



An Improved Interaction Method for Calculating Exhaust Nozzle Boattail Flows

Gary D. Kuhn
Nielsen Engineering & Research, Inc.
Mountain View, California

October 1980

Final Report for Period September 1978 — December 1979

Approved for public release; distribution unlimited.

ARNOLD ENGINEERING DEVELOPMENT CENTER
ARNOLD AIR FORCE STATION, TENNESSEE
AIR FORCE SYSTEMS COMMAND
UNITED STATES AIR FORCE

NOTICES

When U. S. Government drawings, specifications, or other data are used for any purpose other than a definitely related Government procurement operation, the Government thereby incurs no responsibility nor any obligation whatsoever, and the fact that the Government may have formulated, furnished, or in any way supplied the said drawings, specifications, or other data, is not to be regarded by implication or otherwise, or in any manner licensing the holder or any other person or corporation, or conveying any rights or permission to manufacture, use, or sell any patented invention that may in any way be related thereto.

Qualified users may obtain copies of this report from the Defense Technical Information Center.

References to named commercial products in this report are not to be considered in any sense as an indorsement of the product by the United States Air Force or the Government.

This report has been reviewed by the Office of Public Affairs (PA) and is releasable to the National Technical Information Service (NTIS). At NTIS, it will be available to the general public, including foreign nations.

APPROVAL STATEMENT

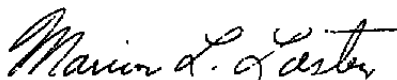
This report has been reviewed and approved.



ELTON R. THOMPSON
Project Manager
Directorate of Technology

Approved for publication:

FOR THE COMMANDER



MARION L. LASTER
Director of Technology
Deputy for Operations

UNCLASSIFIED

REPORT DOCUMENTATION PAGE		READ INSTRUCTIONS BEFORE COMPLETING FORM
1 REPORT NUMBER AEDC-TR-80-19	2 GOVT ACCESSION NO.	3 RECIPIENT'S CATALOG NUMBER
4 TITLE (and Subtitle) AN IMPROVED INTERACTION METHOD FOR CALCULATING EXHAUST NOZZLE BOATTAIL FLOWS	5 TYPE OF REPORT & PERIOD COVERED Final Report, September 1978 - December 1979	
	6 PERFORMING ORG. REPORT NUMBER NEAR TR 213	
7 AUTHOR(s) Gary D. Kuhn	8 CONTRACT OR GRANT NUMBER(s) F40600-77-C-00068-P00064	
9 PERFORMING ORGANIZATION NAME AND ADDRESS Nielsen Engineering & Research, Inc. 510 Clyde Avenue Mountain View, CA 94043	10 PROGRAM ELEMENT, PROJECT, TASK AREA & WORK UNIT NUMBERS Program Element 65807F	
11 CONTROLLING OFFICE NAME AND ADDRESS Arnold Engineering Development Center/DOS Air Force Systems Command Arnold AFS, TN 37389	12 REPORT DATE October 1980	
	13. NUMBER OF PAGES 102	
14 MONITORING AGENCY NAME & ADDRESS (if different from Controlling Office)	15 SECURITY CLASS (of this report) UNCLASSIFIED	
	15a DECLASSIFICATION/DOWNGRADING SCHEDULE N/A	
16 DISTRIBUTION STATEMENT (of this Report) Approved for public release; distribution unlimited.		
17 DISTRIBUTION STATEMENT (of the abstract entered in Block 20, if different from Report)		
18 SUPPLEMENTARY NOTES Available in Defense Technical Information Center (DTIC).		
19 KEY WORDS (Continue on reverse side if necessary and identify by block number) <div style="display: flex; justify-content: space-between;"> <div style="width: 45%;"> interaction methods separated flow computer programs integral methods turbulent boundary layers </div> <div style="width: 45%;"> inviscid flow entrainment exhaust plumes methods of characteristics </div> </div>		
20 ABSTRACT (Continue on reverse side if necessary and identify by block number) <p>A turbulent boundary-layer, inviscid flow interaction method for calculating axisymmetric nozzle boattail configurations is presented. The method is applicable to flows with subsonic or supersonic free streams with Mach number in the range .5 - 1.5, including flows with shock-wave induced separation and to bodies with either high pressure exhaust plumes or solid plume simulators. The theory and some sample calculations are presented along with detailed instructions for preparation of input data, description of</p>		

UNCLASSIFIED

UNCLASSIFIED

20. ABSTRACT, Concluded.

output, and instructions for operation of the computer program on an IBM 370 computer.

UNCLASSIFIED

PREFACE

The results reported herein were developed for the Arnold Engineering Development Center, Air Force Systems Command, by Nielsen Engineering & Research, Inc., under Contract F40600-77-C-0008-P00024. The Air Force Project Manager for this contract was E. R. Thompson, AEDC/DOT. This report covers the work done during the period September 1, 1978 to December 31, 1979. The reproducibles used in the reproduction of this report were provided by the author.

TABLE OF CONTENTS

<u>Section</u>	<u>Page No.</u>
1. INTRODUCTION	1
2. SUBSONIC INTERACTIONS	2
3. SUPERSONIC INTERACTIONS	4
4. EXHAUST PLUME ENTRAINMENT MODEL	8
4.1 INTEGRAL EQUATIONS	9
4.2 ENTRAINMENT LAYER VELOCITY PROFILES	10
4.3 DENSITY PROFILES	11
4.4 TURBULENT EDDY VISCOSITY	11
4.5 EQUATIONS SOLVED	11
5. RESULTS	12
5.1 CIRCULAR ARC BOATTAILS WITH SOLID PLUME SIMULATORS	12
5.2 CIRCULAR ARC BOATTAILS WITH HIGH PRESSURE EXHAUST JETS	14
5.3 SUMMARY OF RESULTS	14
6. COMPUTER PROGRAM ORGANIZATION	15
7. INPUT TO THE PROGRAMS	17
7.1 TABULAR FORM	17
7.2 DICTIONARY OF INPUT VARIABLES	18
8. PROGRAM OPTIONS	26
8.1 BOUNDARY-LAYER OPTION	26
8.2 INVISCID-FLOW OPTION	27
8.3 VISCID-INVISCID ITERATION OPTION	27
8.4 BOUNDARY-LAYER INITIAL CONDITIONS	28
8.5 OPTIONS FOR DETERMINING THE SEPARATION POINT	29
9. PROGRAM OUTPUT	30

TABLE OF CONTENTS (Concluded)

<u>Section</u>	<u>Page No.</u>
9.1 STANDARD OUTPUT	30
9.2 SPECIAL OUTPUT MESSAGES	34
10. PROGRAM OPERATING PROCEDURE	36
10.1 GENERAL JOB CONTROL SEQUENCE	36
10.2 JOB CONTROL EXAMPLES	36
10.2.1 <u>Creating Partitioned Data Sets</u>	37
10.2.2 <u>Starting an Iteration Sequence</u>	37
10.2.3 <u>Restarting an Iteration Sequence</u>	38
10.2.4 <u>Executing the Boundary-Layer Program Alone</u>	40
10.2.5 <u>Executing the Inviscid Program Alone</u>	40
11. NUMERICAL EXAMPLES	41
11.1 AXISYMMETRIC INTERACTION	41
11.2 EXAMPLE OF RESTARTING AN INTERACTION CALCULATION	42
11.3 TWO-DIMENSIONAL BOUNDARY LAYER	42
11.4 AXISYMMETRIC INVISCID FLOW	42
REFERENCES	43
TABLES I THROUGH III	45
FIGURES 1 THROUGH 20	49
LIST OF SYMBOLS	97

1. INTRODUCTION

The flow over the afterbody of jet aircraft is often characterized by separation which increases the drag and decreases engine performance. For subsonic flows the separation occurs in an adverse pressure gradient which causes the flow to break away from the wall and form a local area of reversed flow. The point along the wall dividing the forward and reversed flows is defined as the separation point. While an exact flow solution for the separated region can theoretically be obtained from finite difference calculations of the fully turbulent compressible Navier-Stokes equations, the complexity and expense of such calculations at the present time make that approach unrealistic for engineering requirements. Consequently, calculative techniques have been developed which consist of patching together approximate models of the flow in the various regions.

All of the methods to be discussed herein apply to axisymmetric bodies at zero angle of attack. In the method of Presz, et al. (ref. 1), the separated region is represented by a discriminating streamline which determines the effective shape of a solid body upon which an attached boundary layer is calculated. Control volume analyses locate the separation point and determine the shape of the discriminating streamline. Boundary layers and exhaust plume entrainment are modeled using integral methods. The technique is applicable to subsonic flows with Mach numbers less than that for the onset of shock induced separation, typically a free stream Mach number of about 0.9. Another approach, developed by Cosner (ref. 2), employs an integral boundary layer method for the entire body including the separated region. Empirical relations are used to extend the calculations across the separation and reattachment points for bodies with solid plume simulators. Exhaust plume entrainment is calculated by simply extending the boundary layer analysis to the plume boundary treated as a moving wall. Comparisons with data indicate the method is not successful for bodies with extensive separation. The most sophisticated approach to the problem of exhaust plume entrainment is that of Dash et al. (ref. 3) wherein finite difference methods are used for the flow calculations in all regions of the flow. Separated flow on the nozzle boattail is not considered. However, studies described by Wilmoth (ref. 4) indicate that the method correctly accounts for exhaust plume entrainment. The present author developed a method (ref. 5) which combines a finite difference inviscid flow method with integral methods for the boundary layer and exhaust plume mixing layer. The approach employed a displacement surface calculated from the viscous layer which forms an effective boundary for the inviscid flow and is compatible with the resulting inviscid pressure distribution. For separated boundary layers, the displacement surface was assumed to take the form of

a conic section. The method also included an approximate one-dimensional exhaust jet model including entrainment of the boattail boundary layer. The method was found to provide an accurate engineering prediction method for boattail flow fields with moderately underexpanded exhaust flows and for bodies with solid plume simulators for free stream Mach numbers less than that for which shock induced separation would occur on the boat-tail.

In this report improvements and extensions of the method of reference 5 are discussed. The improvements are the removal of the assumption that the separated displacement surface is conical and the use of a more accurate inviscid jet model based on the method of characteristics. The calculation method is extended to include shock induced separation.

2. SUBSONIC INTERACTIONS

The particular boundary layer and inviscid external flow method used in the calculations were described in references 5 and 6 and will not be described in detail here. The boundary layer method is an integral method which can be applied in a direct mode (boundary layer edge velocity, u_e prescribed) or an inverse mode (boundary layer displacement thickness, δ^* prescribed). The inviscid flow method used is the South-Jameson (ref. 7) theory as implemented by Keller and South (ref. 8) with minor modifications to accommodate the iterative interaction procedure.

In the method described in reference 5, the first step in calculating the viscous/inviscid interaction is to calculate the inviscid flow over the basic body. The resulting distribution of the velocity at the boundary is then prescribed in the second iteration step as the boundary layer edge velocity u_e for the boundary layer calculation in the direct mode up to the separation point. The boundary layer calculation is then switched to the inverse mode and the solution is carried on into the separated flow using a prescribed distribution of the boundary layer displacement thickness δ^* . The result of the inverse calculation is a solution for the boundary layer edge velocity (the "viscous velocity") which, in general, will not agree with the "inviscid velocity" produced by the inviscid flow theory. The effective displacement surface between separation and a point downstream of reattachment or in the plume entrainment region is assumed to be conical (see fig. 1). An iterative procedure is used to find the particular cone angle θ_s and the separation point location x_s for which the "viscous velocity" and the "inviscid velocity" will agree within an acceptable

tolerance. In the remainder of this report, this procedure will be referred to as the " x_s - θ_s iteration".

In the improved interaction procedure the separation point location x_s is assumed known. Also, in order to obtain a first approximation for the shape of the displacement surface an angle θ_s is assumed known. These quantities can be obtained from the method of reference 5 or several other available methods such as those evaluated by Abeyounis (ref. 9). The angle θ_s is usually estimated to be 10° as a first approximation. Thus, the new interaction procedure begins in the same manner as in reference 5. The first step is to calculate the inviscid flow over the basic body. The second step is to calculate a boundary layer displacement thickness assuming a conical displacement surface in the separated region. The next step in the new interaction procedure is the computation of the new displacement thickness distribution in which the assumption of a conical surface is dropped and the new displacement thickness is deduced from the mismatch of the viscous and inviscid velocities by

$$\delta_{\text{new}}^* = \delta_{\text{old}}^* \frac{u_{e_v}}{u_{e_I}} \quad (1)$$

The displacement surface is prescribed in this manner for all subsequent iterations. Also, it is no longer necessary to operate the boundary layer method in a direct mode up to the separation point but the inverse method is used with the displacement surface prescribed over the entire afterbody flow region. Carter (ref. 10) has shown that this update procedure for the displacement thickness follows logically from an approximate analysis of the von Kármán momentum integral equation.

It is noted that the extension of the calculations across both the separation point and the reattachment point in the present method is accomplished in the same manner as for the method of reference 5. The approach employs an engineering approximation based on the assumptions that upstream influences are transmitted predominantly through the external inviscid flow and that violations of the boundary layer assumptions such as significant normal pressure gradients associated with separation can be neglected on the grounds that they are only important in a small neighborhood of the separation point and have negligible effect on the rest of the flow. In keeping with these assumptions, the location of the separation point is obtained independently from the boundary layer calculation and the skin friction is specified to be zero at that point keeping the boundary layer edge velocity and the displacement thickness δ^*

continuous. By specifying the displacement thickness over the entire calculative region a smoothly converging iteration is produced. The update procedure on the displacement thickness, including a relaxation parameter, ω , can be written as

$$\delta_n^* = \delta_{n-1}^* \left[1 + \omega \left(\frac{u_{eV}}{u_{eI}} - 1 \right) \right] \quad (2)$$

where, if $\omega = 1$, equation (1) is obtained. It was found that overrelaxation ($\omega > 1$) could be used to accelerate the convergence of the interaction process. However, with overrelaxation an oscillatory pattern was found to be produced in the convergence so that for practical calculations, underrelaxation is usually used ($\omega < 1$). In the remainder of this report, this procedure will be referred to as the " δ^* -update procedure".

It is noted that the new procedure does not provide any new information for locating the separation point, x_s . Abeyounis (ref. 8) examined eight empirical and semi-empirical separation criteria and prediction methods (not including that of reference 5, the " $x_s-\theta_s$ iteration") using experimental data from boattailed afterbodies with solid exhaust plume simulators. Abeyounis found that none of the methods accurately predicted the separation locations for all the conditions included in the data. The method of reference 5 has been found to compare favorably with the best of the criteria examined by Abeyounis. The $x_s-\theta_s$ iteration procedure remains an option in the revised computer code.

3. SUPERSONIC INTERACTIONS

The interaction between a boundary layer and a shock wave of sufficient strength to cause separation of the boundary layer is very complex and presents formidable difficulties for developing approximate models for engineering calculations. The most detailed experimental studies of shock-wave-boundary-layer interactions in the Mach number range 1.2-1.5 have concerned normal shock waves. While the shock waves encountered on axisymmetric nozzle boattails are not necessarily normal to the surface, a similar degree of complexity of the flow to that associated with a normal shock is to be expected. Therefore, some understanding of the nature of the flow can be gained by examination of a normal-shock-boundary layer interaction. An important work for this purpose is that of Seddon (ref. 11) which discusses the

fundamental nature of normal shock and turbulent boundary layer interaction from detailed examination of velocity profiles.

An interesting feature of Seddon's work is evidence obtained that the wake hypothesis of Coles holds true over the greater part of the flow except in the immediate vicinity of the shock wave or other regions of strong pressure gradient. This is an important observation for the present work. The boundary layer method used previously for subsonic flows is based on the Coles law of the wall and law of the wake so that the work of Seddon suggests the possibility of extending the method to flows with shock waves.

In developing the calculative technique to be described here, it was found that straightforward application of the calculative techniques used in reference 5 and discussed in the previous section was not possible. Calculations using those techniques were found to be unstable. A new calculative technique was derived which employs Prandtl-Meyer theory and the semiempirical approach of Mager (ref. 12).

In order to produce a stable calculation, it was found to be necessary to eliminate from iterative calculations the boundary layer upstream of the separation point. Thus, for supersonic interactions, the first two steps of the calculation are the same as for subsonic interactions, that is, calculation of the inviscid flow over the basic body followed by a calculation of the boundary layer. The separation point is determined from the inviscid pressure distribution by an approximate method and the first boundary layer calculation is made assuming a conical separated displacement surface as in the method of reference 5. In subsequent iterations, the starting point for the boundary layer calculations is the separation point. Thus, the boundary layer upstream of the separation point is calculated only once and is assumed to be the same for all subsequent iterations. Downstream of the separation point the theory for prescribed displacement thickness is modified by replacing the arbitrarily specified δ^* distribution with an equation employing the Prandtl-Meyer function.

$$\frac{d\delta^*}{dx} = \tan \phi - \frac{dr_w}{dx} \quad (3)$$

where

$$\phi = -\sqrt{\frac{\gamma+1}{\gamma-1}} \tan^{-1} \left[\sqrt{\frac{\gamma-1}{\gamma+1}} \left(M_e^2 - 1 \right) \right] + \tan^{-1} \left[\sqrt{M_e^2 - 1} \right] + \phi_c \quad (4)$$

with

$$\phi_c = \phi_s + \sqrt{\frac{\gamma+1}{\gamma-1}} \tan^{-1} \left[\sqrt{\frac{\gamma-1}{\gamma+1}} \left(M_{e_s}^2 - 1 \right) \right] + \tan^{-1} \left[\sqrt{M_{e_s}^2 - 1} \right] \quad (5)$$

$$\phi_s = \tan^{-1} \left[\left(\frac{d\delta^*}{dx} \right)_s + \left(\frac{dr_w}{dx} \right)_s \right] \quad (6)$$

$$M_e = u_e/a_e \cos \phi \quad (7)$$

In the implementation of this theory the Mach number M_e in the Prandtl-Meyer function is evaluated using the velocity component u_e as calculated from the boundary layer theory for the current iteration with the tangential angle, ϕ , evaluated from equation (3) at the previous step of the current boundary layer integration.

The separation point used in supersonic cases is not so easily predicted as for subsonic flows. In the present method, two options are available for predicting the separation point. In one option the separation point is determined from the inviscid solution on the basic body at the first iteration. This option depends somewhat on the arbitrary spacing of the calculative mesh of the external inviscid flow in that the separation position is placed at the inviscid mesh point previous to the point at which the maximum Mach number is calculated on the boattail. In the second option, the user of the method is allowed to input any arbitrary separation point location. With the separation point known, calculation requires an initial value for the angle of the displacement surface after separation. This is determined from the theory of Mager. This theory employs the following equations:

$$p_s/p_i = 1 + 0.225 \gamma M_i^2 / \left[1 + \frac{1}{2} (\gamma - 1) M_i^2 \right] \quad (8)$$

$$(p_f/p_i)_v = p_s/p_i \left\{ 1 + 0.18 \gamma M_i^2 e_f / \left[1 + 0.275 (\gamma - 1) M_i^2 \right] \right\} \quad (9)$$

$$(p_f/p_i)_I = \left[2 \gamma M_i^2 \sin^2 \theta_s - (\gamma - 1) \right] / (\gamma + 1) \quad (10)$$

$$\tan \theta_f = \left\{ \left[\frac{1}{2} (\gamma + 1) M_i^2 / (M_i^2 \sin^2 \theta_s - 1) - 1 \right] \tan \theta_s \right\}^{-1} \quad (11)$$

The required angle θ_f is determined by an iterative procedure as follows. The value of M_i is the maximum Mach number ahead of the shock, obtained from the inviscid solution. Then p_s/p_i is determined from equation (8), and the first approximation to p_f/p_i is determined from equation (9) with θ_f approximated by

$$\theta_f \approx \left[\sqrt{M_i^2 - 1} / \gamma M_i^2 \right] \left[(p_f/p_i) - 1 \right] \quad (12)$$

so that

$$\frac{p_f}{p_i} \approx \frac{p_s}{p_i} \left\{ (1 + G) / \left[1 + (p_s/p_i) G \right] \right\} \quad (13)$$

where

$$G \equiv -0.18 \sqrt{M_i^2 - 1} / \left[1 + 0.275(\gamma - 1) M_i^2 \right] \quad (14)$$

Then θ_s is computed from the oblique shock relation, equation (10), and θ_f from equation (11). Substituting θ_f into equation (9) and calculating a new θ_s from equation (10) allows a second value of θ_f to be determined from equation (11). The second value of θ_f is used as the initial value of the turning angle of the displacement surface following Mager's advice that further iteration will not improve the accuracy.

With the Prandtl-Meyer equation replacing the arbitrarily specified δ^* distribution, there are three equations for the three unknowns, u_e , δ_i , and δ^* of the boundary layer theory. However, the overall flow problem is not closed since the calculation of the flow in the limited region of separation does not necessarily satisfy the boundary conditions on the flow at downstream infinity. In order to provide final closure of the problem, the Prandtl-Meyer analysis stops at the reattachment point and the calculation method returns to the u_e prescribed procedure as in the theory of reference 5. In this procedure the value of u_e that was obtained from the boundary-layer-Prandtl-Meyer theory is faired into the inviscid u_e solution obtained from the previous iteration. The result of this procedure is as in the subsonic case, two velocity distributions, one from the boundary-layer-Prandtl-Meyer theory and one from

the external inviscid-flow theory. In order to cause these velocity distributions to agree as closely as possible, another parameter must be adjusted. The parameter selected for this purpose is the boundary layer edge velocity at the separation point u_{es} . Because of the approximations inherent in the present model, the velocity at the separation point for the boundary-layer calculation cannot be forced to be equal to the velocity at that point in the inviscid flow for any arbitrary iteration step. Thus, the value of the initial velocity for the boundary-layer calculation is iterated until the mean squared error between the boundary-layer velocity and the inviscid velocity is minimized as for the subsonic flows discussed previously.

Due to the approximate nature of the model, it is generally not possible to cause the boundary layer and inviscid solutions to agree as closely as for subsonic cases. While it is typically possible in subsonic cases to achieve agreement to an rms error of less than one percent, an error of four-to five percent is more typical of supersonic cases calculated to date. However, as will be shown subsequently, the pressure coefficient distribution determined from the boundary layer velocity solution compares very well with measured values.

4. EXHAUST PLUME ENTRAINMENT MODEL

The effect of an exhaust jet plume on the flow on an after-body has been found to consist of two separate effects. First is the effect of the shape of the plume. Second is the effect of the entrainment of external air into the plume boundary. The two effects oppose each other since the entrainment of low speed external air by the high speed jet tends to decrease the effective expansion of the jet boundary.

The shape effect of the jet plume is accounted for by the expansion of the inviscid jet core flow. The entrainment effect is determined by calculating a jet mixing displacement thickness and defining an effective body shape using that surface.

The basis of the new exhaust plume entrainment model is the technique developed by Peters, et al. (ref. 13) in which an integral method for the exhaust plume mixing layer is coupled with a method of characteristics inviscid jet calculation. The modifications to Peters' technique for the present calculation method include use of a prescribed external pressure distribution, calculation of integrals in the integral mixing layer method across the mixing layer only, that is, omitting the

external inviscid flow from the integrals, and determination of derivatives of flow quantities at the inner boundary of the mixing layer by numerical differences rather than by solution of a set of simultaneous equations. The boundary of the jet is taken to be the midpoint of the mixing layer and the displacement thickness of the mixing layer is calculated in a manner analogous to that for a boundary layer (see fig. 2). The entrainment of the boundary layer is thus accounted for to a first approximation by using the displacement surface of the jet as the effective boundary upon which to calculate a boundary layer. The boundary layer of the boattail is then simply extended onto this approximate surface as though the jet were a solid surface. Entrainment is accounted for by the fact that the displacement surface of the mixing layer velocity profile is a negative quantity relative to the jet boundary.

4.1 INTEGRAL EQUATIONS

The basic equations of the entrainment in the coordinates shown in figure 2 are:

Continuity

$$(\rho u r)_x + \left\{ \rho r [v - u(r_w)_x] \right\}_r = 0 \quad (15)$$

Axial Momentum

$$r \rho u u_x + r \rho [v - u(r_w)_x] u_r = -r p_x + (r \mu \beta u_r)_r \quad (16)$$

The energy equation is represented by the approximation

$$S = (T_t/T_{t_e} - 1) = (T_{t_i}/T_{t_e} - 1) (u - u_e)/(u_i - u_e) \quad (17)$$

where

$$r_w = r_i + \frac{1}{2} b \quad (\text{see figure 2}) \quad (18)$$

Integrating across the mixing/entrainment layer and using the continuity equation to eliminate the radial velocities yields

$$\begin{aligned}
& \int_{r_i}^{r_w} r \left[\rho (2u - u_w) u_x + u (u - u_w) \rho_x \right] dr \\
& + \frac{1}{2} (r_w^2 - r_i^2) (p_e)_x - r_w \mu_w \beta_w (u_r)_w \\
& + r_i \rho_i \left[v_i - u_i (r_w)_x \right] (u_w - u_i) = 0 \quad (19)
\end{aligned}$$

and

$$\begin{aligned}
& \int_{r_i}^{r_e} r \left[\rho (2u - u_e) u_x + u (u - u_e) \rho_x \right] dr + \frac{1}{2} (r_e^2 - r_i^2) (p_e)_x \\
& + r_i \rho_i \left[v_i - u_i (r_w)_x \right] (u_e - u_i) = 0 \quad (20)
\end{aligned}$$

The results of the solution of these equations are used to define a displacement thickness

$$\delta^* = \int_{r_w}^{r_i+b} \left(1 - \frac{\rho u}{\rho_e u_e} \right) \frac{r}{r_w} dr \quad (21)$$

As a first approximation, it is assumed that the effective boundary of the jet is defined by

$$r_b = r_w + \delta^* = r_i + \frac{1}{2} b + \delta^*$$

The boundary r_b is then used as an effective solid boundary on which a boundary layer is computed in the usual manner.

4.2 ENTRAINMENT LAYER VELOCITY PROFILES

The velocity profiles of the plume mixing layer are represented by

$$u = u_e + \frac{1}{2} (u_i - u_e) \left[1 + \cos \pi \left(\frac{r - r_i}{b} \right) \right] \quad (22)$$

4.3 DENSITY PROFILES

The mixing/entrainment zone density profiles are determined in terms of the temperature profiles for isentropic flow

$$\frac{\rho_e}{\rho} = \frac{T}{T_e} = (1 + m_e) (S + 1) - M_e \left(\frac{u}{u_e} \right)^2 \quad (23)$$

where $m_e = \frac{1}{2} (\gamma - 1) M_e^2$

4.4 TURBULENT EDDY VISCOSITY

The term $r_w \mu_w \beta_w (u_r)_w$ in equation (19) represents the turbulent shear stress at the half radius surface. The factor β_w is the eddy viscosity factor. The model for the eddy viscosity used in this work is the same as that used by Peters, et al. (ref. 13).

4.5 EQUATIONS SOLVED

Evaluation of the integrals of equations (19) and (20) with the profiles of equations (22) and (23) results in a set of two ordinary differential equations of the form

$$A_{i1} \frac{dr_i}{dx} + A_{i2} \frac{db}{dx} + A_{i3} \frac{dp_e}{dx} = B_i \quad (24)$$

with $i = 1$ and 2 , where A_{ij} and B_i are functions of r_i , b , u_e , and u_i .

The equations (24) are numerically integrated using a simple first-order predictor-corrector method as described in reference 5.

Many terms appearing in the coefficients of equation (24) depend on the flow conditions at the inner mixing zone boundary. In order to solve the equations, the following quantities must

be evaluated at $r_i: \theta_i, \partial u / \partial x, \partial u / \partial r, \partial p / \partial x, \partial p / \partial r$. To provide these parameters, the inviscid jet core flow is computed using the irrotational method of characteristics simultaneously with the numerical solution of equations (24) in a manner similar to that of reference 13. This calculation is carried out until the inner mixing layer radius, r_i , becomes zero, or for a specified distance downstream of the nozzle. Downstream of that point, the jet boundary is assumed to be cylindrical.

5. RESULTS

In this section, the theory is compared with experimental results on axisymmetric boattail-sting and boattail-exhaust plume configurations.

5.1 CIRCULAR ARC BOATTAILS WITH SOLID PLUME SIMULATORS

Wind tunnel studies of the configuration shown in figure 3 were described in reference 14. The configuration is a cone-cylinder, with a circular arc boattail. Three of the boattails are examined here to illustrate the capabilities of the calculative method. The first example is for a boattail (configuration 1 in fig. 3) for which extensive separation is evident experimentally. Surface static pressure distributions were measured along the boattail and along the sting for free-stream Mach numbers from 0.4 to 1.2. Boundary-layer transition was tripped at $x/D = .167$. Calculations were made for Mach numbers of 0.6, 0.8, and 0.9.

In figure 4 is shown a typical variation of the rms error

$$s = \left[\sum_{i=1}^N \left(u_{e_v} - u_{e_I} \right)^2 / N u_{e_o}^2 \right]^{1/2} \quad (25)$$

between the viscous and inviscid solutions for configuration 1 in subsonic flow. During the first four iterations a conical displacement surface was used to generate an approximate shape, and then the new procedure [eq. (2)] was used with $\omega = .5$. Large oscillations in the error occur in the first four iterations, followed by a smoothly convergent sequence. When the error is reduced to a value of the order of one percent, oscillations again appear, although of smaller amplitude. The error appears to approach an asymptotic nonzero value. The

value of the minimum error depends on a number of factors, including the coarseness of the calculation mesh used for the external inviscid flow and the smoothness of the boundary. No consistent relationship was found between the value of the minimum error and the location of the separation point.

In figure 5 is shown the effect of the new interaction model on the calculated pressure distribution for the model with the circular arc boattail of configuration 1 and cylindrical plume simulator. The separation point used for the calculations was the value predicted using the x_s - θ_s iteration method of reference 5. The pressure coefficients shown were calculated from the viscous velocity, u_{eV} . The new δ^* update iteration procedure using equation (2) with $\omega = 0.5$ results in small adjustments to the shape and in turn to the pressure distribution. In figure 6 is shown other comparisons between the new theory and data from reference 14 for Mach numbers of 0.4, 0.6, 0.8, and 0.9 on the same boattail as in figure 5. The location of separation was predicted in each case as the location where

$$H_i = \delta_i^* / \theta_i = 1.2$$

for the first and second boundary layer iterations. The calculated pressure coefficients were determined from the average of the viscous and inviscid velocity distributions, u_{eV} and u_{eI} . The comparisons for $M_o = 0.4, 0.6$, and 0.8 are excellent. The comparison for $M_o = 0.9$ is good although the expansion of the flow at the beginning of the boattail is slightly under-predicted. The difference for $M_o = 0.9$ is probably due to the fact that a weak shock occurs which is almost of sufficient strength to cause separation. Attempts to calculate the flows using the theory for shock-induced separation were unsuccessful, but the improved subsonic theory predicts the pressure distribution well.

In figure 7 is shown the results of calculations for two cases of shock-induced separation on the same body as for the results shown in figures 5 and 6. The separation point in each case was determined by the procedure described previously. That is, x_s was derived to be the location of the inviscid calculative point previous to the point at which the maximum Mach number is calculated on the boattail at the first iteration. The pressure coefficients were determined from the viscous velocity distributions, u_{eV} , for which the best agreement with the inviscid velocity was obtained. The results for a Mach number of 1.15 are very good with the predicted shock location and plateau pressure agreeing very closely with the data. For a Mach number of 1.3, the predicted shock location is very good while the predicted plateau pressure is in fair agreement with the data.

The afterbody drag on the model of figures 5, 6, and 7 is shown in figure 8. The predicted drag is slightly high for low subsonic Mach numbers but is well predicted for high subsonic Mach numbers and underpredicted for transonic Mach numbers. The prediction is excellent for the low subsonic Mach number of 1.15, but is slightly low at the higher Mach number of 1.3.

A comparison with data on configuration 2 is shown in figure 9. The boattail of configuration 2 is slightly longer than that of configuration 1 resulting in a shorter region of separated flow. The predicted pressure distribution is in excellent agreement with the data.

5.2 CIRCULAR ARC BOATTAILS WITH HIGH PRESSURE EXHAUST JETS

Four cases with real exhaust jets are shown in figure 10. The configuration 1 afterbody, was used with a sonic nozzle and jet total pressure to free-stream static pressure ratios of 2.0, 3.0, 4.0, and 5.0. The data shown are for a free-stream Mach number of 0.8. The calculations were made for a nozzle Mach number of 1.01 and pressure ratios of 2.1, 3.0, 4.0, and 5.0, respectively. These adjustments were necessary for two reasons. First, the present method of characteristics jet theory cannot calculate for a nozzle Mach number of exactly 1.0. Second, the external static pressure at the end of the boattail tends to be slightly higher than the free-stream pressure, P_o , so that in order to achieve a supersonic flow in the jet as required by the method of characteristics, a slightly higher pressure ratio was necessary for the lowest pressure than was used in the experiment. The separation point locations shown in figure 9 were determined by the same criterion used in the previous comparisons shown in figure 6. Good comparisons with the experimental data are calculated for all four pressure ratios although the comparison appears to improve with increasing nozzle pressure.

The predicted afterbody drag for the body with an exhaust jet is compared with experimental values in figure 11. The new theory appears to underpredict the drag for low pressure ratios and overpredict the drag for high pressure ratios. The comparison could probably be improved by using a different separation location in the calculations.

5.3 SUMMARY OF RESULTS

The calculative method developed previously was improved by removing the restriction that the separation flow region have a conical shape and by extending the Mach number range to include

flows with shock-induced separation. Also, an improved exhaust jet calculative method was incorporated based on a simultaneous solution of the method of characteristics for the inviscid jet core flow and an integral method for the jet mixing boundary.

The results of sample calculations indicate that for subsonic flows, the conical displacement surface is a very good approximation and relaxing the requirement of a conical surface yields only a small adjustment to calculated pressure distributions while providing a substantial increase in computational speed and reduction in cost.

Calculations for supersonic flows indicate the theory produces a good approximation for the pressure distribution and consequently for the afterbody drag for Mach numbers up to 1.3.

6.0 COMPUTER PROGRAM ORGANIZATION

In this section, the general organization of the programs will be described. Specific information on data required for input and data developed for output will be described in sections 7, 8, and 9. Sample Job Control Card decks for a typical IBM 370 installation are presented in section 10.

The overall program consists of a mainline program (program 1) and three main subprograms each consisting of several sub-routines. The first main subprogram is the inviscid-flow program (program 2). It is a modified version of the program described in reference 8. The second main subprogram is the boundary-layer program (program 3). It is based on the integral theory described in reference 5. The third subprogram is the inviscid exhaust plume, mixing layer program (program 4). The mainline program controls the iteration between the other three programs. Either of the first two subprograms may be used separately, without iterating by appropriate choice of the input parameters.

Both the viscous-flow programs and the inviscid-flow programs require some punched card input and may require some input data from disc or tape data files. The data files must be identified by specific Logical Unit numbers. The general relationship of the programs and the various data files are shown in figure 12. The specific Logical Unit numbers required for input and output are listed in Table I. Two Logical Unit numbers are associated with each data file shown in figure 12. One unit is used for input, the other for output.

Program 2 requires initially data from cards describing the free-stream conditions, the computational mesh and the body

shape. Alternately, the program can accept the input body shape from data file 1. It can also accept an initial solution for the perturbation velocity potential from another data file (data file 2). Program 2 produces printed output lists of the appropriate flow field quantities, quantities describing the configurations and the computational mesh and several data files. Data file 2 is rewritten using the new solution for the potential. A third file (data file 3) is written containing the distribution of the axial velocity component at the inviscid boundary for use by the viscous flow program.

Program 3 requires initially the free-stream conditions and gas constants as well as parameters describing the shape of the surface over which the boundary layer is flowing. On the first iteration of a viscous-inviscid interaction, the surface shape is the same as that for program 2. On subsequent iterations, the body shape for the boundary-layer program remains the same, except when it is modified by the calculation of a new plume shape, while that for the inviscid flow is modified by the addition of the boundary layer. Program 3 can also accept data from data files as optional input. The boundary-layer-edge velocity distribution, u_e , can be input from data file 3, produced by program 2. The distribution of the body shape augmented by the displacement thickness can be input from data file 4. That file differs from data file 1 because it contains the raw data for $\delta^* + r_w$ versus x as calculated by the boundary-layer program while data file 1 contains the shape interpolated to the x stations of the original input shape. If program 3 is being used separately from program 2 (i.e., without iterating), two additional options are available for card input. Either the boundary-layer-edge velocity, u_e , can be input as mentioned previously, or the displacement thickness, δ^* , may be input. These options are described more fully in sections 8.1 and 8.2.

Program 3 produces as output lists of the boundary layer and flow quantities as they are calculated along the body. In addition, program 3 produces an updated version of data file 4 and the augmented body shape (data file 1) required by program 2. Data file 4 also contains a list of the velocity ratio u_e/u_{e0} corresponding to the boundary layer.

Program 3 can be used in a two-dimensional boundary layer mode if desired. However, calculation of a viscous-inviscid interaction or exhaust plume entrainment can only be done for axisymmetric cases with the present inviscid program.

All card input pertaining to programs 2 and 3 is input through an input subroutine called by program 1. Program 1 also produces a file of the quantities needed to restart and continue the calculation if the calculation should terminate before all iterations are completed. These data are stored on data file 5.

Detailed instructions regarding restarting are presented in sections 10.2.3 and 11.2.

7. INPUT TO THE PROGRAMS

The data required by the programs generally fall into three categories: (1) geometrical data; (2) flow field data; and (3) control parameters. The control parameters are indices for specifying options and iteration counters. It will be noted by comparison with reference 8 that a number of input quantities required for the inviscid-flow program have been eliminated in the present version. This has been done by incorporating the calculations required to obtain some of the quantities into the present code or by simply defining fixed values which have been found to be successful. Specifically, a value of 1.4 is used for the initial value of the subsonic relaxation factor, a value of 0.1 is used for the initial value of the supersonic relaxation factor and a value of 1.3 is used for the exponent in the normal coordinate stretching function. Also, it is assumed that the computational grid has equal step sizes in both coordinate directions at the nose of the body. Finally, the number of relaxation steps allowed in the inviscid program is fixed at 20 for the first four interaction iterations and is changed to 40 and 80 after four and eight iterations, respectively.

The general requirement of the input data is that the tabular lists of the various distributions required represent smooth curves. This is especially true of the list of body shape coordinates. The inviscid program uses cubic splines to fit the input coordinates, so those coordinates must accurately represent a smooth curve with continuous second derivatives.

7.1 TABULAR FORM

The input data required for calculating transonic viscous, inviscid-flow interactions consist of several punched cards containing parameters describing the free-stream flow conditions, the computational mesh for the inviscid calculation, initial values for the viscous flow calculation, and certain options that are available in the program. A dictionary of the input data is presented in the next section. Table II shows the input variables as they are to be punched on the data cards. More detailed explanation of the requirements for the inviscid-flow program (program 2) are presented in reference 8 and are not repeated herein.

7.2 DICTIONARY OF INPUT VARIABLES

The variables required for input on punched cards are defined in this section in the order in which they are required. Additional details on the format of the punched data are given in Table II. The first three cards of any input data deck contain a description of the case being calculated. Any or all of these three cards may be blank, but all three are required. The remaining variables in Table II are as follows:

NRSTRT	Integer indicating whether calculation is being re-started to continue a previous calculation. Only valid for interaction calculations (LPROG = 0, and LITER = TRUE. See below).
= 0	Start from zero. Input all quantities on cards or data files as required.
> 0	Restart. Input data file 5 (Logical Unit 11) containing data from previous iteration plus all other input data files plus other card data as indicated in Table II.
N3	Integer indicating whether restart is to begin with new values of x_s and θ_s (see section 11.2 and Table III).
ILIM	Integer number of seconds corresponding to estimated length of calculation. When the time from the beginning of the calculation is within 10 seconds of this limit, the final restart files will be written. This assures that the job will not terminate while writing such files.
LPROG	Integer indicating level of calculation.
= -1	Inviscid flow only.
= 0	Viscous-Inviscid interaction.
= 1	Boundary layer only.
N1	Integer iteration counter for inner viscous-inviscid iteration
N2	Integer iteration counter for x_s - θ_s iteration presently limited to a maximum of 20.
IBL	Integer indicating how interaction calculations are to begin.

= 3 Start with inviscid flow.

= 0 Start with boundary layer.

IUNIT Integer indicating which value of the gas constant, RGAS, the energy conversion factor, XJ, the acceleration of gravity, GC, and the constants in Sutherlands temperature-viscosity relation are to be used. The choice depends on whether air is the gas being calculated and the units of the input quantities.

= 1 Input units must be pounds, feet, seconds, and °R.

= 2 Input units must be pounds, inches, seconds, and °R.

= 3 Input units must be newtons, meters, seconds, and °K.

For another gas, or other units, put in anything for IUNIT and put in nonzero values of VISC, RGAS, XJ, GC, and SCON. Any units are allowed. The basic rule is that all input quantities must be consistent with regard to units.

MIT Number of relaxation cycles allowed for the inviscid-flow program (program 2). If a value of zero is input, a value of 20 is used. Otherwise, the input value is used.

GAM Ratio of specific heats of the external inviscid flow.

AMINF Free-stream Mach number.

IXY Integer number of values of coordinate pairs, XO,YO, to be input for inviscid body shape. If IXY = 0, the required shape must be input from data file 1 (Logical Unit 14). Maximum value is 200.

XO,YO Axial and radial coordinates of body shape for inviscid-flow calculation, 2 per card.

The next series of variables, items 7 and 8 in Table II, are for the inviscid-flow program (program 2). Detailed information on how these data are to be obtained is contained in reference 1.

IMAX Number of grid lines in the tangential direction; I = 1 is the forward stagnation line, I = IMAX is the rear stagnation line for closed bodies and downstream

infinity for open bodies. For each grid refinement IMAX is increased such that $IMAX_{NEW} = 2(IMAX_{OLD}) - 1$. The present limit on IMAX is 81. Instructions for changing this limit appear as comments in the program listing (subroutine ONE0). The grid refinement option is generally not used for viscous-inviscid interaction calculations.

JMAX Number of grid lines in the normal direction; $J = 1$ corresponds to an infinite distance from the body and $J = JMAX$ is on the body. The same formula and limit that apply to IMAX also apply to JMAX.

MHALF Number of grid refinements to be done. For interaction calculations a value of zero should be used with a grid fine enough for adequate resolution.

KLOSE Body type.

= 0 Open body (i.e., one with a sting or wake).

= 1 Closed body.

LREADP Integer indicating whether initial estimate of potential distribution is to be input from data file 2 (Logical Unit 13).

= 0 No.

= 1 Yes.

If any one, or all of the next four input quantities are input as zero, the pre-programmed values are used.

DNDZO Step size of the normal coordinate at the body. The pre-programmed value is 7 percent of the maximum body diameter.

XIXM Value of the computational coordinate, X , at the matching point of the two stretching functions used in the finite-difference scheme (see ref. 3), for open bodies only. Since X varies from zero to one, XIXM is the fraction of the total number of grid points which will be in the first stretching region (ahead of x_m). The pre-programmed value is 0.75.

XM Axial location, x_m (in physical coordinates), of the junction (or matching point) between the two tangential stretching functions, for open bodies only, see reference 8. Must be less than $XO(IXY)$. This parameter is

used to concentrate computational mesh points in a certain region. The usual approach for interaction calculations (the preprogrammed value) is to let x_m be equal to the length of the body to the beginning of the sting, or plume, XBT.

DSDXIM	Step size of the tangential coordinate at the junction between the two tangential stretching functions. The preprogrammed value is 8 percent of the length of the afterbody (XBT-XZNEW).
XBT	Length of the body.
DMAX	Maximum body diameter.
XZNEW	Length of forebody. Also, this is the axial location at which boundary-layer calculations will begin after four iterations have been calculated. The usual procedure is to start the boundary-layer calculations close to the nose of a long body at XZ (see item 17 in Table II) and then after four iterations move the starting point to XZNEW (XZNEW > XZ). In subsequent iterations, the boundary layer does not change for $X < XZNEW$. For long slender bodies with boattails, XZNEW should be the beginning of the boattail.
PLUMIN	Logical variable indicating whether an exhaust plume is being calculated.
GAMAP	Ratio of specific heats of exhaust gas.
PTPPFS	Ratio of nozzle total pressure to free-stream static pressure.
AMP	Nozzle exit Mach number.
THETAP	Nozzle exit divergence angle.
TTP	Nozzle total temperature.
GMP	Ratio of gas constant of air to that of the exhaust gas.
XJ	Energy conversion factor. If one of the preprogrammed values is acceptable, put in a value of 0.0. The value used will then be determined by the value of IUNIT on item number 3 as follows:

IUNIT	XJ
1	778.0
2	9336.0
3	1.0

GC Gravity constant. If one of the preprogrammed values is acceptable, put in a value of 0.0. The value used will then be determined by the value of IUNIT on item number 3 as follows.

IUNIT	GC
1	32.2
2	386.4
3	9.81

The remaining input variables are related to the boundary-layer program alone or to the viscous-inviscid interaction method.

LSEP Logical variable indicating whether the location of separation (XSEP) is known (TRUE) or not (FALSE).

LITER Logical variable indicating whether the conical separated interaction procedure is to be used. If LITER = TRUE, the calculation procedure is the same as that described in reference 5 for bodies with solid plume simulators until a solution is reached. When the $x_g - \theta_g$ iteration terminates, the calculation then begins the δ^* -update procedure described in section 2 of this report. If LITER = FALSE, the calculation follows the procedure described in section 2 or 3 of this report, depending on the value of the next input variable, LNSHK.

LNSHK Logical variable indicating whether the shock-induced separation procedure is to be used. If LNSHK = TRUE, the calculation procedure for subsonic flow (no shock) is used even if supersonic flow with a shock wave occurs. This parameter is used to override the shock-separated flow procedure for transonic flows where weak shock waves occur and the supersonic procedure does not yield a good result. If LNSHK = FALSE, the supersonic procedure will be followed automatically if a shock wave with Mach number greater than 1.25 is found on the boattail on the first iteration.

XSEP Axial location of separation. Put in only if LSEP = TRUE.

DTHET Angle of δ^* surface with the boattail tangent at x_s .
 Put in only if LSEP = TRUE. A value of 0.0 will cause
 the program to use value of 10.0 (degrees).

IOPT Integer indicating the mode of the calculation.

 = 1 u_e is to be input.
 = 2 δ^* is to be input.

 Put in a value of 1 for starting an interaction calcu-
 lation.

K Integer indicating whether flow is axisymmetric.

 = 0 Two dimensional.
 = 1 Axisymmetric.

LVAR1 Integer indicator for method of input of u_e when
 IOPT = 1.

 = 0 Input u_e (dimensional) on cards.
 = 1 Input u_e/u_{e0} on cards.
 = 2 Input u_e/u_{e0} from data file 3 on Logical Unit
 12.

LSHAPE Integer indicating option for calculating all initial
 conditions (I.C.) except u_e (see section 8.4).

 = 0 Input initial values per LIC.
 = 1 Calculate I.C. for flat plate.
 = 2 Calculate I.C. for cylinder.
 = 3 Calculate I.C. for cone.

LIC Integer indicating initial condition options for
 IOPT = 1 and LSHAPE = 0.

 = 1 Put in CFCL and DELTA1.
 = 2 Put in CFCL and DELST1.

LDSTAR Integer indicating whether a file of $\delta^* + r_w$ is to be
 input.

= 0 No input.

= 1 File of $\delta^* + r_w$ versus x is required on Logical Unit 15 (data file 4).

LSHPBL Integer indicating whether body shape is to be input for boundary-layer calculations.

= 0 XRL and RL are assumed to be the same as XO and YO. This is usually the case when starting an interaction calculation.

= 1 XRL and RL will be required.

NOTE: The next three variables, NVAR, XVAR, VAR, are only required on cards if LPROG = 1 and LVAR1 = 0 or 1.

NVAR Integer indicating the number of values to be input for the prescribed variable (u_e or δ^*). Maximum value is 100.

XVAR,VAR Axial location and value of prescribed variable as follows:

IOPT = 1 and LVAR1 = 0, VAR = u_e

IOPT = 1, and LVAR1 = 1, VAR = u_e/u_{e0}

IOPT = 2, VAR = δ^*

EL Reference length. Needed if input data lengths are nondimensionalized. If lengths are dimensional, put in EL = 1.0.

PT Total pressure, p_t (lb/ft²), (lb/in²), or (newton/m²).

TT Total temperature, T_t (°R) or (°K).

TWONTT Ratio of body surface temperature to total temperature, T_w/T_t .

VISC Constant λ in Sutherlands formula for viscosity.

$$\mu = \lambda \frac{T^{3/2}}{T + T_s}$$

If one of the programmed values is acceptable, put in a value of 0.0. The value used will then be determined by the value of IUNIT on item number 3 as follows:

IUNIT	VISC
1	$2.27(10^{-8}) \text{ lb sec/ft}^2 (\text{°R})^{1/2}$
2	$1.5764(10^{-10}) \text{ lb sec/in}^2 (\text{°R})^{1/2}$
3	$1.4582(10^{-6}) \text{ Newton sec/m}^2 (\text{°K})^{1/2}$

RGAS Gas constant. If one of the programmed values is acceptable, put in a value of 0.0. The value used will be determined by the value of IUNIT as follows:

IUNIT	RGAS
1	$1716.0 \text{ ft}^2/\text{sec}^2 \text{ °R}$
2	$247104.0 \text{ in}^2/\text{sec}^2 \text{ °R}$
3	$286.96 \text{ m}^2/\text{sec}^2 \text{ °K}$

SCON Constant T_s , in Sutherlands viscosity law (see definition for VISC). If one of the programmed values is acceptable, put in a value of 0.0. The value used will be determined by the value of IUNIT as follows:

IUNIT	SCON
1	198.6 °R
2	198.6 °R
3	110.333 °K

DFACT Relaxation factor for adding δ^* to body in the $x_s-\theta_s$ iteration scheme. Usual value is 1.0. If a value of 0.0 is put in, a value of 1.0 will be used.

XZ Axial location of beginning of boundary-layer calculation.

RLEN Axial location of end of boundary-layer calculation. Usually at least one maximum diameter larger than XBT.

XT Axial location of transition from laminar to turbulent boundary-layer flow.

DXP Axial interval at which velocity profiles are to be printed. If a value of 0.0 is put in, no profiles are printed. In any case, profiles will not be printed more often than the output step size for individual output quantities (see section 9.1).

HLIM Limit value of $H_i = \delta_i^*/\theta_i$ to indicate separation as discussed in reference 5. Input of a blank or a value

of 0.0 will cause a value of 1.2 to be used. To move the value of x_s forward, decrease HLIM. To move x_s downstream, increase HLIM. A value greater than 4.0 will allow the calculation to proceed to a separation singularity if one should occur. The calculation will terminate at that point. See section 5 for a discussion of the use of HLIM in sample calculations.

CFC1	Value of skin-friction coefficient at initial boundary-layer station (see section 8.4).
DELTA1	Value of boundary-layer thickness, δ (compressible), at initial boundary-layer station (see section 8.4).
DELST1	Value of boundary-layer displacement thickness, δ^* , at initial boundary-layer station (see section 8.4).
UE1	Value of boundary-layer-edge velocity u_e at initial boundary-layer station.
DUEDX	Value of boundary-layer-edge velocity gradient at initial boundary-layer station.
NR	Integer number of values of XRP and RL to be input for body shape. If NSHPBL = 0, this is assumed to be the same as IXY. Maximum value is 200.
XRP,RL	Axial and radial coordinates of body shape for boundary-layer calculation. If LSHPBL = 0, these are assumed to be the same as XO and YO, respectively. For two-dimensional configurations, these represent the x and y coordinates of a surface measured from a reference plane.

8. PROGRAM OPTIONS

Several optional modes of calculation are available through the input parameters. A description of the options and the corresponding values of the pertinent parameters follows.

8.1 BOUNDARY-LAYER OPTION

To use only the boundary-layer program, put in the three card description, then all values on the fourth input data card, Item 2 in Table II, should be zero. Then the first value on the fifth input data card should be:

LPROG=1 (see Table II, Item 3)

Of the remaining variables shown on item number 3 in Table II, only IUNIT is required. The remaining cards would be those corresponding to item 4 and items 13 to 21 as described in Table II. With this option, the user has the choice of specifying either the free-stream velocity, u_e , or the displacement thickness, δ^* , through the variables NVAR, XVAR, and VAR on items 14 and 15. The boundary-layer calculation can be restarted at any station by inputting the value of the variables at that station as listed in the output. The calculated list of $\delta^* + r_w$ and u_e/u_{e0} will be written on Logical Unit 10 (data file 4) when the calculation terminates.

Another method is also available for calculating the boundary layer alone. The boundary-layer step of a viscid-inviscid iteration can be executed separately. The appropriate values on the fifth card would be:

```
LPROG = 0
  N1 = 1
  N2 = 21
  IBL = 0
  IUNIT = 1, 2, or 3
```

This option requires LITER = TRUE and input of all other quantities as though the iterative sequence were to be completed. With the values just described, only the boundary layer will be calculated and then the run will be terminated. If it is desired to continue the iteration, simply make N2 less than 21. The free-stream velocity distribution must be provided on Logical Unit 12 for this case. All other optional inputs are the user's choice.

8.2 INVISCID-FLOW OPTION

To use only the inviscid-flow program, put in the three card description, then all values on the fourth card should be zero. Then put in LPROG = -1 on the fifth card (item number 3 in Table II). Of the remaining values on that card, only IUNIT is required and that quantity is required only if PLUMIN is TRUE. After the first five cards only the data for items 4 to 9 or 10 as described in Table II and section 7.2 are required for this option.

8.3 VISCID-INVISCID ITERATION OPTION

To use both the boundary-layer and the inviscid-flow programs iteratively, put in LPROG = 0 and all other quantities as

appropriate. Such iterations can be started with only the body shape and free-stream flow quantities known. The $x_s-\theta_s$ iteration procedure (LITER = TRUE) may be restarted to continue a prematurely terminated iteration. Several options are available to the user for restarting an unfinished iteration. See section 11.2 for an example of restarting. The simplest option is to put in NRSTRT = 1 as the first value on the fourth input data card and to provide the required input data files on Logical Units 11, 12, 13, 14, and 15 (see fig. 12 and Table I). The only other data required for restarting are the three-card description of the case. The calculation then proceeds from where the previous iteration stopped. Another method of restarting, which is valid for all iteration procedures, would be to omit the restart file and put in NRSTRT = 0. The user can then vary any of the other input quantities, using the data files or punched cards as desired. Note that the $x_s-\theta_s$ calculation terminates when N2 reaches a value of 21. The value of N1 increases continuously throughout the calculation while the value of N2 is reset to 1 each time the $x_s-\theta_s$ cycle finds a minimum error without satisfying the convergence criterion.

8.4 BOUNDARY-LAYER INITIAL CONDITIONS

Initial values of boundary-layer quantities can be obtained in several ways. The user can obtain values of the skin-friction coefficient, C_f , and either the boundary-layer thickness, δ , or the displacement thickness, δ^* . These are shown on item 18 in Table II. The appropriate values LSHAPE = 0 and LIC = 1 or 2 are punched on the card corresponding to item 13. For the case when no other source of this information is available, formulas have been included in the program based on the Blasius solution for laminar boundary layers and based on one-seventh power law velocity profiles for turbulent flows. These formulas are only available if u_e is being specified (IOPT = 1). The basic formulas calculate C_f and δ in the transform plane (incompressible, two-dimensional). The formulas are as follows:

Laminar Flow

$$C_{f_i} = \frac{0.664}{\sqrt{\frac{U_e}{\nu_{e_0}} x}} \quad (26)$$

$$\delta_i = \frac{5x}{\sqrt{\frac{U_e}{\nu_{e_0}} x}} \quad (27)$$

Turbulent Flow

$$C_{f_i} = 0.0592 \left(\frac{U_e}{v_{e_o}} x \right)^{-0.2} \quad (28)$$

$$\epsilon_i = 0.37 x \left(\frac{U_e}{v_{e_o}} x \right)^{-0.2} \quad (29)$$

These formulas provide initial values for boundary layers on flat plates. They are chosen by inputting LSHAPE = 1. For other geometries, the value of the x coordinate is transformed. Thus, LSHAPE = 2 chooses the values for a circular cylinder where

$$x = \frac{r_w^2}{x_a} \quad (30)$$

where x_a is the axial coordinate and LSHAPE = 3 chooses the values for a cone, where

$$x = \frac{1}{3} \left(\frac{r_w^2}{x_a} \right) \quad (31)$$

These formulas have been found to be quite adequate for calculating flows over long bodies. Small initial errors in the calculated boundary layer become negligible in a few boundary-layer thicknesses.

8.5 OPTIONS FOR DETERMINING THE SEPARATION POINT

The logical variables LSEP, LNSHK, and LITER and the input quantity HLIM are used to select a particular method of specifying x_s . The options are summarized as follows:

<u>LSEP</u>	<u>LITER</u>	<u>LNSHK</u>	<u>Instructions</u>	<u>Calculation Mode</u>
T	T	-	input x_s	$x_s - \theta_s$
F	T	-	input HLIM	$x_s - \theta_s$
T	F	T	input x_s	δ^* -update
F	F	T	input HLIM	δ^* -update
T	F	F	input x_s	shock
F	F	F	x_s from 1st inviscid solution	shock

The entire $x_s - \theta_s$ iteration procedure is a prediction method for x_s . The options which require input of x_s or HLIM for that mode are used to obtain a first approximation for starting the $x_s - \theta_s$ iteration. In addition, those options can be used with the δ^* -update procedure to provide a fixed value of x_s . Shock separated cases have the two options discussed in section 3.

9. PROGRAM OUTPUT

9.1 STANDARD OUTPUT

The complete program output is presented in the following list. Options for reducing the amount of printed output as discussed in reference 5 for the previous version of the program have been omitted from the present version of the program.

1. Three-line title or discription
2. List of all values of integers on first and second data cards
3. List of body geometry input
4. List of other input values for inviscid flow
5. List of input indices for boundary-layer calculation
6. List of body shape data for boundary layer
7. List of other boundary-layer input quantities

8. Plume velocity and shape distributions. These lists are printed at the beginning and after the 4th iteration.
9. Computed geometric parameters in normal direction for inviscid flow
 - J - normal grid index
 - AN - normal coordinate
 - G - stretching function derivatives (refs. 7 and 8)
 - GH - stretching function derivatives at half intervals
10. Computed geometric parameters in tangential direction
 - I - tangential grid index
 - S - arc length along reference surface
 - X - axial coordinate
 - Y - radial coordinate
 - THET - angle of reference coordinate surface, θ . For closed bodies, θ is the same as the body angle, θ_B . For open bodies, $\theta = \theta_B$ on the forebody and $\theta = 0$ on the afterbody.
 - THETB - body angle, θ_B .
 - AK - surface curvature on closed bodies. For open bodies AK is the surface curvature on the forebody and $AK = -(d^2r_w/dx^2)$ on the afterbody.
 - F - derivative of the tangential stretch function (refs. 7 and 8)
11. Inviscid relaxation iteration history
 - IT - iteration number
 - DPMAX - maximum ϕ correction, $\max_{ij} |\phi_{ij}^{IT} - \phi_{ij}^{IT-1}|$
 - ID,JD - I and J location of DPMAX
 - RMAX - maximum residual, $\max_{ij} |R_{ij}|$, where R_{ij} is the right-hand side of the difference equation

- IR,JR - I and J location of RMAX
- ISUB,ISUP - indicates if maximum residual occurred at a subsonic or supersonic point
- RAVG - average value of the residual
- RF1 - relaxation factor for subsonic points
- QF3 - relaxation factor for supersonic points
- NS - number of supersonic points
- SEC/CY - time for iteration cycle
12. Tabulated values of surface pressure coefficient, C_p , Mach number, and axial velocity on the body along with a rough plot of C_p along the body. This plot is distorted in the axial direction because it is for equal spacing in the computational space. The asterisks show the level of sonic C_p . The inviscid velocity distribution is used to calculate C_p unless otherwise indicated. For example, the label "(AVERAGE OF INVISCID AND VISCOUS SOLUTIONS)" indicates that C_p is derived from $1/2(u_{eV} + u_{eI})$.
13. Drag coefficients by trapezoidal integration of the C_p 's on the real body. The displacement surface is removed for calculation of the drag.
14. Coordinates x and y of the sonic line
15. Boundary-layer reference velocity, u_{e0} , unit Reynolds number, Re_0/L and viscosity, ν_{e0} . This is only printed on the first step (N1 = 1).
16. List of boundary-layer quantities with profiles at intervals governed by DXP.
- X - axial distance from the nose, x
- UTAU - friction velocity, u_τ
- UE/UZ - boundary-layer-edge velocity ratio, u_e/u_{e0}
- DSTPR - augmented body radius, $\delta^* + r_w$
- HTR - transformed shape factor, δ_i^*/θ_i

DELTA	- boundary-layer thickness, δ
DELST	- displacement thickness, δ^*
THETA	- momentum thickness, θ
CF	- skin friction coefficient, C_f
DELI	- tranformed boundary-layer thickness, δ_i
DUEDX	- boundary-layer-edge velocity gradient, du_e/dx
RW	- body radius, r_w

17. Quantities showing status of iteration

XMAX	- location of maximum difference between u_{eV} and u_{eI}
UECHK	- maximum value of $(u_{eV} - u_{eI})/u_e$ (percent)
DRMS	- value of rms error (percent)

These quantities are printed each cycle during the iteration procedures described in section 2 and 3 of this report

18. Quantities showing status of x_s - θ_s iteration when the procedure described in reference 5 is being used to calculate x_s and θ_s (LITER = TRUE). The following status quantities are printed each time the boundary-layer, inviscid-flow iteration sequence converges.

XSEP	- the current value of x_s
DTHET	- the current value of θ_s
DRMS	- the current value of the rms error (percent)

If the calculation proceeds to a normal completion, a message will be printed indicating the iteration number at which the minimum error occurred and the value of other pertinent parameters for that iteration. The drag value and inviscid flow and boundary-layer data representing the solution will be found in the output list under the indicated iteration number.

9.2 SPECIAL OUTPUT MESSAGES

Several special messages are contained in the output to call attention to specific conditions that may occur. The messages are listed in this section with instructions about what to do when they are encountered.

(1) -----DIVERGENCE.RMAX EXCEEDS RCHEK,-----

This message is printed by the inviscid-flow program if the relaxation procedure diverges. Check all input to verify that it is correct. If no obvious errors appear, the difficulty is probably either in the choice of parameters for the computational mesh, or the smoothness of the data defining the body shape.

(2) RFL DECREASED TO ____ BECAUSE 10-CYCLE AVG FOR RMAX INCREASED.

This message refers to the subsonic relaxation factor in the inviscid-flow program. The initial value is 1.4. The value is automatically reduced by 10 percent if: (1) the maximum residual, averaged over 10 cycles, is greater than that for the previous 10 cycles, and (2) the last maximum residual occurred at a subsonic point.

(3) QF3 INCREASED TO ____ BECAUSE 10-CYCLE AVG FOR RMAX INCREASED.

This message refers to the supersonic damping factor in the inviscid-flow program. The initial value is 0.1. The value is automatically increased if: (1) the maximum correction, averaged over 10 cycles, is greater than that for the previous 10 cycles, and (2) the last maximum residual is at a supersonic point.

(4) INPUT FROM TAPE13 HAS INCOMPATIBLE DIMENSIONS

This message is printed if the dimensions of the ϕ_{ij} solution read from Logical Unit 13 (data file 2 in figure 12) are not the same as the values of IMAX and JMAX put on item number 7 in Table II.

(5) METHOD FOR CALCULATING UTAU IN DERIV DOES NOT CONVERGE

This message refers to the iteration used to solve for U_τ when β^* is prescribed in the boundary-layer calculation. The only known cause of the iteration failing to converge is an error in the input data (see ref. 5 for details).

(6) DELTA1 HAS BECOME NEGATIVE STOP INTEGRATION, PRINT PROFILE AT PREVIOUS STEP

This message refers to the transformed boundary-layer thickness, δ_i . The error condition may occur due to the initial integration step size DXZ being too large. Another possible cause might be a too sudden change in the body shape, or in the prescribed u_e or δ^* distribution.

- (7) DELTA HAS BECOME NEGATIVE
STOP INTEGRATION, PRINT VALUES AT PREVIOUS STEP

This message is not expected to occur in the finished program. If it does, check the input data carefully.

- (8) METHOD FOR CALCULATING INITIAL VALUE OF DELI DOES NOT CONVERGE

When initial values of C_f , δ , or δ^* are known, the calculation must solve an integral equation for the initial value of the tranformed thickness, δ_i . This is done by iteration in a similar manner as for U_t described in message (5). If the iteration does not converge, it is usually due to errors in the input quantities.

- (9) RESULTS OF ITERATION

This message is printed at the end of each step of the x_s - θ_s cycle. It is followed by the current value of x_s , XSEP, the current value of θ_s , DTHET, and the value of the rms error, DRMS.

- (10) ***FINAL RESULTS***
BEST SOLUTION WAS ITERATION NO. ____

This message is printed whenever the smallest root-mean-squared error has been found.

- (11) SKIN FRICTION HAS BECOME NEGATIVE IN AN INCORRECT MANNER.
CHECK ALL INPUT CAREFULLY

This message will be printed if the skin-friction coefficient changes sign. It may indicate that the initial estimate of the separation point location was too far downstream. It has usually been observed to occur when strong shocks are present, or when too few relaxation steps, MIT were used initially.

- (12) ATTACHED BOUNDARY LAYER SOLUTION TERMINATED AFTER ____
ITERATIONS

This message will be printed if the viscous-inviscid interaction converges and no separation occurred or the separation point for the next iteration would have been downstream of the end of the body.

10. PROGRAM OPERATING PROCEDURE

In this section, the construction of card decks for operation of the computer programs is described. First, a general description of the operations required is given. Then the specific Job Control cards needed for operation on an IBM 370 computer are listed. The same card decks should be applicable at any 370 installation with minor modifications.

10.1 GENERAL JOB CONTROL SEQUENCE

The following list is the general Job Control procedure that would be required to run the programs for a complete viscid-inviscid interaction calculation. The reader is referred to figure 16 and Table I.

1. Create partitioned data sets for restart files (files 1-5 in fig. 12).
2. Define units 2, 3, 8, 9, and 10. These unit numbers are needed for output.
3. Define units 11, 12, 13, 14, and 15 if NRSTRT = 1 in the input data. These unit numbers correspond to the input files. They contain data created in a previous run.

For starting an initial calculation, the partitioned data sets would be created in a separate operation. Then, since no data would be on file, only units 2, 3, 8, 9, and 10 need to be defined. For restarting an iterative calculation, all data files would exist, so units 11 to 15 must also be defined.

To execute the boundary-layer program alone, unit 10 must be defined in order to output the $\delta^* + r_w$ and u_e/u_{e0} list. Unit 12 must be defined when LVAR1 = 2, and unit 15 must be defined when LDSTAR = 1.

To execute the inviscid program alone, units 2 and 8 must be defined. Unit 13 is also required when LREADP = 1, and unit 14 is required when IXY = 0.

10.2 JOB CONTROL EXAMPLES

In this section, specific examples of Job Control cards used for the operations discussed previously are presented. In the examples, the computer program is referred to as "ITER" with

the source code names "SITER" and the load module or binary version named "BITER". The account ID used in the examples is WYL.XM.K01. Logical units 5 and 6 are the standard input/output file numbers. It is not necessary to specifically define these unit numbers in the JCL deck. An estimated core memory size of 256K will be adequate for all cases except when the restart procedure is being used. Then the estimate should be increased to 512K.

10.2.1 Creating Partitioned Data Sets

Partitioned data sets for use as input/output disk files must be created before the normal program operation can proceed. The following procedure is suggested:

Use IBM Utility Program IEFBR14.

Use default values for DCB (DSORG=PO,RECFM=VS).

On 3330 disk, use SPACE in tracks as follows (refer to fig. 12 and Table I for explanation of file numbers):

VELBOD (File 3)	SPACE = (TRK,(2,1,10))
RESTRT (File 5)	SPACE = (TRK,(10,2,10))
PHI (File 2)	SPACE = (TRK,(20,4,10))
XOFILE (File 1)	SPACE = (TRK,(4,1,10))
DSFILE (File 4)	SPACE = (TRK,(6,1,10))

Example of creating a partitioned data set called VELBOD:

```
//EXEC PGM=IEFBR14
//A DD DSN=WYL.XM.K01.VELBOD,VOL=volume,
//    UNIT=3330,DISP=(,CATLG),
//    SPACE=(TRK,(2,1,10))
```

10.2.2 Starting an Iteration Sequence

To start an iteration sequence, unit numbers, 2, 3, 8, 9, and 10 must be defined. When LITER = TRUE in the input data set, the following sequence of cards should be used:

```

// EXEC PORTGO,PROG=ITER,VOL=volume
//      LIB='WYL.XM.K01.BITER'
//GO.FT02F001 DD DSN=WYL.XM.K01.VELBOD(RUN1),
//      DISP=OLD
//GO.FT03F001 DD DSN=WYL.XM.K01.RESTRT(RUN1),
//      DISP=OLD
//GO.FT08F001 DD DSN=WYL.XM.K01.PHI(RUN1),
//      DISP=OLD
//GO.FT09F001 DD DSN=WYL.XM.K01.XOFILE(RUN1),
//      DISP=OLD
//GO.FT10F001 DD DSN=WYL.XM.K01.DSFILE(RUN1),
//      DISP=OLD
//GO.SYSIN DD *
      {
        Input data cards
      }
/*

```

In the example presented in section 11.1, LITER = FALSE and the restart procedure is not available. However, the JCL cards corresponding to unit numbers 2, 3, 8, 9, and 10 must still be defined as follows:

```

//GO.FT02F001 DD DUMMY
//GO.FT03F001 DD DUMMY
//GO.FT08F001 DD DUMMY
//GO.FT09F001 DD DUMMY
//GO.FT10F001 DD DUMMY

```

10.2.3 Restarting an Iteration Sequence

The specific cards used to perform a restart of the calculation started in the previous section (when LITER = TRUE) are:

```

// EXEC FORTGO,PROG=ITER,VOL=volume,
//      LIB='WYL.XM.K01BITER'
//GO.FT02F001 DD DSN=WYL.XM.K01.VELBOD(RUN2),
//      DISP=OLD
//GO.FT03F001 DD DSN=WYL.XM.K01.RESTRT(RUN2),
//      DISP=OLD
//GO.FT08F001 DD DSN=WYL.XM.K01.PHI(RUN2),
//      DISP=OLD
//GO.FT09F001 DD DSN=WYL.XM.K01.XOFILE(RUN2),
//      DISP=OLD
//GO.FT10F001 DD DSN=WYL.XM.K01.DSFILE(RUN2),
//      DISP=OLD
//GO.FT11F001 DD DSN=WYL.XM.K01.RESTRT(RUN1),
//      DISP=OLD,LABEL=(,,,IN)
//GO.FT12F001 DD DSN=WYL.XM.K01.VELBOD(RUN1),
//      DISP=OLD,LABEL=(,,,IN)
//GO.FT13F001 DD DSN=WYL.XM.K01.PHI(RUN1),
//      DISP=OLD,LABEL=(,,,IN)
//GO.FT14F001 DD DSN=WYL.XM.K01.XOFILE(RUN1),
//      DISP=OLD,LABEL=(,,,IN)
//GO.FT15F001 DD DSN=WYL.XM.K01.DSFILE(RUN1),
//      DISP=OLD,LABEL=(,,,IN)
//GO.SYSIN DD *
      {
        Input data cards
      }
/*

```

These cards were used with the example discussed in section 11.2. The input data cards required for restarting are summarized in Table III.

10.2.4 Executing the Boundary-Layer Program Alone

The specific cards used to perform the calculations discussed in section 11.3 are listed in this section. In the example shown here, all input is assumed to be from cards, but the output list of $\delta^* + r_w$ and u_e/u_{e0} is to be saved on unit 10. Unit 12 would be required for input if LVAR1 = 2, and unit 15 would be required if LDSTAR = 1. The cards used in the example in section 11.3 are:

```
// EXEC FORTGO,PROG=ITER,VOL=volume
//      LIB='SYL.XM.K01.BITER'
//GO.FT10F001 DD DSN=WYL.XM.K01.DSFILE(RUN1),
//      DISP=OLD
//GO.SYSIN DD *
```

Input data cards

/*

10.2.5 Executing the Inviscid Program Alone

The cards used to perform the calculations discussed in section 11.4 are listed in this section. In this example, the velocity potential, ϕ , is input from unit 13, and the new solution for ϕ is output on unit 8. The calculated velocity on the body is output on unit 2. Input from unit 13 corresponds to LREADP = 1 in the card input data. In addition, unit 14 would be required for input of the body shape if IXY = 0 in the card input data. The specific cards used in the example are:

```
// EXEC FORTGO,PROG=ITER,VOL=volume,
//      LIB='WYL.XM.K01.BITER'
//GO.FT02F001 DD DSN=WYL.XM.K01.VELBOD(RUN2),
//      DISP=OLD
//GO.FT08F001 DD DSN=WYL.XM.K01.PHI(RUN2),
//      DISP=OLD
//GO.FT13F001 DD DSN=WYL.XM.K01.PHI(RUN1),
//      DISP=OLD,LABEL=(,,IN)
//GO.SYSIN DD *
```

{ Input data cards

/*

11. NUMERICAL EXAMPLES

In this section, several example calculations are presented to aid in program checkout. An example is presented of a complete viscid-inviscid interaction using the δ^* -update procedure described in section 2. An example is also presented of the use of the boundary-layer program alone for a two-dimensional geometry. That example also demonstrates the two options for boundary conditions, having u_e specified in the beginning of the calculation, and δ^* specified in the second part. Input data for another sample case are also presented to demonstrate the use of the program to calculate the inviscid flow alone.

11.1 AXISYMMETRIC INTERACTION

A list of the punched card input data for a sample calculation on the boattailed body shown in figure 3a and b is presented in figure 13. The case being calculated is for a free-stream Mach number of 0.8. The body corresponds to the ogive-cylinder body with a circular-arc boattail described in reference 14. The JCL card deck for this case has been presented in section 10.2.2. The running time for the complete calculation is about 3.0 minutes on the IBM 370/165. The calculations shown were made by an IBM 3033 computer in 1.04 minutes. Small numerical differences will occur when the program is run on a different machine.

Selected output for the sample case is shown in figure 14. A total of 14 iterations were performed, with the minimum error of 0.74 percent occurring on the 13th iteration.

The complete list of output for this case consisted of a total of approximately 5000 lines. Output steps 1-7 as listed in section 9.1 have been omitted from this presentation since they simply verify the input data. The output pages shown are those corresponding to steps 8-18 of the set described in section 9.1. Finally, figure 14 concludes with the inviscid solution and boundary-layer solutions corresponding to the best result, iteration number 13, and the final page, from iteration 14 showing the final messages.

11.2 EXAMPLE OF RESTARTING AN INTERACTION CALCULATION

For a case where the $x_s-\theta_s$ iteration is being used, the calculation may terminate prematurely. The punched card input data for restarting such a case is presented in figure 15. The JCL card deck for this calculation was presented in section 10.2.3. Note that the iterative calculations cannot be restarted at any arbitrary iteration using the restart file, unit 11. That file and the other output files contain only the data that were output just prior to the termination. It will be recalled that this restart procedure is only available when the input quantity `LITER = TRUE`.

11.3 TWO-DIMENSIONAL BOUNDARY LAYER

A list of the punched card input data for a sample calculation on the two-dimensional configuration shown in figure 16 is presented in figure 17. Note that two sets of input are presented for this case, giving an example of the options of prescribed u_e and prescribed δ^* . The data for u_e and δ^* were obtained from the experimental results of reference 15 which indicate separation occurring in an adverse pressure gradient region downstream of a shock wave. The output for the complete boundary-layer calculation are presented in figure 18. No external data files were used for input for this case. The JCL card deck for this case was presented in section 10.2.4.

11.4 AXISYMMETRIC INVISCID FLOW

The punched card input data for a sample calculation of the inviscid flow alone are presented in figure 19. The output for this case is shown in figure 20.

REFERENCES

1. Presz, W. M., Jr., King, R. W., and Buteau, J. D.: An Improved Analytical Model of the Separation Region on Boat-tail Nozzles at Subsonic Speeds. NASA CR-3028, July 1978.
2. Cosner, R. R. and Bower, W. W.: A Patched Solution of the Transonic Flow Fields About an Axisymmetric Boattail. AIAA Paper No. 77-227, 15th Aerospace Sciences Meeting, Los Angeles, CA, Jan. 1977.
3. Dash, S. M. and Pergament, H. S.: A Computational Model for the Prediction of Jet Entrainment in the Vicinity of Nozzle Boattails (The BOAT code). NASA CR-3075, Aug. 1978.
4. Wilmoth, R. G., Dash, S. M., and Pergament, H. S.: A Numerical Study of Jet Entrainment Effects on the Subsonic Flow Over Nozzle Afterbodies. AIAA Paper No. 79-0135, 17th Aerospace Sciences Meeting, New Orleans, LA, Jan. 1979.
5. Kuhn, G. D.: Computer Program for Calculation of Separated Turbulent Flows on Axisymmetric Afterbodies Including Exhaust Plume Effects. AEDC TR-79-4, Mar. 1979.
6. Kuhn, G. D.: Calculation of Separated Turbulent Flows on Axisymmetric Afterbodies Including Exhaust Plume Effects. AIAA Paper No. 79-0303, 17th Aerospace Sciences Meeting, New Orleans, LA, Jan. 1979.
7. South, J. C., Jr. and Jameson, A.: Relaxation Solutions for Inviscid Axisymmetric Transonic Flow Over Blunt or Pointed Bodies. Preceedings of the AIAA Computational Fluid Dynamics Conference, Palm Springs, CA, July 19-20, 1973.
8. Keller, J. D. and South, J. C., Jr.: RAXBOD: A FORTRAN Program for Inviscid Transonic Flow Over Axisymmetric Bodies. NASA TM X-72831, Feb. 1976.
9. Abeyounis, W. K.: Boundary Layer Separation on Isolated Boattail Nozzles. NASA TP-1226, Aug. 1978.
10. Carter, J. E.: A New Boundary-Layer Inviscid Iteration Technique for Separated Flow. AIAA Paper No. 79-1450. Presented at the AIAA 4th Computational Fluid Dynamics Conference, Williamsburg, VA, July 1979.

REFERENCES (Concluded)

11. Seddon, J.: The Flow Produced by Interaction of a Turbulent Boundary Layer with a Normal Shock Wave of Strength Sufficient to Cause Separation. ARC R&M 3502, 1967.
12. Mager, A.: On the Model of the Free, Shock-Separated Turbulent Boundary Layer. J. Aero. Sci., Vol. 23, 1956, pp. 181-184.
13. Peters, C. E., Phares, W. J., and Cunningham, T. H. M.: Theoretical and Experimental Studies of Ducted Mixing and Burning of Coaxial Streams. J. Spacecraft, Vol. 6, No. 12, Dec. 1969, pp. 1435-1441.
14. Reubush, D. E.: Experimental Study of the Effectiveness of Cylindrical Plume Simulators for Predicting Jet-On Boattail Drag at Mach Numbers up to 1.3. NASA TN D-7795, Nov. 1974.
15. Alber, I. E., Bacon, J. W., Masson, B. S., and Collins, D. J.: An Experimental Investigation of Turbulent Transonic Viscous-Inviscid Interactions. AIAA Journal, Vol. 11, No. 5, 1973, pp. 620-627.

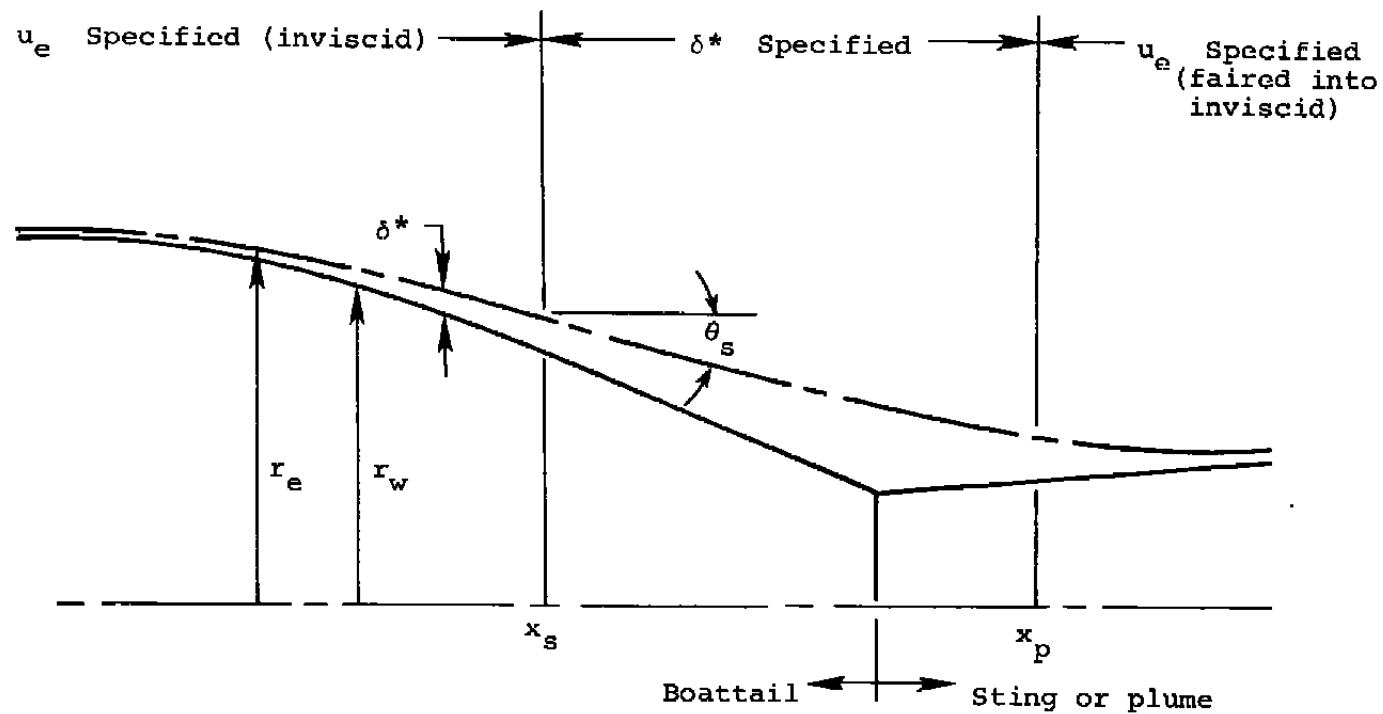


Figure 1.- Effective body shape for separated flow.

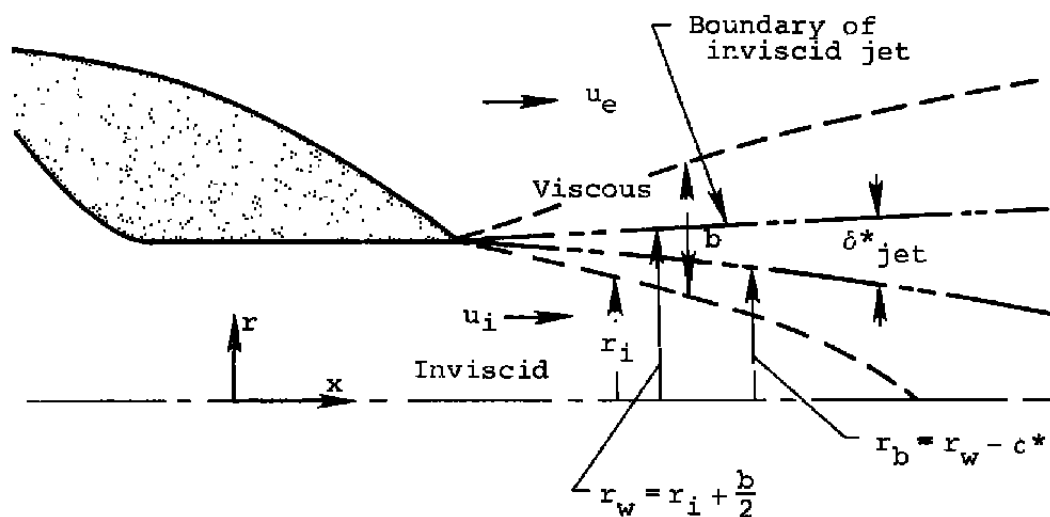
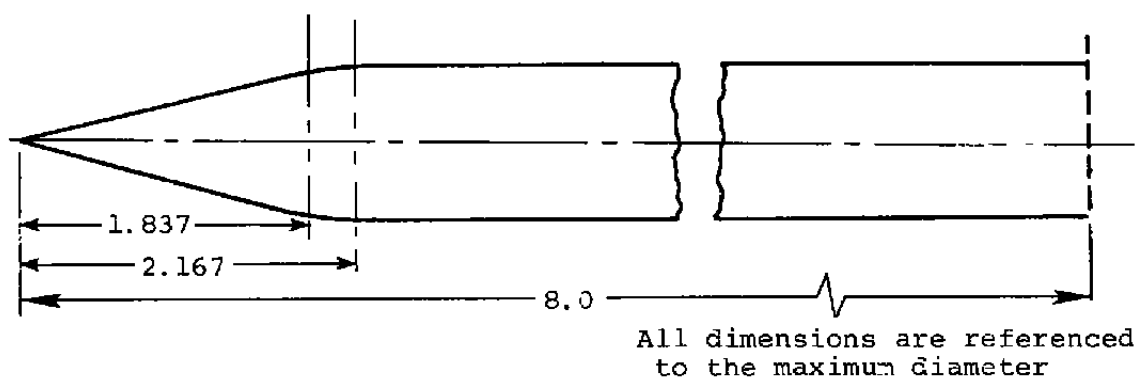
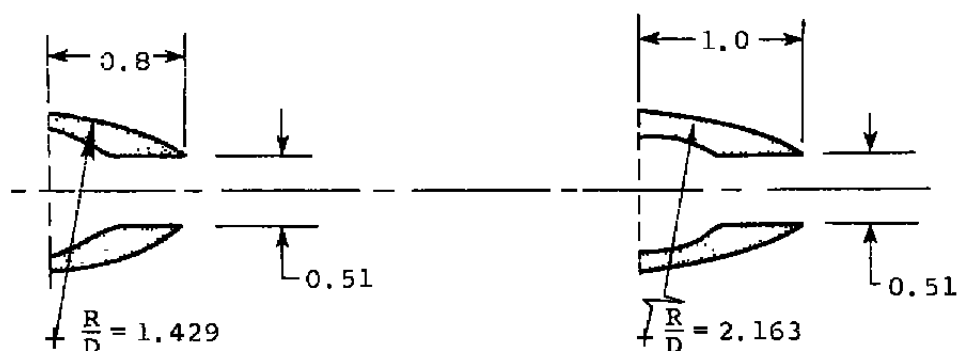


Figure 2.- Schematic of exhaust plume entrainment quantities.

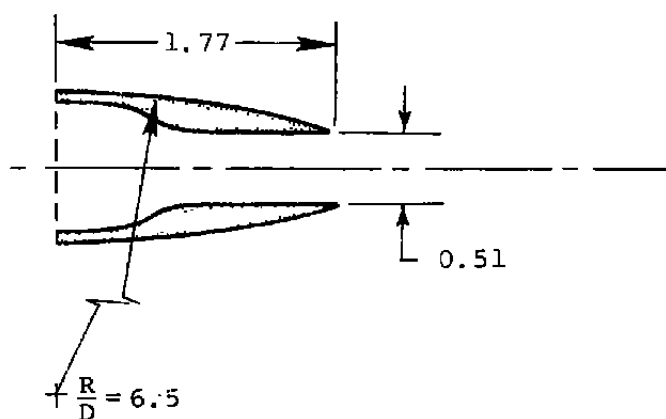


(a) Forebody.



(b) Boattail configuration 1.

(c) Boattail configuration 2.



(d) Boattail configuration 3.

Figure 3.- Body with circular arc boattail (ref. 14).

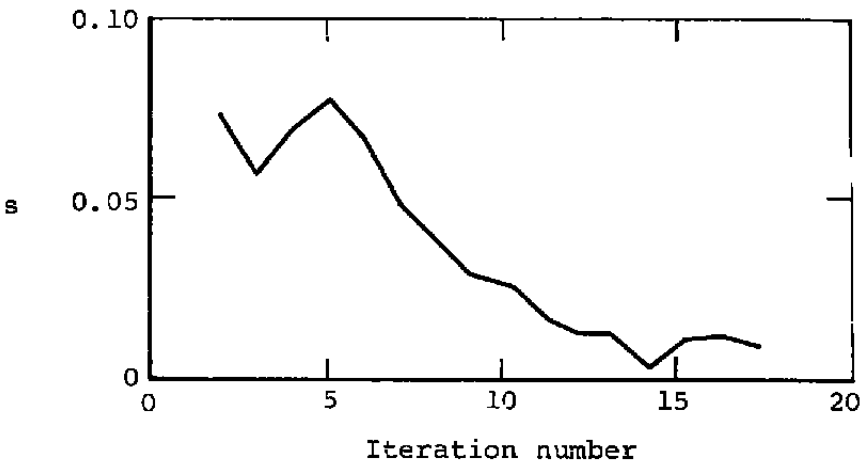


Figure 4.- Typical variation of rms error of a separated flow.

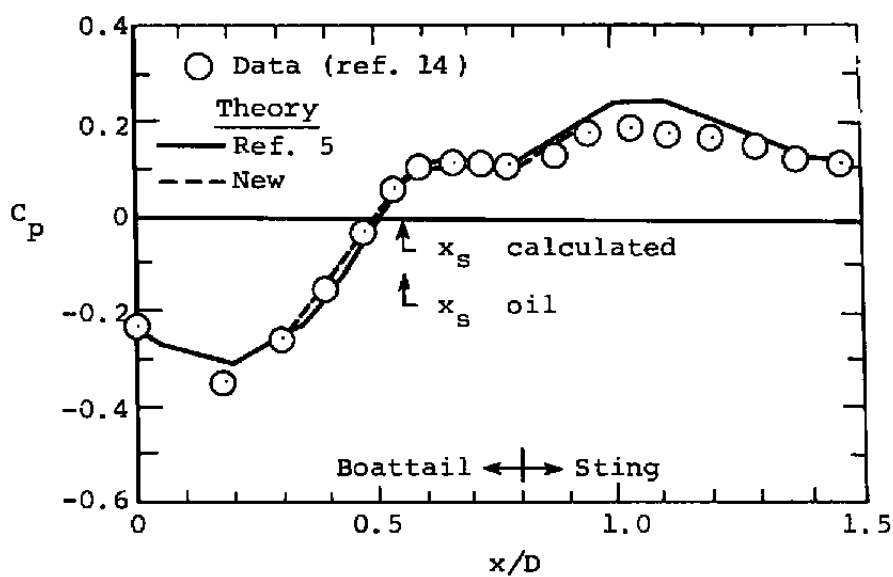


Figure 5.- Effect of new interaction model on separated flow predictions.

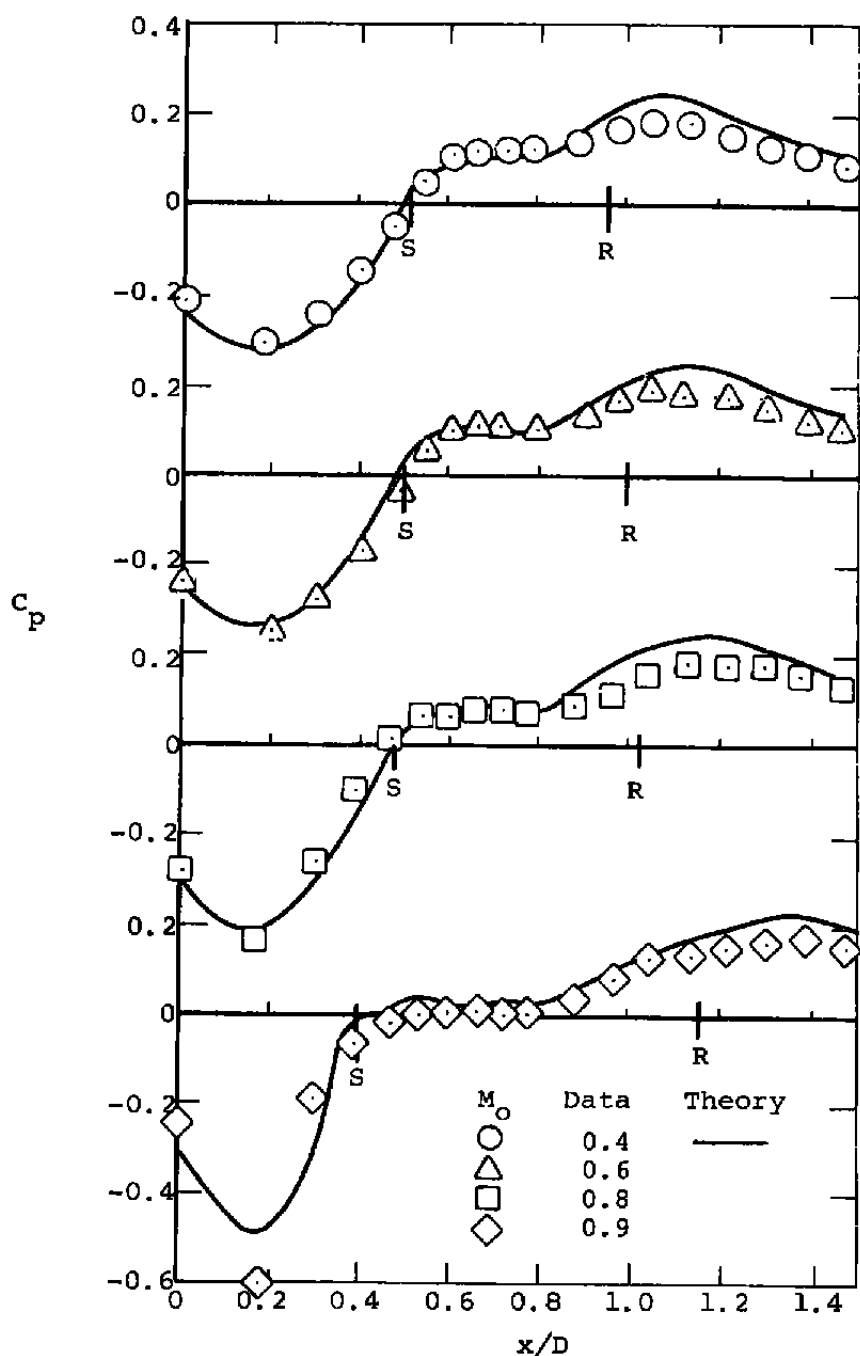


Figure 6.- Comparison of improved subsonic theory and data for a circular arc boattail with a cylindrical plume simulator (ref. 14).

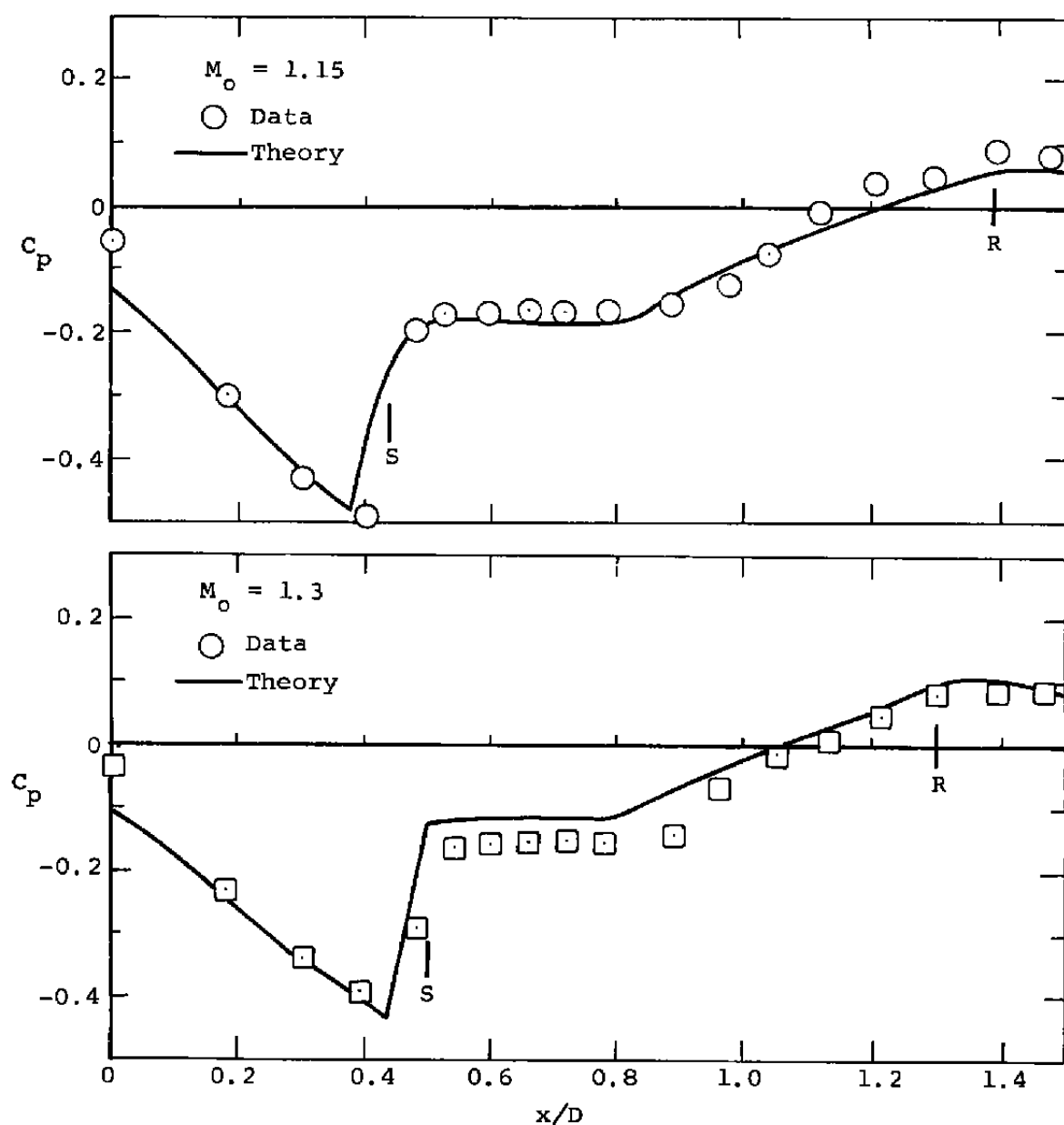


Figure 7.- Comparison of theory with data for supersonic flows.

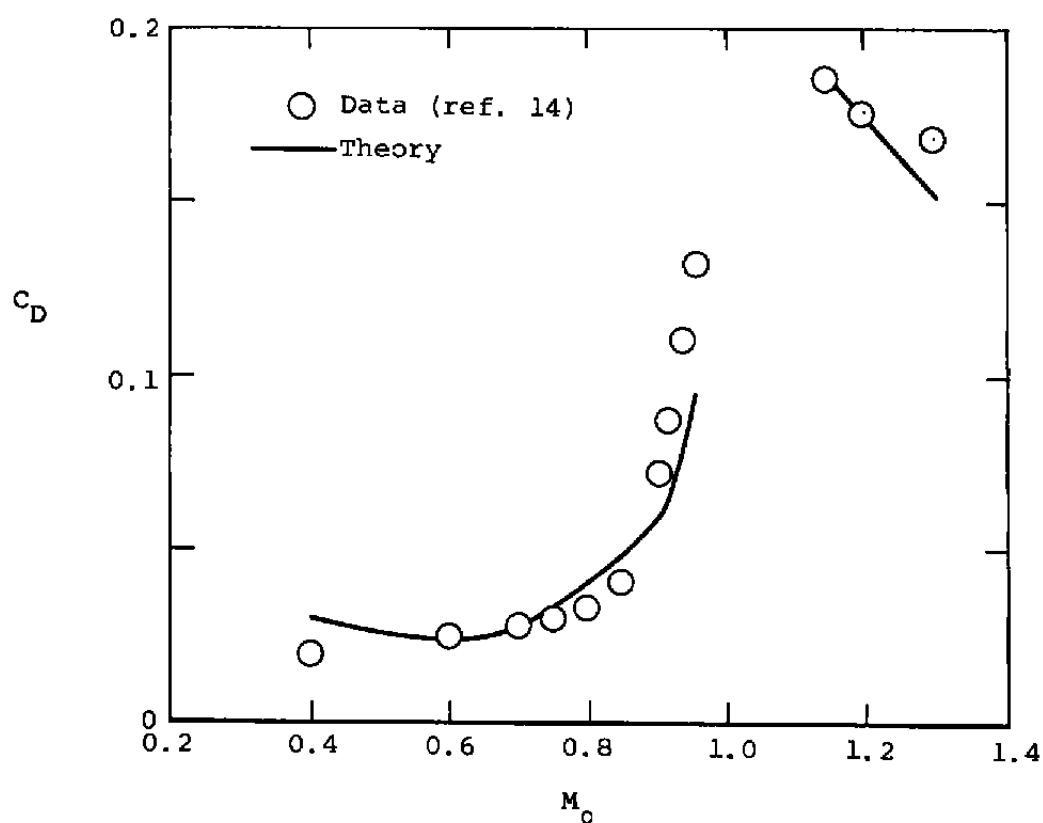


Figure 8.- Afterbody drag on a circular arc boattail with a cylindrical plume simulator.

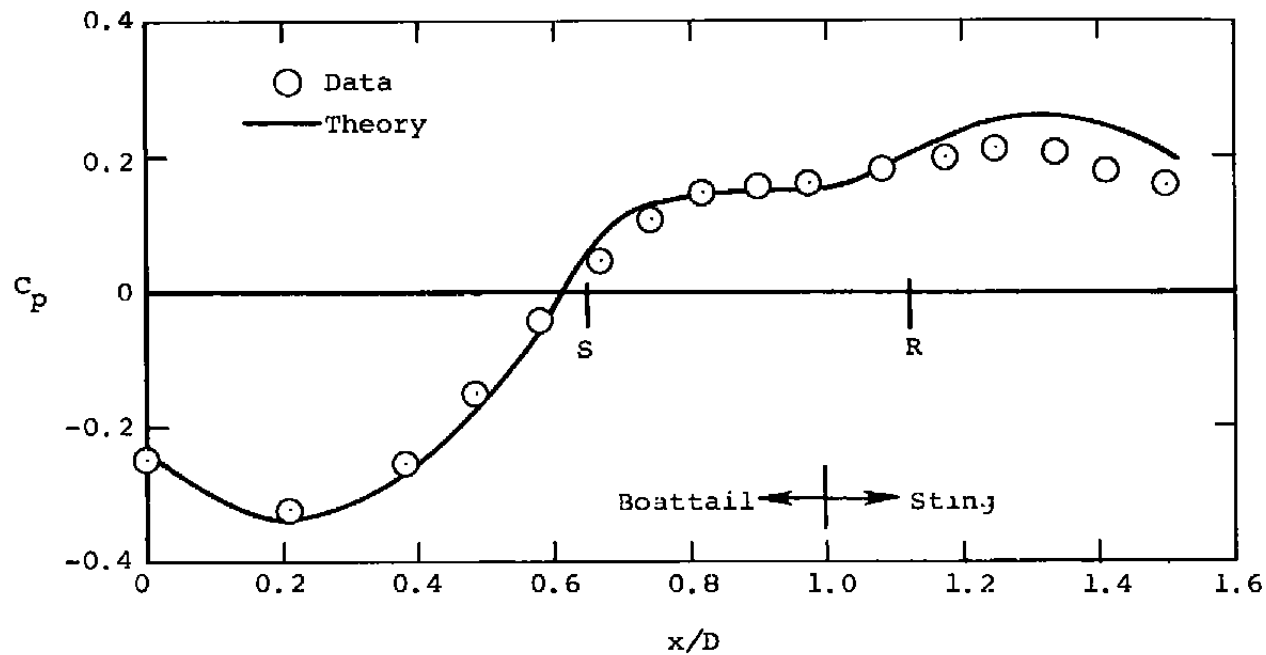


Figure 9.- Comparison between theory and data
for configuration 2; $M_o = 0.8$.

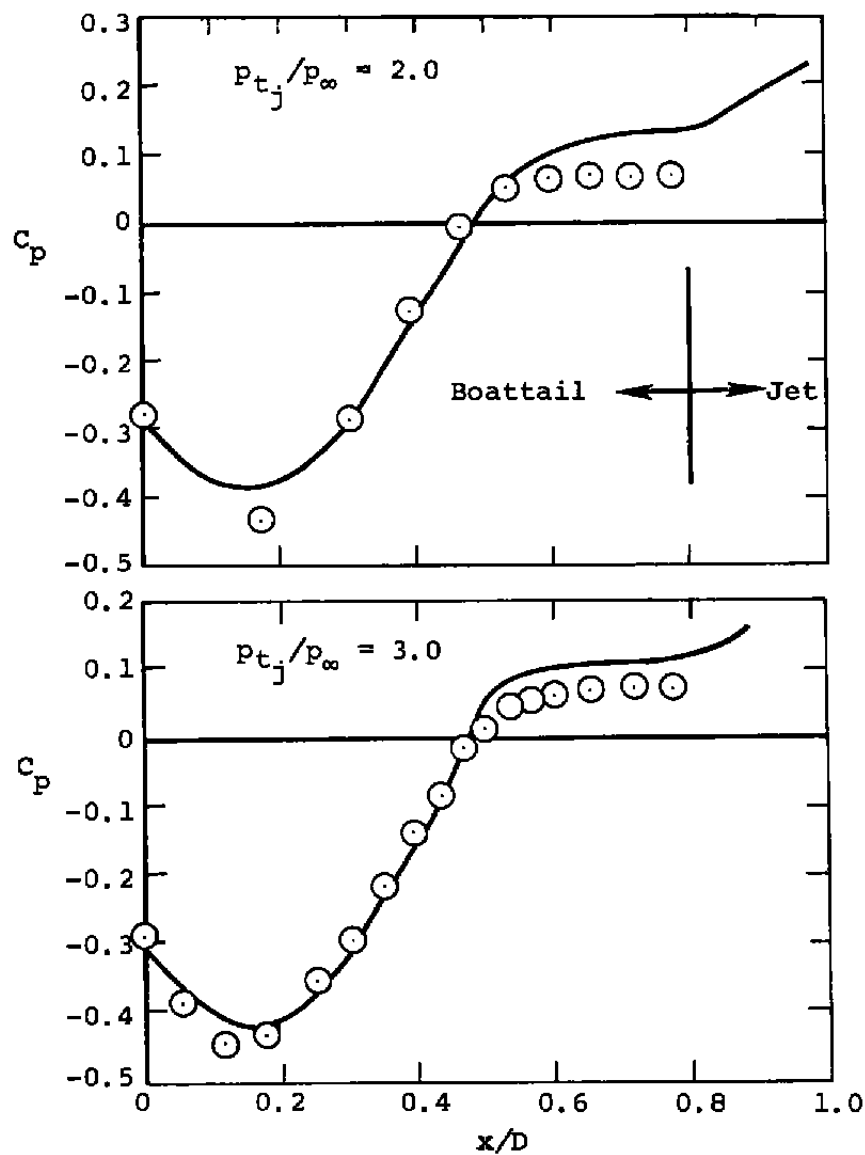


Figure 10.- Comparison between the theory and data for a boattail with a high pressure air jet; $M_o = 0.8$.

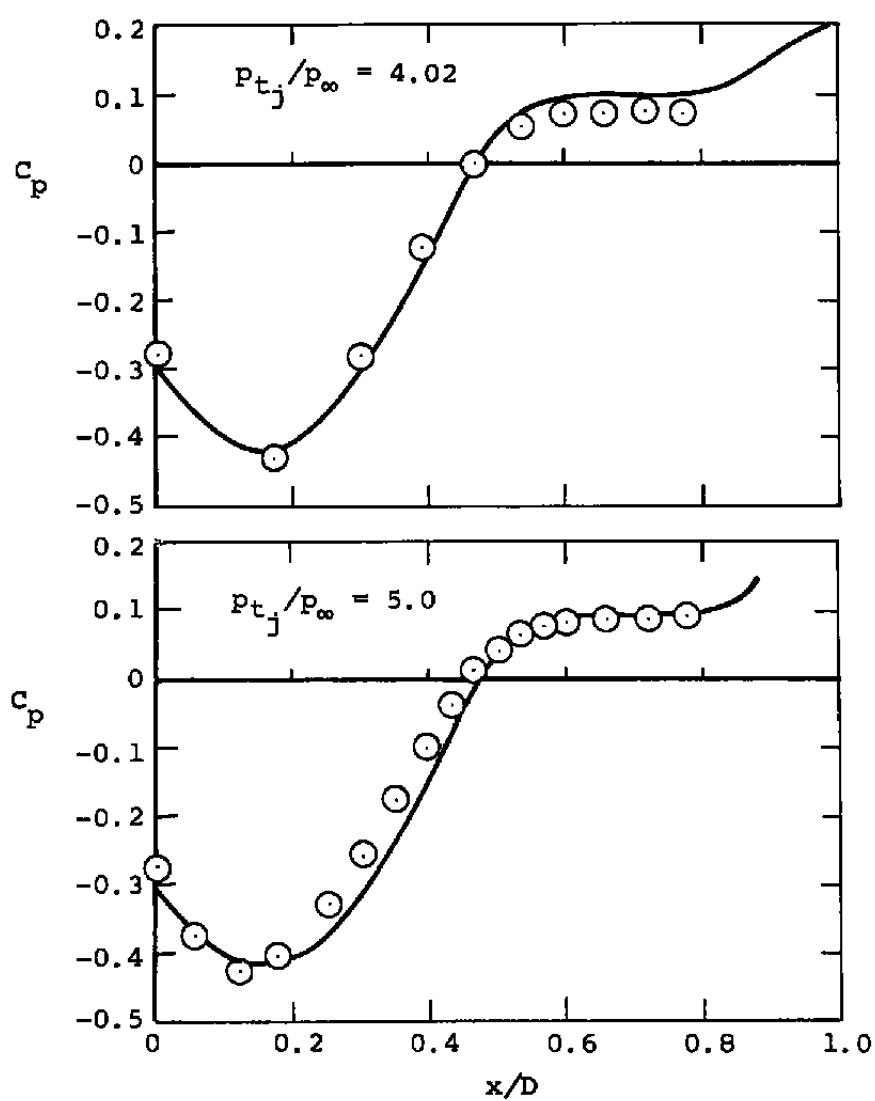


Figure 10.- Concluded.

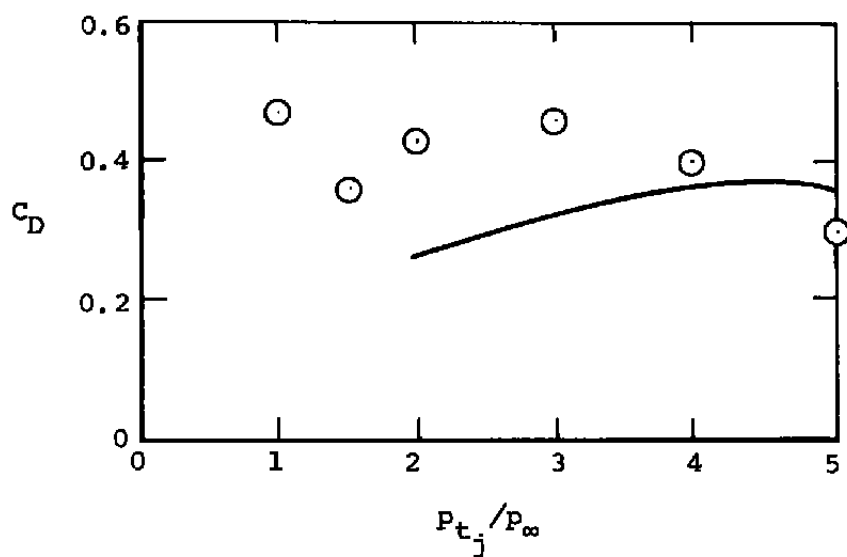


Figure 11.- Afterbody drag on a boattail with high pressure air jets.

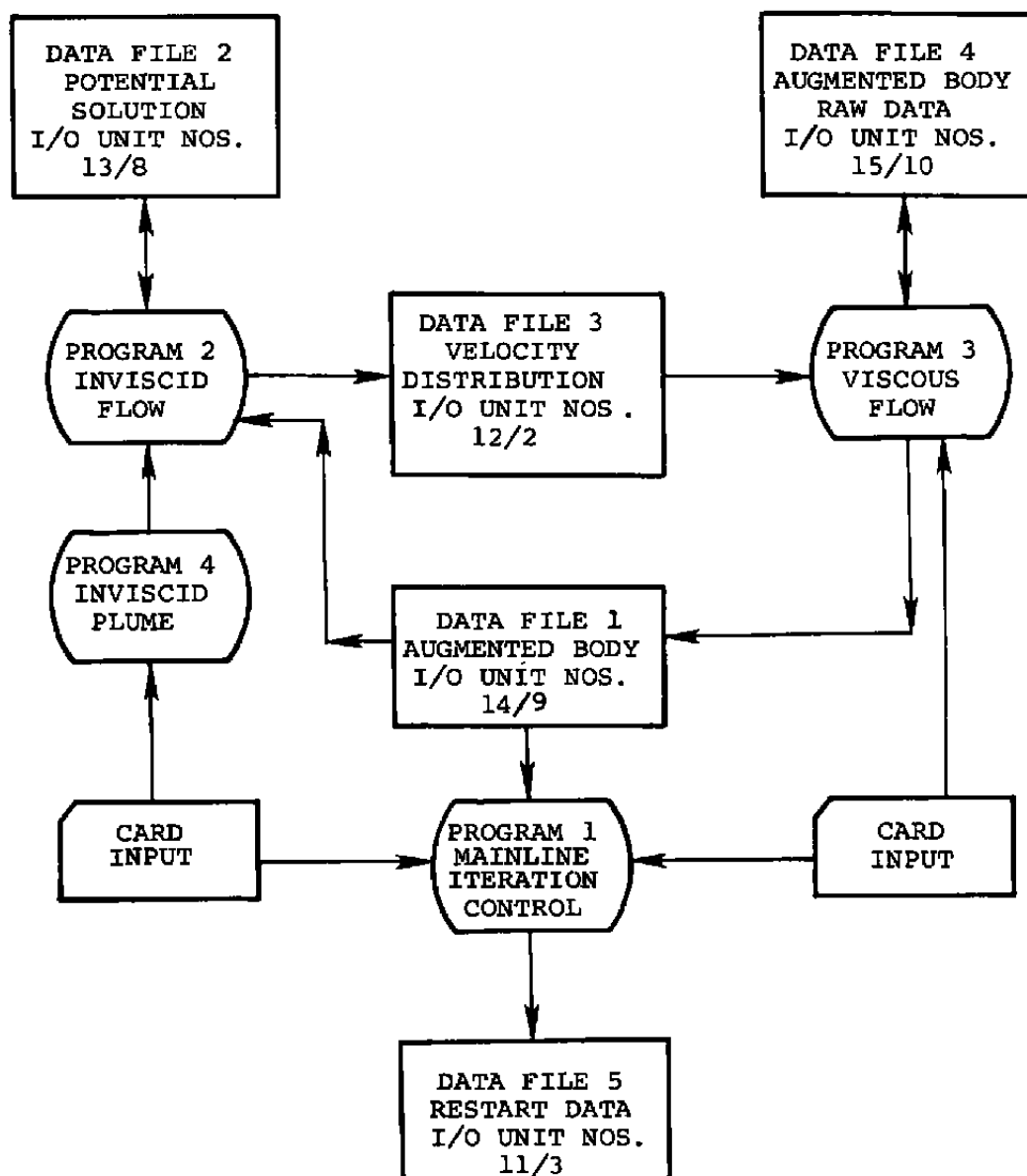


Figure 12.- General relationship of programs and data files.

NASA DATA COMPARISON - CONFIGURATION 1
 JET SIMULATED WITH HIGH PRESSURE AIR
 BOATTAIL L/D = 0.8 DE/D = 0.51

0	0	700			
0	1	1	1	1	0
1.4		0.8			
98					
0.0		0.0			
0.1		0.025013			
0.2		0.050026			
0.3		0.075038			
0.4		0.100051			
0.5		0.125064			
0.6		0.150077			
0.7		0.175090			
0.8		0.200102			
0.9		0.225115			
1.0		0.250128			
1.1		0.275141			
1.2		0.300154			
1.3		0.325166			
1.4		0.350179			
1.5		0.375192			
1.6		0.400205			
1.7		0.425218			
1.8		0.450230			
1.9		0.473630			
2.0		0.489760			
2.1		0.498366			
2.2		0.500000			
2.3		0.500000			
2.5		0.500000			
3.0		0.500000			
3.5		0.500000			
4.0		0.500000			
5.0		0.500000			
6.0		0.500000			
7.0		0.500000			
7.5		0.500000			
8.0		0.500000			
8.025		0.499781			
8.05		0.499125			
8.075		0.498030			
8.1		0.496496			
8.125		0.494521			
8.15		0.492104			
8.175		0.489241			
8.2		0.485931			
8.225		0.482171			

(a) First 49 cards.

Figure 13.- Input data for viscous-inviscid interaction calculation.

8.25	0.477956
8.275	0.473282
8.3	0.468146
8.325	0.462542
8.35	0.456463
8.375	0.449905
8.4	0.442859
8.425	0.435319
8.45	0.427277
8.475	0.418722
8.5	0.409646
8.525	0.400037
8.55	0.389885
8.575	0.379176
8.6	0.367897
8.625	0.356032
8.65	0.343565
8.675	0.330479
8.7	0.316753
8.725	0.302368
8.75	0.287298
8.775	0.271518
8.8	0.255000
8.81	0.255000
8.82	0.255000
8.83	0.255000
8.84	0.255000
8.85	0.255000
8.86	0.255000
8.87	0.255000
8.88	0.255000
8.89	0.255000
8.9	0.255000
8.92	0.255000
8.94	0.255000
8.96	0.255000
8.98	0.255000
9.0	0.255000
9.025	0.255000
9.05	0.255000
9.075	0.255000
9.1	0.255000
9.15	0.255000
9.2	0.255000
9.3	0.255000
9.4	0.255000
9.5	0.255000
9.7	0.255000
9.9	0.255000

(b) Next 49 cards.

Figure 13.- Continued.

10.1		0.255000						
10.3		0.255000						
10.5		0.255000						
10.8		0.255000						
11.2		0.255000						
11.6		0.255000						
12.0		0.255000						
81	31	0	0	0				
0.0		0.70		8.5	0.05	8.8	1.0	8.0
T								
1.4		2.1		1.01	0.0	537.9	1.0	
F	F	T						
1	1	2	3	1	0			
0.5		2134.1		577.8	0.97			
0.15		10.0		0.166667	0.0	1.2		

(c) Remaining 15 cards.

Figure 13.- Concluded.

INITIAL VALUES FOR PLUME

K	A(1,K)	A(2,K)	A(3,K)	A(4,K)
1	8.8000	0.2550	0.5221	0.0
2	8.8000	0.2422	0.5221	0.0
3	8.8000	0.2295	0.5221	0.0
4	8.8000	0.2167	0.5221	0.0
5	8.8000	0.2040	0.5221	0.0
6	8.8000	0.1912	0.5221	0.0
7	8.8000	0.1785	0.5221	0.0
8	8.8000	0.1657	0.5221	0.0
9	8.8000	0.1530	0.5221	0.0
10	8.8000	0.1402	0.5221	0.0
11	8.8000	0.1275	0.5221	0.0
12	8.8000	0.1147	0.5221	0.0
13	8.8000	0.1020	0.5221	0.0
14	8.8000	0.0892	0.5221	0.0
15	8.8000	0.0765	0.5221	0.0
16	8.8000	0.0637	0.5221	0.0
17	8.8000	0.0510	0.5221	0.0
18	8.8000	0.0382	0.5221	0.0
19	8.8000	0.0255	0.5221	0.0
20	8.8000	0.0127	0.5221	0.0
21	8.8000	0.0	0.5221	0.0

I	XPE(I)	YPE(I)
1	8.8000	1400.018
2	10.0000	1400.018

(a) Plume initial conditions.

Figure 14.- Selected output for viscid-inviscid interaction calculation.

PLUME CALCULATION AT ITERATION NO. 1

X	RI	B	RW	UI/UE
8.8510	0.25465	0.00100	0.25508	1.2517
8.9020	0.25416	0.00197	0.25500	1.2518
8.9530	0.25348	0.00292	0.25472	1.2518
9.0040	0.25257	0.00395	0.25420	1.2517
9.0550	0.25148	0.00475	0.25350	1.2517
9.1060	0.25037	0.00567	0.25277	1.2517
9.1570	0.24926	0.00658	0.25205	1.2517
9.2080	0.24814	0.00750	0.25132	1.2517
9.2590	0.24702	0.00843	0.25059	1.2517
9.3099	0.24590	0.00935	0.24987	1.2517
9.3609	0.24478	0.01028	0.24914	1.2517
9.4119	0.24366	0.01121	0.24841	1.2517
9.4629	0.24254	0.01214	0.24768	1.2517
9.5139	0.24141	0.01308	0.24695	1.2517
9.5649	0.24029	0.01402	0.24623	1.2517
9.6159	0.23916	0.01496	0.24550	1.2517
9.6669	0.23803	0.01591	0.24477	1.2517
9.7179	0.23690	0.01685	0.24403	1.2517
9.7689	0.23576	0.01781	0.24330	1.2517
9.8199	0.23463	0.01876	0.24257	1.2517
9.8709	0.23349	0.01972	0.24184	1.2517
9.9219	0.23235	0.02068	0.24111	1.2517
9.9729	0.23121	0.02164	0.24037	1.2517
10.0239	0.23007	0.02261	0.23964	1.2517

(b) Initial plume solution.

Figure 14.- Continued.

----- NORMAL COORD. STRETCH FOR ALF= 1.300 -----

J	AN	G	GH
1	-0.6990E-76	0.0	0.7725E-04
2	0.1617E+03	0.1545E-03	0.4607E-03
3	0.6339E+02	0.7668E-03	0.1365E-02
4	0.3608E+02	0.1964E-02	0.2900E-02
5	0.2391E+02	0.3836E-02	0.5148E-02
6	0.1720E+02	0.6460E-02	0.8183E-02
7	0.1307E+02	0.9905E-02	0.1207E-01
8	0.1022E+02	0.1424E-01	0.1687E-01
9	0.8215E+01	0.1951E-01	0.2265E-01
10	0.6729E+01	0.2579E-01	0.2947E-01
11	0.5598E+01	0.3314E-01	0.3738E-01
12	0.4690E+01	0.4161E-01	0.4643E-01
13	0.3968E+01	0.5126E-01	0.5670E-01
14	0.3377E+01	0.6215E-01	0.6824E-01
15	0.2886E+01	0.7433E-01	0.8110E-01
16	0.2474E+01	0.8787E-01	0.9535E-01
17	0.2123E+01	0.1028E+00	0.1110E+00
18	0.1822E+01	0.1193E+00	0.1282E+00
19	0.1561E+01	0.1372E+00	0.1470E+00
20	0.1334E+01	0.1568E+00	0.1674E+00
21	0.1135E+01	0.1780E+00	0.1895E+00
22	0.9585E+00	0.2010E+00	0.2134E+00
23	0.8020E+00	0.2258E+00	0.2391E+00
24	0.6623E+00	0.2524E+00	0.2657E+00
25	0.5371E+00	0.2810E+00	0.2953E+00
26	0.4245E+00	0.3116E+00	0.3280E+00
27	0.3227E+00	0.3443E+00	0.3617E+00
28	0.2304E+00	0.3792E+00	0.3977E+00
29	0.1465E+00	0.4163E+00	0.4360E+00
30	0.7000E-01	0.4550E+00	0.4767E+00
31	0.1198E-06	0.4976E+00	0.5198E+00

(c) Computed geometric parameters in normal
direction for inviscid flow.
Figure 14.- Continued.

I	S	X	Y	THET	THETB	AK	F
1	0.0	0.0	0.0	0.9000E+02	0.9000E+02	0.3392E-04	0.1786E+00
2	0.7013E-01	0.6804E-01	0.1702E-01	0.1404E+02	0.1404E+02	0.3263E-04	0.1776E+00
3	0.1411E+00	0.1369E+00	0.3423E-01	0.1404E+02	0.1404E+02	0.3508E-04	0.1746E+00
4	0.2136E+00	0.2072E+00	0.5183E-01	0.1404E+02	0.1404E+02	0.1710E-03	0.1698E+00
5	0.2885E+00	0.2799E+00	0.7001E-01	0.1404E+02	0.1404E+02	0.1137E-03	0.1637E+00
6	0.3666E+00	0.3556E+00	0.8896E-01	0.1404E+02	0.1404E+02	0.6476E-04	0.1565E+00
7	0.4486E+00	0.4352E+00	0.1088E+00	0.1404E+02	0.1404E+02	0.3181E-04	0.1486E+00
8	0.5351E+00	0.5191E+00	0.1298E+00	0.1404E+02	0.1404E+02	0.3862E-05	0.1403E+00
9	0.6269E+00	0.6082E+00	0.1521E+00	0.1404E+02	0.1404E+02	0.4738E-04	0.1321E+00
10	0.7246E+00	0.7030E+00	0.1758E+00	0.1404E+02	0.1404E+02	0.2102E-03	0.1240E+00
11	0.8288E+00	0.8040E+00	0.2011E+00	0.1404E+02	0.1404E+02	0.2119E-03	0.1162E+00
12	0.9399E+00	0.9118E+00	0.2281E+00	0.1404E+02	0.1404E+02	0.5890E-04	0.1089E+00
13	0.1050E+01	0.1027E+01	0.2568E+00	0.1404E+02	0.1404E+02	0.2978E-04	0.1021E+00
14	0.1185E+01	0.1149E+01	0.2875E+00	0.1404E+02	0.1404E+02	0.8230E-04	0.9586E-01
15	0.1319E+01	0.1280E+01	0.3201E+00	0.1404E+02	0.1404E+02	0.1697E-03	0.9013E-01
16	0.1462E+01	0.1419E+01	0.3548E+00	0.1404E+02	0.1404E+02	0.9192E-04	0.8493E-01
17	0.1614E+01	0.1566E+01	0.3916E+00	0.1404E+02	0.1404E+02	0.3839E-03	0.8022E-01
18	0.1774E+01	0.1721E+01	0.4304E+00	0.1406E+02	0.1406E+02	0.1258E-03	0.7599E-01
19	0.1943E+01	0.1885E+01	0.4705E+00	0.1221E+02	0.1221E+02	0.7319E+00	0.7220E-01
20	0.2120E+01	0.2060E+01	0.4959E+00	0.4519E+01	0.4519E+01	0.7878E+00	0.6881E-01
21	0.2306E+01	0.2246E+01	0.5000E+00	-0.1302E+00	-0.1302E+00	0.1413E-01	0.6579E-01
22	0.2500E+01	0.2440E+01	0.5000E+00	0.0	0.9817E-02	-0.1476E-02	0.6312E-01
23	0.2702E+01	0.2642E+01	0.5000E+00	0.0	0.1970E-02	0.7913E-03	0.6078E-01
24	0.2911E+01	0.2851E+01	0.5000E+00	0.0	-0.3575E-02	0.1335E-03	0.5873E-01
25	0.3127E+01	0.3068E+01	0.5000E+00	0.0	-0.1543E-02	-0.2756E-03	0.5695E-01
26	0.3350E+01	0.3290E+01	0.5000E+00	0.0	0.7465E-03	-0.8351E-04	0.5544E-01
27	0.3578E+01	0.3518E+01	0.5000E+00	0.0	0.5621E-03	0.9205E-04	0.5417E-01
28	0.3811E+01	0.3751E+01	0.5000E+00	0.0	-0.1860E-03	0.2000E-04	0.5314E-01
29	0.4048E+01	0.3988E+01	0.5000E+00	0.0	0.4014E-04	-0.5329E-04	0.5234E-01
30	0.4289E+01	0.4229E+01	0.5000E+00	0.0	0.5544E-03	-0.1603E-04	0.5176E-01
31	0.4531E+01	0.4471E+01	0.5000E+00	0.0	0.4761E-03	0.2730E-04	0.5140E-01
32	0.4775E+01	0.4715E+01	0.5000E+00	0.0	-0.2088E-03	0.7083E-04	0.5126E-01
33	0.5018E+01	0.4958E+01	0.5000E+00	0.0	-0.1502E-02	0.1144E-03	0.5135E-01
34	0.5261E+01	0.5201E+01	0.5000E+00	0.0	-0.2547E-02	0.1074E-04	0.5169E-01
35	0.5502E+01	0.5442E+01	0.5000E+00	0.0	-0.1779E-02	-0.1221E-03	0.5227E-01
36	0.5739E+01	0.5679E+01	0.5000E+00	0.0	0.7712E-03	-0.2531E-03	0.5314E-01
37	0.5972E+01	0.5912E+01	0.5000E+00	0.0	0.5005E-02	-0.3817E-03	0.5430E-01
38	0.6199E+01	0.6139E+01	0.5000E+00	0.0	0.9360E-02	-0.1481E-03	0.5580E-01
39	0.6419E+01	0.6359E+01	0.5001E+00	0.0	0.8405E-02	0.2994E-03	0.5769E-01
40	0.6632E+01	0.6572E+01	0.5001E+00	0.0	0.2130E-02	0.7309E-03	0.6001E-01
41	0.6836E+01	0.6776E+01	0.5001E+00	0.0	-0.8812E-02	0.1144E-02	0.6285E-01
42	0.7029E+01	0.6970E+01	0.5000E+00	0.0	-0.2370E-01	0.1538E-02	0.6630E-01
43	0.7212E+01	0.7153E+01	0.4999E+00	0.0	-0.2664E-01	-0.1553E-02	0.7049E-01

(d) Computed tangential geometric parameters.

Figure 14.- Continued.

44	0.7384E+01	0.7324E+01	0.4999E+00	0.0	0.6027E-02	-0.5098E-02	0.7556E-01
45	0.7543E+01	0.7483E+01	0.5000E+00	0.0	0.6755E-01	-0.8390E-02	0.8172E-01
46	0.7690E+01	0.7630E+01	0.5002E+00	0.0	0.1002E+00	0.2183E-02	0.8924E-01
47	0.7823E+01	0.7763E+01	0.5004E+00	0.0	0.4047E-01	0.1342E-01	0.9845E-01
48	0.7944E+01	0.7884E+01	0.5004E+00	0.0	-0.8710E-01	0.2356E-01	0.1098E+00
49	0.8051E+01	0.7991E+01	0.5000E+00	0.0	-0.2599E+00	0.3260E-01	0.1237E+00
50	0.8146E+01	0.8086E+01	0.4974E+00	0.0	-0.3447E+01	0.7092E+00	0.1409E+00
51	0.8229E+01	0.8169E+01	0.4900E+00	0.0	-0.6787E+01	0.7148E+00	0.1618E+00
52	0.8301E+01	0.8241E+01	0.4796E+00	0.0	-0.9704E+01	0.7329E+00	0.1866E+00
53	0.8363E+01	0.8303E+01	0.4674E+00	0.0	-0.1225E+02	0.7509E+00	0.2145E+00
54	0.8418E+01	0.8358E+01	0.4544E+00	0.0	-0.1451E+02	0.7702E+00	0.2426E+00
55	0.8467E+01	0.8407E+01	0.4408E+00	0.0	-0.1656E+02	0.7926E+00	0.2647E+00
56	0.8513E+01	0.8453E+01	0.4261E+00	0.0	-0.1850E+02	0.8233E+00	0.2727E+00
57	0.8560E+01	0.8500E+01	0.4097E+00	0.0	-0.2049E+02	0.8550E+00	0.2609E+00
58	0.8610E+01	0.8550E+01	0.3899E+00	0.0	-0.2264E+02	0.8943E+00	0.2396E+00
59	0.8664E+01	0.8605E+01	0.3658E+00	0.0	-0.2503E+02	0.9435E+00	0.2192E+00
60	0.8724E+01	0.8664E+01	0.3362E+00	0.0	-0.2771E+02	0.1031E+01	0.1997E+00
61	0.8790E+01	0.8730E+01	0.2994E+00	0.0	-0.3098E+02	0.1140E+01	0.1812E+00
62	0.8863E+01	0.8803E+01	0.2539E+00	0.0	-0.2027E+02	-0.2850E+02	0.1635E+00
63	0.8943E+01	0.8883E+01	0.2558E+00	0.0	-0.2273E+01	0.1674E+01	0.1467E+00
64	0.9033E+01	0.8974E+01	0.2546E+00	0.0	-0.5810E+00	0.3814E+00	0.1309E+00
65	0.9135E+01	0.9075E+01	0.2532E+00	0.0	-0.8156E+00	0.1670E-01	0.1159E+00
66	0.9250E+01	0.9190E+01	0.2516E+00	0.0	-0.8164E+00	0.5679E-03	0.1019E+00
67	0.9381E+01	0.9321E+01	0.2497E+00	0.0	-0.8173E+00	0.9970E-04	0.8877E-01
68	0.9533E+01	0.9473E+01	0.2475E+00	0.0	-0.8186E+00	0.1406E-03	0.7654E-01
69	0.9710E+01	0.9650E+01	0.2450E+00	0.0	-0.8206E+00	0.1523E-03	0.6522E-01
70	0.9919E+01	0.9859E+01	0.2420E+00	0.0	-0.8225E+00	0.2196E-03	0.5480E-01
71	0.1017E+02	0.1011E+02	0.2396E+00	0.0	0.0	0.0	0.4529E-01
72	0.1048E+02	0.1042E+02	0.2396E+00	0.0	0.0	0.0	0.3669E-01
73	0.1086E+02	0.1080E+02	0.2396E+00	0.0	0.0	0.0	0.2899E-01
74	0.1135E+02	0.1129E+02	0.2396E+00	0.0	0.0	0.0	0.2219E-01
75	0.1201E+02	0.1195E+02	0.2396E+00	0.0	0.0	0.0	0.1630E-01
76	0.1273E+02	0.1267E+02	0.2396E+00	0.0	0.0	0.0	0.1132E-01
77	0.1431E+02	0.1425E+02	0.2396E+00	0.0	0.0	0.0	0.7247E-02
78	0.1661E+02	0.1655E+02	0.2396E+00	0.0	0.0	0.0	0.4076E-02
79	0.2121E+02	0.2115E+02	0.2396E+00	0.0	0.0	0.0	0.1812E-02
80	0.3501E+02	0.3495E+02	0.2396E+00	0.0	0.0	0.0	0.4530E-03
81	0.1000E+31	0.1000E+31	0.2396E+00	0.0	0.0	0.0	0.1000E-29

(d) Concluded.

Figure 14.- Continued.

ITERATION NO. 1

IT	DMAX	ID	JD	RMAX	IR	JR	ISUB	ISUP	RAVG	RF1	QF3	NS	SEC/CYC
1	0.404E-01	62	31	0.312E+02	1	31	1	0	0.159E+00	1.400	0.100	0	0.180
2	0.251E-01	62	31	0.141E+02	62	31	1	0	0.114E+00	1.400	0.100	0	0.180
3	0.224E-01	61	31	0.169E+02	1	31	1	0	0.105E+00	1.400	0.100	0	0.180
4	0.174E-01	60	31	0.283E+01	61	31	1	0	0.916E-01	1.400	0.100	0	0.190
5	0.161E-01	60	31	0.125E+02	1	31	1	0	0.872E-01	1.400	0.100	0	0.180
6	0.138E-01	60	31	0.623E+01	60	31	1	0	0.781E-01	1.400	0.100	0	0.170
7	0.127E-01	59	31	0.525E+01	59	31	1	0	0.705E-01	1.400	0.100	0	0.170
8	0.113E-01	59	31	0.466E+01	62	31	1	0	0.661E-01	1.400	0.100	0	0.180
9	0.107E-01	58	31	0.428E+01	62	31	1	0	0.629E-01	1.400	0.100	1	0.180
10	0.945E-02	58	31	0.395E+01	62	31	1	0	0.608E-01	1.400	0.100	2	0.180
11	0.888E-02	57	31	0.366E+01	62	31	1	0	0.570E-01	1.400	0.100	4	0.180
12	0.782E-02	57	31	0.341E+01	62	31	1	0	0.535E-01	1.400	0.100	4	0.180
13	0.697E-02	56	31	0.322E+01	56	31	0	1	0.512E-01	1.400	0.100	6	0.180
14	0.632E-02	56	31	0.300E+01	62	31	1	0	0.500E-01	1.400	0.100	7	0.180
15	0.558E-02	56	31	0.282E+01	62	31	1	0	0.482E-01	1.400	0.100	8	0.180
16	0.497E-02	55	31	0.266E+01	62	31	1	0	0.462E-01	1.400	0.100	9	0.170
17	0.451E-02	55	31	0.252E+01	62	31	1	0	0.443E-01	1.400	0.100	10	0.170
18	0.408E-02	55	31	0.239E+01	62	31	1	0	0.429E-01	1.400	0.100	9	0.180
19	0.385E-02	60	31	0.227E+01	62	31	1	0	0.418E-01	1.400	0.100	11	0.180
20	0.366E-02	60	31	0.216E+01	62	31	1	0	0.406E-01	1.400	0.100	11	0.180

RMAX= 0.22E+01, COVR= 0.15E-01

(e) Inviscid iteration results from first inviscid solution.

Figure 14.- Continued.

X	UTAU	DELST	UE/UZ	DSTPR	HTR	DELTA	THETA	CF	DELI	DUEDX	RW
1.5000E-01	2.3441E+01	2.9972E-04	0.7691	0.0378	2.3664	8.1286E-04	1.1749E-04	2.482E-03	3.5063E-05	8.0512E+02	0.0375
1.7861E-01	2.5431E+01	2.9944E-04	0.7939	0.0450	2.2692	8.4255E-04	1.2128E-04	2.729E-03	4.2533E-05	8.0512E+02	0.0447
2.0723E-01	2.9081E+01	3.0036E-04	0.8185	0.0521	2.0731	9.2980E-04	1.3124E-04	3.341E-03	5.3611E-05	8.0512E+02	0.0518
2.4357E-01	3.2499E+01	3.4131E-04	0.8315	0.0613	1.8276	1.2437E-03	1.6498E-04	4.033E-03	8.3884E-05	3.3713E+02	0.0609
2.7991E-01	3.4879E+01	3.9504E-04	0.8444	0.0704	1.6482	1.6887E-03	2.0349E-04	4.492E-03	1.3034E-04	3.3713E+02	0.0700
3.1778E-01	3.5288E+01	4.6823E-04	0.8517	0.0800	1.5514	2.1734E-03	2.4785E-04	4.512E-03	1.9005E-04	1.8341E+02	0.0795
3.5565E-01	3.5332E+01	5.3310E-04	0.8590	0.0895	1.4945	2.6096E-03	2.8872E-04	4.440E-03	2.5450E-04	1.8341E+02	0.0890
3.9540E-01	3.5053E+01	6.1186E-04	0.8639	0.0995	1.4603	3.0278E-03	3.3080E-04	4.316E-03	3.2745E-04	1.1837E+02	0.0989
4.3515E-01	3.4881E+01	6.7732E-04	0.8689	0.1095	1.4339	3.4180E-03	3.6930E-04	4.221E-03	4.0565E-04	1.1837E+02	0.1088
4.7713E-01	3.4652E+01	7.4901E-04	0.8727	0.1201	1.4135	3.8131E-03	4.0894E-04	4.126E-03	4.9506E-04	8.7110E+01	0.1193
5.1911E-01	3.4512E+01	8.1404E-04	0.8765	0.1307	1.3957	4.1945E-03	4.4606E-04	4.054E-03	5.9108E-04	8.7110E+01	0.1298
5.6355E-01	3.4354E+01	8.8153E-04	0.8798	0.1419	1.3805	4.5887E-03	4.8455E-04	3.983E-03	7.0060E-04	7.1651E+01	0.1410
6.0818E-01	3.4249E+01	9.4569E-04	0.8832	0.1531	1.3667	4.9731E-03	5.2123E-04	3.926E-03	8.1750E-04	7.1651E+01	0.1521
6.5556E-01	3.4141E+01	1.0124E-03	0.8864	0.1650	1.3543	5.3735E-03	5.5935E-04	3.871E-03	9.5012E-04	6.4544E+01	0.1640
7.0295E-01	3.4067E+01	1.0767E-03	0.8895	0.1769	1.3431	5.7658E-03	5.9605E-04	3.824E-03	1.0908E-03	6.4544E+01	0.1758
7.5347E-01	3.4002E+01	1.1434E-03	0.8928	0.1896	1.3326	6.1761E-03	6.3415E-04	3.779E-03	1.2496E-03	6.2406E+01	0.1885
8.0399E-01	3.3950E+01	1.2081E-03	0.8961	0.2023	1.3230	6.5789E-03	6.7109E-04	3.739E-03	1.4170E-03	6.2406E+01	0.2011
8.5789E-01	3.3935E+01	1.2750E-03	0.8997	0.2159	1.3135	7.0007E-03	7.0901E-04	3.701E-03	1.6049E-03	6.3940E+01	0.2146
9.1179E-01	3.3925E+01	1.3404E-03	0.9032	0.2294	1.3051	7.4151E-03	7.4637E-04	3.667E-03	1.8021E-03	6.3940E+01	0.2281
9.6929E-01	3.3949E+01	1.4073E-03	0.9073	0.2439	1.2965	7.8484E-03	7.8434E-04	3.636E-03	2.0217E-03	6.8527E+01	0.2424
1.0268E+00	3.3978E+01	1.4731E-03	0.9114	0.2583	1.2888	8.2740E-03	8.2152E-04	3.606E-03	2.2510E-03	6.8527E+01	0.2568
1.0881E+00	3.4059E+01	1.5393E-03	0.9162	0.2737	1.2806	8.7175E-03	8.5884E-04	3.501E-03	2.5043E-03	7.6638E+01	0.2722
1.1494E+00	3.4139E+01	1.6049E-03	0.9210	0.2891	1.2734	9.1521E-03	8.9553E-04	3.557E-03	2.7673E-03	7.6638E+01	0.2875
1.2146E+00	3.4301E+01	1.6688E-03	0.9271	0.3055	1.2650	9.6021E-03	9.3111E-04	3.539E-03	3.0543E-03	9.0135E+01	0.3038
1.2799E+00	3.4452E+01	1.7328E-03	0.9331	0.3219	1.2580	1.0041E-02	9.6634E-04	3.519E-03	3.3500E-03	9.0135E+01	0.3201
1.3492E+00	3.4744E+01	1.7909E-03	0.9412	0.3393	1.2488	1.0489E-02	9.9784E-04	3.511E-03	3.6667E-03	1.1359E+02	0.3375
1.4185E+00	3.5011E+01	1.8504E-03	0.9492	0.3567	1.2415	1.0922E-02	1.0296E-03	3.479E-03	3.9891E-03	1.1359E+02	0.3548
1.4920E+00	3.5569E+01	1.8930E-03	0.9613	0.3751	1.2296	1.1353E-02	1.0510E-03	3.511E-03	4.3207E-03	1.6176E+02	0.3732
1.5655E+00	3.6068E+01	1.9406E-03	0.9733	0.3935	1.2208	1.1757E-02	1.0742E-03	3.511E-03	4.6500E-03	1.6176E+02	0.3716
1.6432E+00	3.7626E+01	1.9193E-03	0.9994	0.4129	1.1949	1.2124E-02	1.0552E-03	3.600E-03	4.9305E-03	3.3434E+02	0.4110
1.7209E+00	3.8972E+01	1.9231E-03	1.0252	0.4324	1.1791	1.2419E-02	1.0476E-03	3.646E-03	5.1764E-03	3.3434E+02	0.4304
1.8029E+00	4.3250E+01	1.7736E-03	1.0905	0.4527	1.1217	1.2713E-02	9.3874E-04	3.898E-03	5.2516E-03	8.1564E+02	0.4509
1.8849E+00	4.6918E+01	1.7246E-03	1.1540	0.4718	1.0930	1.2892E-02	8.8142E-04	4.020E-03	5.2311E-03	8.1564E+02	0.4701
1.9726E+00	4.7669E+01	1.8575E-03	1.1846	0.4872	1.1167	1.2909E-02	9.3684E-04	3.900E-03	5.2308E-03	3.7594E+02	0.4853
2.0604E+00	4.8491E+01	2.0018E-03	1.2148	0.4970	1.1314	1.3206E-02	9.9465E-04	3.800E-03	5.2797E-03	3.7594E+02	0.4950
2.1532E+00	4.8692E+01	2.5882E-03	1.1664	0.5018	1.2357	1.3609E-02	1.2774E-03	3.245E-03	5.7310E-03	-5.6742E+02	0.4992
2.2461E+00	3.7735E+01	3.1366E-03	1.1169	0.5031	1.3110	1.4987E-02	1.5932E-03	2.808E-03	6.6206E-03	-5.6742E+02	0.5000
2.3431E+00	3.4864E+01	3.6791E-03	1.0811	0.5037	1.3412	1.6867E-02	1.6812E-03	2.584E-03	7.7121E-03	-3.6357E+02	0.5000
2.4401E+00	3.2263E+01	4.2836E-03	1.0448	0.5043	1.3680	1.9091E-02	2.2042E-03	2.393E-03	8.9902E-03	-3.8357E+02	0.5000
2.5411E+00	3.2443E+01	4.5124E-03	1.0361	0.5045	1.3298	2.1075E-02	2.3621E-03	2.466E-03	1.0086E-02	-8.7737E+01	0.5000
2.6420E+00	3.2393E+01	4.7793E-03	1.0274	0.5048	1.3065	2.3064E-02	2.5310E-03	2.493E-03	1.1156E-02	-8.7737E+01	0.5000
2.7467E+00	3.2372E+01	5.0055E-03	1.0226	0.5050	1.2820	2.5020E-02	2.6773E-03	2.530E-03	1.2187E-02	-4.5551E+01	0.5000
2.8513E+00	3.2298E+01	5.2498E-03	1.0179	0.5052	1.2648	2.6905E-02	2.8287E-03	2.545E-03	1.3192E-02	-4.5551E+01	0.5000
2.9594E+00	3.2304E+01	5.4778E-03	1.0151	0.5055	1.2480	2.8780E-02	2.9702E-03	2.562E-03	1.4182E-02	-2.6644E+01	0.5000
3.0675E+00	3.2238E+01	5.7157E-03	1.0122	0.5057	1.2351	3.0602E-02	3.1146E-03	2.568E-03	1.5152E-02	-2.6644E+01	0.5000
3.1788E+00	3.2215E+01	5.9456E-03	1.0104	0.5059	1.2227	3.2426E-02	3.2538E-03	2.575E-03	1.6116E-02	-1.6391E+01	0.5000
3.2901E+00	3.2153E+01	6.1811E-03	1.0086	0.5062	1.2127	3.4208E-02	3.3947E-03	2.575E-03	1.7064E-02	-1.6391E+01	0.5000
3.4041E+00	3.2113E+01	6.4133E-03	1.0074	0.5064	1.2031	3.5996E-02	3.5331E-03	2.576E-03	1.8012E-02	-1.0632E+01	0.5000

(f) First boundary layer calculation (incomplete).

Figure 14.- Continued.

ITERATION NO. 4 (AVERAGE OF INVISCID AND VISCOUS SOLUTIONS)

PLOT OF CP AT EQUAL XI-INCREMENTS

I	XB	YB	FM	QS	CP
1	0.0	0.0	0.0	0.0	1.1704
2	0.068	0.017	0.538	0.694	0.5626
3	0.137	0.034	0.564	0.726	0.5091
4	0.207	0.052	0.640	0.817	0.3499
5	0.280	0.070	0.663	0.844	0.3004
6	0.356	0.089	0.677	0.860	0.2707
7	0.435	0.109	0.687	0.872	0.2495
8	0.519	0.131	0.695	0.881	0.2327
9	0.608	0.153	0.701	0.889	0.2177
10	0.703	0.177	0.708	0.896	0.2034
11	0.804	0.202	0.715	0.904	0.1868
12	0.911	0.229	0.722	0.912	0.1732
13	1.026	0.258	0.730	0.921	0.1558
14	1.149	0.289	0.739	0.931	0.1354
15	1.280	0.322	0.750	0.944	0.1103
16	1.418	0.357	0.765	0.961	0.0770
17	1.565	0.393	0.788	0.986	0.0276
18	1.720	0.432	0.838	1.042	-0.0845
19	1.885	0.471	0.955	1.166	-0.3389
20	2.060	0.496	1.001	1.213	-0.4372
21	2.246	0.503	0.913	1.122	-0.2489
22	2.440	0.504	0.852	1.056	-0.1140
23	2.642	0.505	0.832	1.036	-0.0719
24	2.851	0.505	0.822	1.025	-0.0493
25	3.067	0.506	0.816	1.018	-0.0355
26	3.290	0.506	0.812	1.014	-0.0276
27	3.518	0.507	0.810	1.011	-0.0227
28	3.751	0.507	0.809	1.009	-0.0186
29	3.988	0.508	0.807	1.008	-0.0153
30	4.229	0.508	0.806	1.006	-0.0130
31	4.471	0.509	0.805	1.006	-0.0114
32	4.715	0.509	0.805	1.005	-0.0102
33	4.958	0.510	0.804	1.005	-0.0095
34	5.201	0.510	0.804	1.005	-0.0091
35	5.442	0.510	0.804	1.005	-0.0092
36	5.679	0.511	0.804	1.005	-0.0096
37	5.912	0.511	0.805	1.005	-0.0104
38	6.139	0.512	0.805	1.006	-0.0116

(g) Solution after 4 iterations.

Figure 14.- Continued.

39	6.359	0.512	0.806	1.007	-0.0133
40	6.572	0.512	0.807	1.008	-0.0156
41	6.776	0.513	0.809	1.010	-0.0197
42	6.969	0.513	0.812	1.013	-0.0264
43	7.152	0.513	0.816	1.018	-0.0356
44	7.324	0.513	0.821	1.023	-0.0455
45	7.483	0.513	0.827	1.029	-0.0593
46	7.630	0.513	0.838	1.042	-0.0840
47	7.763	0.513	0.854	1.059	-0.1200
48	7.884	0.512	0.877	1.084	-0.1698
49	7.991	0.511	0.928	1.138	-0.2810
50	8.086	0.507	0.984	1.193	-0.4008
51	8.169	0.500	0.997	1.202	-0.4277
52	8.241	0.491	0.978	1.176	-0.3876
53	8.303	0.480	0.944	1.133	-0.3162
54	8.358	0.468	0.908	1.090	-0.2386
55	8.407	0.456	0.866	1.043	-0.1455
56	8.453	0.446	0.821	0.993	-0.0464
57	8.500	0.433	0.775	0.944	0.0543
58	8.550	0.423	0.760	0.937	0.0895
59	8.605	0.412	0.767	0.945	0.0722
60	8.664	0.401	0.770	0.949	0.0667
61	8.730	0.398	0.770	0.950	0.0654
62	8.803	0.374	0.762	0.938	0.0848
63	8.893	0.358	0.741	0.917	0.1298
64	8.974	0.340	0.723	0.896	0.1712
65	9.075	0.320	0.690	0.858	0.2437
66	9.190	0.304	0.690	0.872	0.2438
67	9.321	0.295	0.722	0.911	0.1726
68	9.473	0.290	0.742	0.934	0.1288
69	9.650	0.285	0.758	0.952	0.0938
70	9.859	0.281	0.755	0.960	0.0784
71	10.110	0.279	0.774	0.971	0.0578
72	10.417	0.279	0.786	0.985	0.0308
73	10.800	0.279	0.792	0.991	0.0184
74	11.293	0.279	0.795	0.995	0.0109
75	11.950	0.279	0.797	0.997	0.0062
76	12.870	0.279	0.799	0.998	0.0033
77	14.250	0.279	0.799	0.999	0.0015
78	16.550	0.279	0.800	1.000	0.0006
79	21.150	0.279	0.800	1.000	0.0001
80	34.948	0.279	0.800	1.000	0.0000
81*****	0.279	0.800	1.000	0.0	



(g) Continued.

Figure 14.- Continued.

TOTAL BODY DRAG COEFFICIENT= 0.05813

AFTERBODY DRAG COEFFICIENT= 0.04588

STATUS OF ITERATION

XMAX	=	8.4071
UECHK	=	6.2636
DRMS	=	2.8226

(g) Concluded.

Figure 14.- Continued.

INITIAL VALUES FOR PLUME

K	A(1,K)	A(2,K)	A(3,K)	A(4,K)
1	8.8000	0.2550	0.5221	0.0
2	8.8000	0.2422	0.5221	0.0
3	8.8000	0.2295	0.5221	0.0
4	8.8000	0.2167	0.5221	0.0
5	8.8000	0.2040	0.5221	0.0
6	8.8000	0.1912	0.5221	0.0
7	8.8000	0.1785	0.5221	0.0
8	8.8000	0.1657	0.5221	0.0
9	8.8000	0.1530	0.5221	0.0
10	8.8000	0.1402	0.5221	0.0
11	8.8000	0.1275	0.5221	0.0
12	8.8000	0.1147	0.5221	0.0
13	8.8000	0.1020	0.5221	0.0
14	8.8000	0.0892	0.5221	0.0
15	8.8000	0.0765	0.5221	0.0
16	8.8000	0.0637	0.5221	0.0
17	8.8000	0.0510	0.5221	0.0
18	8.8000	0.0382	0.5221	0.0
19	8.8000	0.0255	0.5221	0.0
20	8.8000	0.0127	0.5221	0.0
21	8.8000	0.0	0.5221	0.0

I	XPE(I)	YPE(I)
1	8.7300	1442.714
2	8.6026	1466.081
3	8.6833	1488.626
4	8.9735	1510.610
5	9.0750	1579.031
6	9.1900	1577.453
7	9.3214	1524.848
8	9.4731	1487.343
9	9.6500	1462.437
10	9.8591	1452.112
11	10.1100	1435.264
12	10.4166	1419.318
13	10.8000	1411.542
14	11.2928	1406.852
15	11.9499	1403.809
16	12.8697	1402.060
17	14.2499	1400.970
18	16.5498	1400.381
19	21.1495	1400.110
20	34.9480	1400.026
21	*****	1400.018

(h) Plume solution after 4 iterations.
Figure 14.- Continued.

PLUME CALCULATION AT ITERATION NO. 4

X	RI	B	RW	UI/UE
8.8510	0.25436	0.00106	0.25480	1.2929
8.9020	0.25368	0.00201	0.25452	1.3005
8.9530	0.25282	0.00304	0.25407	1.3114
9.0040	0.25180	0.00424	0.25352	1.3426
9.0550	0.25068	0.00558	0.25289	1.3878
9.1060	0.24947	0.00705	0.25223	1.4059
9.1570	0.24824	0.00853	0.25159	1.4050
9.2080	0.24703	0.01001	0.25099	1.3943
9.2590	0.24586	0.01142	0.25043	1.3667
9.3099	0.24476	0.01273	0.24993	1.3405
9.3609	0.24371	0.01398	0.24944	1.3228
9.4119	0.24270	0.01517	0.24897	1.3077
9.4629	0.24173	0.01632	0.24852	1.2930
9.5139	0.24078	0.01742	0.24807	1.2837
9.5649	0.23986	0.01849	0.24762	1.2756
9.6159	0.23895	0.01954	0.24719	1.2677
9.6669	0.23807	0.02057	0.24676	1.2616
9.7179	0.23719	0.02158	0.24632	1.2589
9.7689	0.23632	0.02259	0.24589	1.2562
9.8199	0.23545	0.02359	0.24546	1.2535
9.8709	0.23459	0.02458	0.24503	1.2507
9.9219	0.23373	0.02556	0.24461	1.2473
9.9729	0.23289	0.02653	0.24420	1.2439
10.0239	0.23205	0.02749	0.24379	1.2406

TIME TO CALCULATE PLUME = 1.42 SECS

(h) Concluded.

Figure 14.- Continued.

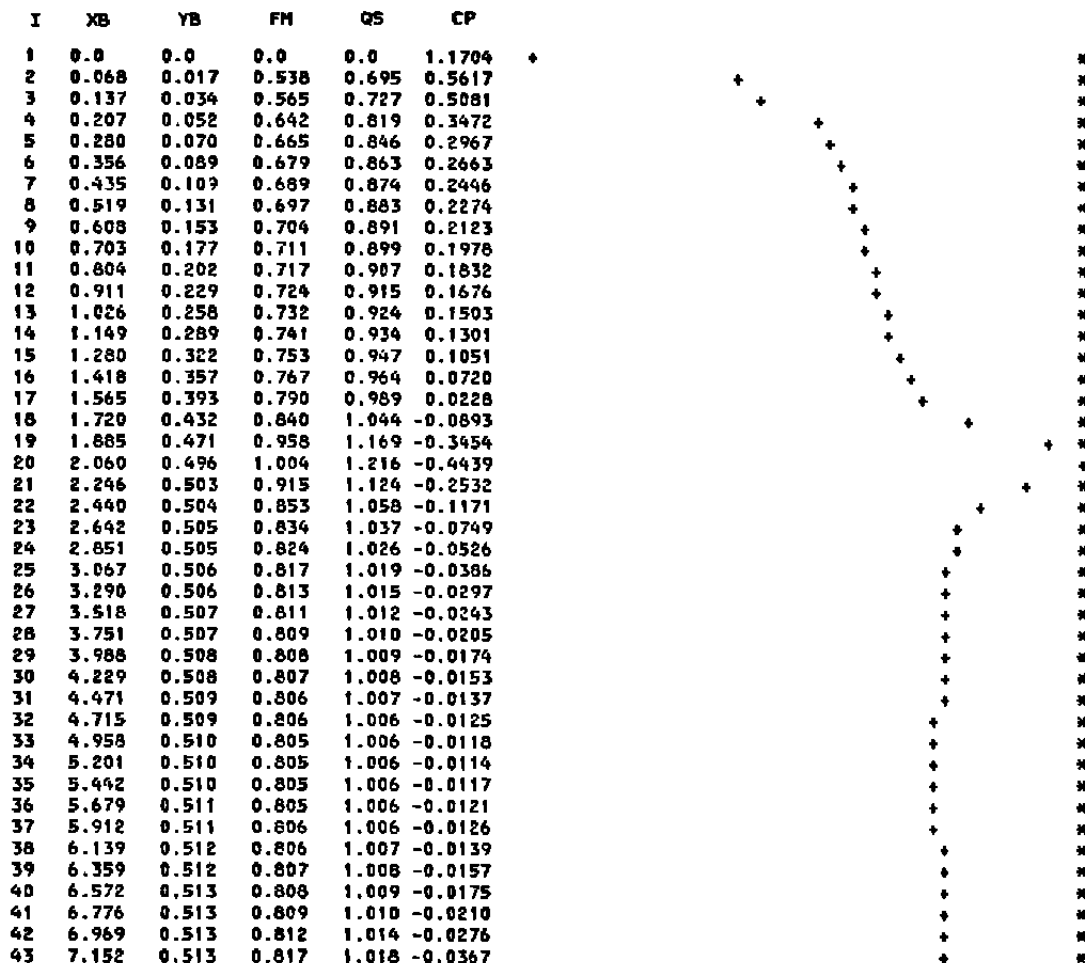
ITERATION NO. 13

X	UTAU	DELST	UE/UZ	DSTPR	HTR	DELTA	THETA	CF	DELI	DUEDX	RW
8.0029E+00	3.8902E+01	1.0922E-02	1.1422	0.5109	0.8889	1.0487E-01	5.6459E-03	2.831E-03	5.0246E-02	4.4055E+02	0.5000
8.0444E+00	4.0015E+01	1.0420E-02	1.1599	0.5097	0.8576	1.0728E-01	5.2556E-03	2.889E-03	5.0646E-02	4.7102E+02	0.4993
8.0859E+00	4.1076E+01	9.9785E-03	1.1772	0.5073	0.8259	1.1024E-01	4.8922E-03	2.939E-03	5.1198E-02	4.6055E+02	0.4974
8.1273E+00	4.1137E+01	1.0057E-02	1.1793	0.5044	0.8260	1.1077E-01	4.9258E-03	2.935E-03	5.1073E-02	7.3560E+01	0.4943
8.1680E+00	4.1187E+01	1.0164E-02	1.1915	0.5001	0.8261	1.1156E-01	4.9740E-03	2.930E-03	5.0954E-02	6.2985E+01	0.4900
8.2048E+00	4.0411E+01	1.0701E-02	1.1711	0.4959	0.8521	1.1027E-01	5.3517E-03	2.880E-03	5.0328E-02	-2.9314E+02	0.4852
8.2408E+00	3.9605E+01	1.1287E-02	1.1603	0.4908	0.8768	1.0953E-01	5.7518E-03	2.827E-03	4.9894E-02	-3.0370E+02	0.4795
8.2720E+00	3.8220E+01	1.2207E-02	1.1410	0.4860	0.9159	1.0815E-01	6.3840E-03	2.741E-03	4.9502E-02	-6.2442E+02	0.4738
8.3033E+00	3.6792E+01	1.3240E-02	1.1210	0.4807	0.9540	1.0749E-01	7.0693E-03	2.646E-03	4.9411E-02	-6.2734E+02	0.4674
8.3306E+00	3.5280E+01	1.4391E-02	1.0999	0.4756	0.9926	1.0726E-01	7.8126E-03	2.542E-03	4.9573E-02	-8.9099E+02	0.4612
8.3580E+00	3.3702E+01	1.5711E-02	1.0781	0.4701	1.0319	1.0759E-01	8.6382E-03	2.430E-03	4.9978E-02	-9.2379E+02	0.4544
8.3826E+00	3.2212E+01	1.7082E-02	1.0576	0.4649	1.0688	1.0837E-01	9.4702E-03	2.320E-03	5.0554E-02	-7.9508E+02	0.4478
8.4071E+00	3.0677E+01	1.8550E-02	1.0367	0.4594	1.1072	1.0963E-01	1.0393E-02	2.203E-03	5.1330E-02	-7.9985E+02	0.4407
8.4303E+00	2.9205E+01	2.0327E-02	1.0167	0.4540	1.1449	1.1128E-01	1.1349E-02	2.086E-03	5.2246E-02	-7.9622E+02	0.4336
8.4534E+00	2.7699E+01	2.2253E-02	0.9965	0.4484	1.1848	1.1340E-01	1.2411E-02	1.964E-03	5.3350E-02	-7.9334E+02	0.4261
8.4767E+00	2.6073E+01	2.4595E-02	0.9750	0.4427	1.2304	1.1609E-01	1.3655E-02	1.827E-03	5.4732E-02	-8.2590E+02	0.4181
8.5000E+00	2.4489E+01	2.7229E-02	0.9545	0.4369	1.2776	1.1933E-01	1.5000E-02	1.691E-03	5.6286E-02	-7.9077E+02	0.4097
8.5250E+00	2.3220E+01	2.9812E-02	0.9384	0.4299	1.3171	1.2305E-01	1.6285E-02	1.578E-03	5.7740E-02	-6.3127E+02	0.4000
8.5125E+00	0.0	2.6432E-02	0.9384	0.4333	4.0000	5.0946E-02	6.4299E-03	0.0	2.1794E-02	3.9267E+02	0.4049
8.5312E+00	-3.1415E-01	3.0503E-02	0.9312	0.4280	4.0295	5.4283E-02	6.2631E-03	-2.939E-07	2.3057E-02	-3.6211E+02	0.3975
8.5500E+00	-1.0975E+00	3.3597E-02	0.9253	0.4235	4.1941	5.8701E-02	7.2939E-03	-3.638E-06	2.4737E-02	-2.9916E+02	0.3899
8.5773E+00	-2.3545E+00	3.8874E-02	0.9201	0.4170	4.5581	6.5704E-02	7.8564E-03	-1.696E-05	2.7256E-02	-1.7411E+02	0.3782
8.6045E+00	-3.5154E+00	4.5333E-02	0.9166	0.4111	5.0125	7.3882E-02	8.4393E-03	-3.811E-05	3.0109E-02	-1.2076E+02	0.3657
8.6344E+00	-4.3414E+00	5.2579E-02	0.9131	0.4039	5.4403	8.2887E-02	9.1253E-03	-5.862E-05	3.3042E-02	-1.1501E+02	0.3513
8.6643E+00	-5.3876E+00	6.1762E-02	0.9136	0.3979	6.1165	9.3355E-02	9.6869E-03	-9.019E-05	3.6249E-02	4.3254E+00	0.3361
8.6971E+00	-6.0852E+00	7.2171E-02	0.9136	0.3905	6.7277	1.0489E-01	1.0435E-02	-1.151E-04	3.9448E-02	-1.3684E+01	0.3183
8.7300E+00	-6.5800E+00	8.3744E-02	0.9136	0.3831	7.2883	1.1708E-01	1.1316E-02	-1.345E-04	4.2502E-02	-2.3791E+01	0.2994
8.7633E+00	-7.1720E+00	1.0018E-01	0.9149	0.3772	8.1145	1.3296E-01	1.2370E-02	-1.593E-04	4.6272E-02	4.4767E+00	0.2770
8.8026E+00	-7.5276E+00	1.1528E-01	0.9128	0.3703	8.8064	1.4600E-01	1.3313E-02	-1.764E-04	4.6604E-02	1.3542E+02	0.2550
8.8430E+00	-6.1886E+00	1.0739E-01	0.9015	0.3622	7.1732	1.4110E-01	1.4768E-02	-1.225E-04	4.7042E-02	-2.8402E+02	0.2548
8.8933E+00	-4.8179E+00	1.0002E-01	0.8906	0.3546	6.0297	1.3650E-01	1.5999E-02	-7.629E-05	4.5568E-02	-2.4612E+02	0.2546
8.9284E+00	-2.5653E+00	8.9353E-02	0.8769	0.3436	4.7932	1.2978E-01	1.7509E-02	-2.237E-05	4.3311E-02	-2.5805E+02	0.2543
8.9735E+00	3.4428E-01	7.9877E-02	0.8659	0.3337	3.9418	1.2405E-01	1.8687E-02	4.191E-07	4.1346E-02	-2.1382E+02	0.2538
9.0242E+00	2.3924E+00	7.4796E-02	0.8567	0.3281	3.4605	1.2219E-01	1.9683E-02	2.048E-05	4.0842E-02	-1.4132E+02	0.2533
9.0750E+00	4.0573E+00	7.0375E-02	0.8503	0.3230	3.1020	1.2071E-01	2.0415E-02	5.987E-05	4.0393E-02	-9.8622E+01	0.2526
9.1325E+00	1.6597E+01	5.8517E-02	0.8509	0.3104	1.5452	1.6541E-01	2.9921E-02	1.000E-03	5.9773E-02	5.6225E+02	0.2519
9.1612E+00	1.7335E+01	5.6072E-02	0.8580	0.3076	1.5038	1.6462E-01	2.9134E-02	1.071E-03	5.9094E-02	2.5016E+02	0.2515
9.1900E+00	1.8103E+01	5.3642E-02	0.8659	0.3048	1.4634	1.6385E-01	2.8295E-02	1.145E-03	5.8397E-02	2.7694E+02	0.2512
9.2557E+00	1.9730E+01	4.8920E-02	0.8838	0.2994	1.3849	1.6264E-01	2.6524E-02	1.301E-03	5.7032E-02	2.8957E+02	0.2505
9.3214E+00	2.1240E+01	4.5000E-02	0.9018	0.2948	1.3195	1.6200E-01	2.4896E-02	1.442E-03	5.6034E-02	2.8777E+02	0.2498
9.3972E+00	2.2415E+01	4.2329E-02	0.9161	0.2914	1.2714	1.6237E-01	2.3725E-02	1.552E-03	5.5545E-02	1.9564E+02	0.2491
9.4731E+00	2.3519E+01	4.0002E-02	0.9302	0.2884	1.2289	1.6298E-01	2.2636E-02	1.651E-03	5.5165E-02	1.9301E+02	0.2484
9.5615E+00	2.4370E+01	3.8421E-02	0.9412	0.2861	1.1964	1.6424E-01	2.1875E-02	1.727E-03	5.5153E-02	1.2685E+02	0.2477
9.6500E+00	2.5183E+01	3.6978E-02	0.9522	0.2839	1.1664	1.6558E-01	2.1144E-02	1.798E-03	5.5174E-02	1.2683E+02	0.2469
9.7345E+00	2.5559E+01	3.6345E-02	0.9582	0.2824	1.1476	1.6748E-01	2.0834E-02	1.840E-03	5.5590E-02	5.8010E+01	0.2450
9.8591E+00	2.6116E+01	3.5745E-02	0.9642	0.2809	1.1296	1.6938E-01	2.0528E-02	1.880E-03	5.6001E-02	5.8299E+01	0.2451
9.9845E+00	2.6637E+01	3.5085E-02	0.9714	0.2792	1.1095	1.7166E-01	2.0177E-02	1.923E-03	5.6497E-02	5.7361E+01	0.2441

(i) Best fit boundary layer solution.

Figure 14.- Continued.

ITERATION NO. 13 (AVERAGE OF INVISCID AND VISCOUS SOLUTIONS)
PLOT OF CP AT EQUAL XI-INCREMENTS



(j) Best fit C_p plot.

Figure 14.- Continued.

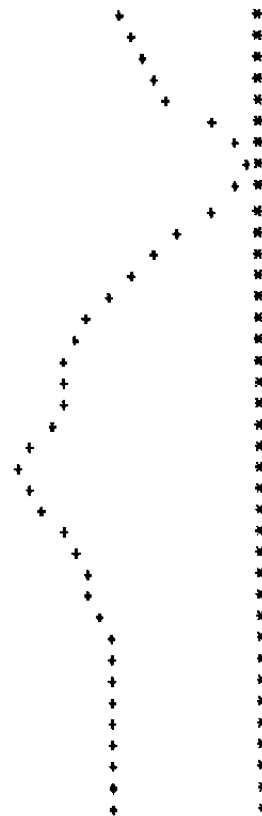
44	7.324	0.513	0.821	1.023	-0.0461
45	7.483	0.513	0.827	1.030	-0.0595
46	7.630	0.513	0.839	1.042	-0.0846
47	7.763	0.514	0.855	1.061	-0.1223
48	7.884	0.513	0.879	1.036	-0.1739
49	7.991	0.511	0.930	1.140	-0.2852
50	8.086	0.507	0.970	1.179	-0.3714
51	8.169	0.500	0.978	1.183	-0.3890
52	8.241	0.491	0.962	1.161	-0.3549
53	8.303	0.491	0.930	1.122	-0.2849
54	8.358	0.470	0.895	1.030	-0.2086
55	8.407	0.459	0.860	1.039	-0.1336
56	8.453	0.443	0.828	1.002	-0.0519
57	8.500	0.437	0.792	0.957	0.0173
58	8.550	0.423	0.764	0.933	0.0796
59	8.605	0.411	0.752	0.921	0.1065
60	8.664	0.398	0.745	0.918	0.1219
61	8.730	0.383	0.741	0.918	0.1307
62	8.803	0.370	0.739	0.914	0.1354
63	8.883	0.354	0.719	0.890	0.1782
64	8.974	0.334	0.698	0.873	0.2253
65	9.075	0.322	0.680	0.851	0.2653
66	9.190	0.305	0.666	0.858	0.2517
67	9.321	0.295	0.713	0.901	0.1913
68	9.473	0.288	0.736	0.928	0.1414
69	9.650	0.284	0.755	0.949	0.1003
70	9.859	0.281	0.765	0.961	0.0769
71	10.110	0.279	0.775	0.972	0.0543
72	10.417	0.279	0.786	0.984	0.0314
73	10.800	0.279	0.791	0.990	0.0194
74	11.293	0.279	0.795	0.994	0.0119
75	11.950	0.279	0.797	0.996	0.0070
76	12.870	0.279	0.795	0.993	0.0039
77	14.250	0.279	0.799	0.999	0.0019
78	16.550	0.279	0.800	1.000	0.0008
79	21.150	0.279	0.800	1.000	0.0002
80	34.948	0.279	0.800	1.000	0.0000
81*****	0.279	0.800	1.000	0.0	

TOTAL BODY DRAG COEFFICIENT= 0.03337

AFTERBODY DRAG COEFFICIENT= 0.02644

STATUS OF ITERATION

XMAX	=	8.5312
UECHK	=	-1.7347
DRMS	=	0.7385



(j) Concluded.
Figure 14.- Continued.

53	8.303	0.481	0.929	1.121	-0.2839		*
54	8.358	0.470	0.894	1.079	-0.2079		*
55	8.407	0.459	0.860	1.039	-0.1325		*
56	8.453	0.448	0.828	1.001	-0.0610		*
57	8.500	0.437	0.792	0.955	0.0177		*
58	8.550	0.423	0.765	0.935	0.0766		*
59	8.605	0.411	0.753	0.922	0.1042		*
60	8.664	0.397	0.745	0.918	0.1222		*
61	8.730	0.383	0.740	0.917	0.1325		*
62	8.803	0.370	0.738	0.914	0.1368		*
63	8.883	0.354	0.718	0.887	0.1822		*
64	8.974	0.334	0.693	0.868	0.2357		*
65	9.075	0.322	0.678	0.851	0.2694		*
66	9.190	0.305	0.695	0.879	0.2309		*
67	9.321	0.295	0.724	0.913	0.1690		*
68	9.473	0.289	0.746	0.939	0.1195		*
69	9.650	0.284	0.765	0.961	0.0777		*
70	9.859	0.281	0.776	0.973	0.0538		*
71	10.110	0.279	0.775	0.972	0.0555		*
72	10.417	0.279	0.755	0.984	0.0310		*
73	10.800	0.279	0.791	0.990	0.0191		*
74	11.293	0.279	0.795	0.994	0.0118		*
75	11.950	0.279	0.797	0.997	0.0070		*
76	12.570	0.279	0.798	0.998	0.0038		*
77	14.250	0.279	0.799	0.999	0.0019		*
78	16.550	0.279	0.800	1.000	0.0008		*
79	21.150	0.279	0.800	1.000	0.0002		*
80	34.948	0.279	0.800	1.000	0.0000		*
81	*****	0.279	0.800	1.000	0.0		*

TOTAL BODY DRAG COEFFICIENT= 0.03315

AFTERBODY DRAG COEFFICIENT= 0.02622

STATUS OF ITERATION

XMAX = 9.9845
 UECHK = 3.0180
 DRHS = 1.1709

**** ITERATION FOR BOUNDARY LAYER/INVISCID FLOW EQUILIBRIUM CONVERGED ****

*** FINAL RESULTS ***

BEST SOLUTION WAS ITERATION NO. 13

XSEP = 8.5125
 DRHS = 0.7385

(k) Final page of output.
 Figure 14.- Concluded.

```
NASA CONFIGURATION 1
(BLANK CARD)
RESTARTING ITERATION SCHEME AFTER    ITERATIONS FOR RUN
  1      0  600
```

Figure 15.- Sample input data for restart.

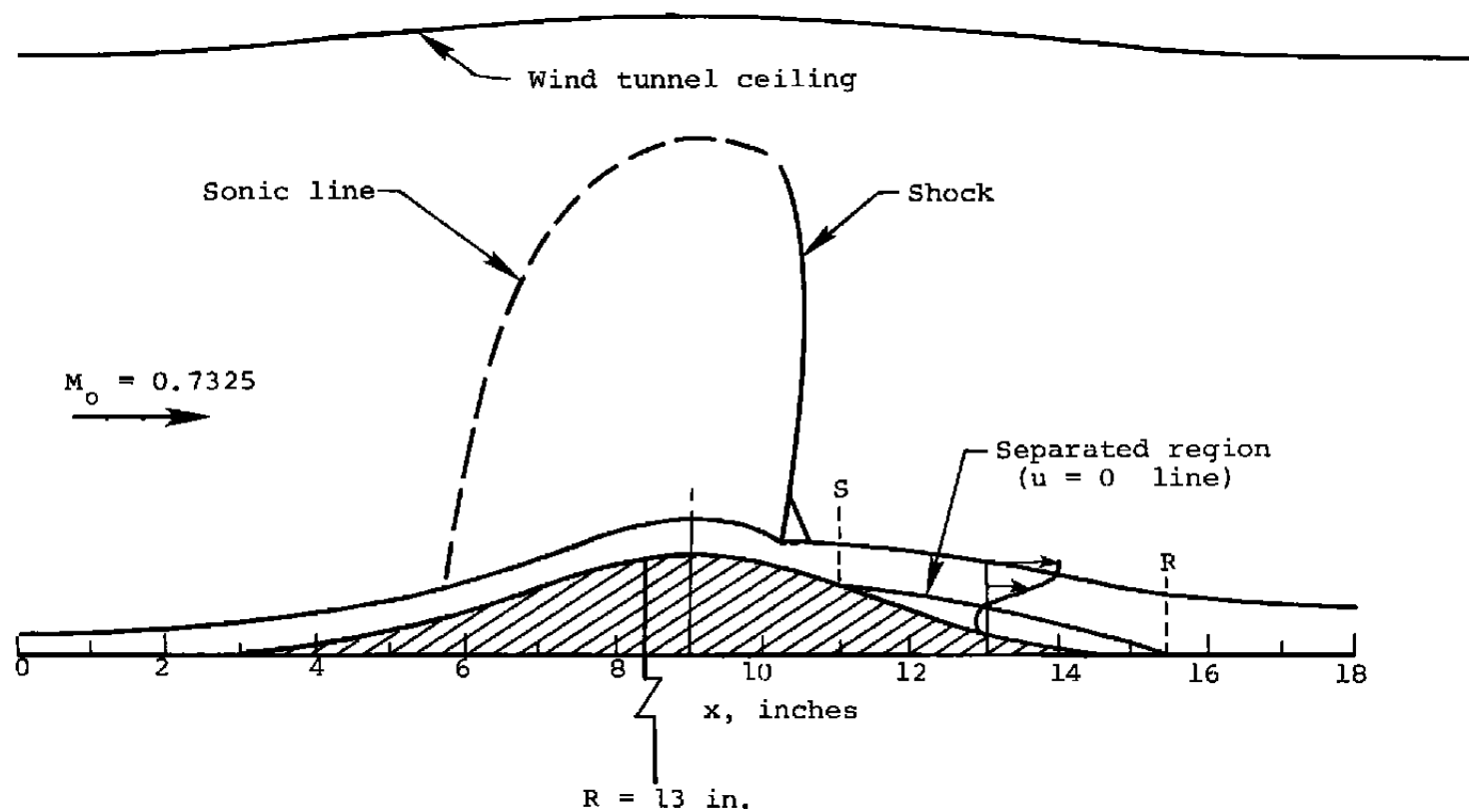


Figure 16.- Two-dimensional configuration for boundary-layer calculation.

```

      AL3ER TEST CASE
      TWO-DIMENSIONAL BOUNDARY LAYER CALCULATION
      SPECIFYING VELOCITY DISTRIBUTION FROM X=0
0      0      0
1      0      0      0      2      0
1.4    .7325
1      0      0      0      2      0      0
22
0.0    9750.
1.0    9480.
2.0    9400.
3.0    8500.
4.0    8650.
5.0    9750.
6.0    11650.
7.0    12980.
8.0    14200.
9.0    15480.
10.0   16100.
10.25  14800.
10.75  13400.
11.0   12600.
11.50  12100.
12.0   11150.
13.0   10900.
14.0   10800.
15.0   10300.
16.0   9900.
17.0   9800.
18.0   10200.
19.0   15.0   585.0   .99   0.0   0.0   0.0   0.0
20.0   15.0   -5.0   0.0   0.0   0.0   0.0   0.0
.00233 .065
19
0.0    0.0
1.0    0.0
2.0    0.0
3.0    0.0
4.0    0.25
5.0    0.50
6.0    0.70
7.0    0.85
8.0    0.98
9.0    1.0
10.0   0.98
11.0   0.85
12.0   0.70
13.0   0.50
14.0   0.25
15.0   0.0
16.0   0.0
17.0   0.0
18.0   0.0

```

(a) Input for case with u_e specified.

Figure 17.- Input data for two-dimensional boundary-layer calculation.

```

      ALBER TEST CASE
      TWO-DIMENSIONAL BOUNDARY LAYER CALCULATION
      SPECIFYING DELST DISTRIBUTION FROM X=10.75
3      0      0
1      0      0      0      2      0
1.4    .7325
2      0      0      0      2      0      0
13
10.0    .03
10.25   .05
10.75   .07
11.0    .083
11.5    .112
12.0    .148
13.0    .314
14.0    .435
14.5    .460
15.0    .440
16.0    .306
17.0    .230
18.0    .190
1.0     15.0    585.0    .99    0.0    0.0    0.0    0.0
10.75   18.0    -5.0     0.0    0.0    0.0    0.0    0.0
.00077
13400.  -2820.
19
0.0     0.0
1.0     0.0
2.0     0.0
3.0     0.0
4.0     0.25
5.0     0.50
6.0     0.70
7.0     0.85
8.0     0.98
9.0     1.0
10.0    0.98
11.0    0.85
12.0    0.70
13.0    0.50
14.0    0.25
15.0    0.0
16.0    0.0
17.0    0.0
18.0    0.0

```

(b) Input data for case with δ^* specified.

Figure 17.- Concluded.

U2 = 9.90272E-03
HL2 = 3.02426E-05
NU2 = 3.27443E-02

AX	UTAU	DELTA	DELST	THETA	CF	UE/UY	DELST+R	Ox	HTR
0.0	3.32242E-02	3.90140E-01	6.52716E-02	3.48384E-02	2.33000E-03	0.98458	6.52716E-02	0.0	1.1853
5.00000E-01	3.21310E-02	3.95803E-01	6.53929E-02	3.91283E-02	2.24705E-03	0.97097	6.93925E-02	1.250E-01	1.2071
1.00000E-00	3.10535E-02	4.10471E-01	7.37869E-02	4.15399E-02	2.16527E-03	0.95731	7.37869E-02	1.250E-01	1.2288
1.50000E-00	3.08112E-02	4.20119E-01	7.55540E-02	4.25883E-02	2.15244E-03	0.95328	7.55540E-02	1.250E-01	1.2293
2.00000E-00	3.05810E-02	4.29808E-01	7.73537E-02	4.36547E-02	2.13935E-03	0.94923	7.73537E-02	1.250E-01	1.2300
2.50000E-00	2.67428E-02	4.51450E-01	9.40342E-02	5.19691E-02	1.82001E-03	0.90439	9.40342E-02	1.250E-01	1.3310
3.00000E-00	2.25967E-02	4.65408E-01	1.18051E-01	6.25757E-02	1.45358E-03	0.85835	1.18051E-01	1.250E-01	1.4640
3.50000E-00	2.38377E-02	4.91889E-01	1.12308E-01	6.08659E-02	1.56700E-03	0.86593	2.37308E-01	1.250E-01	1.4072
4.00000E-00	2.49044E-02	4.98707E-01	1.07677E-01	5.93432E-02	1.70071E-03	0.87350	3.57677E-01	1.250E-01	1.3613
4.50000E-00	3.00004E-02	4.87966E-01	8.40818E-02	4.81035E-02	2.15565E-03	0.92949	4.59042E-01	1.250E-01	1.2059
5.00000E-00	3.43194E-02	4.89869E-01	6.54349E-02	3.98973E-02	2.48613E-03	0.98458	5.69435E-01	1.250E-01	1.0984
5.50000E-00	4.12164E-02	5.12647E-01	5.25946E-02	2.88568E-02	2.99462E-03	1.08214	6.52600E-01	1.250E-01	0.9447
6.00000E-00	4.72248E-02	5.79759E-01	4.32235E-02	2.11964E-02	3.15095E-03	1.17644	7.43223E-01	1.250E-01	0.8087
6.50000E-00	5.10831E-02	6.49677E-01	3.95237E-02	1.65049E-02	3.23355E-03	1.24456	8.14524E-01	1.250E-01	0.6903
7.00000E-00	5.46276E-02	4.73384E-01	3.81249E-02	1.73663E-02	3.26948E-03	1.31375	8.88125E-01	1.250E-01	0.6184
7.50000E-00	5.84737E-02	5.41189E-01	3.61652E-02	1.45727E-02	3.34613E-03	1.37327	9.51165E-01	1.250E-01	0.7132
8.00000E-00	6.15961E-02	7.38021E-01	3.61176E-02	1.10344E-02	3.33669E-03	1.43395	1.01612E-00	1.250E-01	0.5954
8.50000E-00	6.63138E-02	3.24316E-01	3.25074E-02	1.35469E-02	3.45291E-03	1.49974	1.02251E-00	1.250E-01	0.6748
9.00000E-00	7.08443E-02	3.51955E-01	3.19577E-02	1.27136E-02	3.54016E-03	1.56321	1.03196E-00	1.250E-01	0.8211
9.50000E-00	7.28881E-02	3.56577E-01	3.25226E-02	1.20038E-02	3.55447E-03	1.54481	1.02252E-00	1.250E-01	0.8151
1.00000E-01	7.49256E-02	3.60902E-01	3.31672E-02	1.14900E-02	3.56767E-03	1.62581	1.01317E-00	1.250E-01	0.8107
1.05000E-01	5.69590E-02	1.97371E-01	3.51045E-02	1.62790E-02	2.09740E-03	1.42514	9.50104E-01	1.250E-01	1.1481
1.10000E-01	4.02644E-02	2.01348E-01	5.12561E-02	2.38486E-02	1.90670E-03	1.27238	9.01250E-01	1.250E-01	1.4164
1.15000E-01	3.53120E-02	2.17810E-01	6.01054E-02	2.76050E-02	1.61324E-03	1.22188	8.35165E-01	1.250E-01	1.5065
1.20000E-01	2.34226E-02	2.56450E-01	8.56149E-02	3.67189E-02	8.57211E-04	1.12595	7.89615E-01	1.250E-01	1.8657
1.25000E-01	2.49922E-02	2.71578E-01	8.52057E-02	3.83132E-02	1.00182E-03	1.11336	6.89206E-01	1.250E-01	1.7627
1.30000E-01	2.57452E-02	2.87398E-01	9.05402E-02	4.00555E-02	1.09042E-03	1.10071	5.90540E-01	1.250E-01	1.7029
1.35000E-01	2.71775E-02	3.00251E-01	8.91904E-02	4.08723E-02	1.22784E-03	1.09586	4.64191E-01	1.250E-01	1.6243
1.40000E-01	2.81568E-02	3.13199E-01	8.67628E-02	4.17275E-02	1.33169E-03	1.09061	3.38763E-01	1.250E-01	1.5686
1.45000E-01	2.62903E-02	3.34089E-01	9.75644E-02	4.54369E-02	1.27371E-03	1.06547	2.22564E-01	1.250E-01	1.6110
1.50000E-01	2.43585E-02	3.57543E-01	1.67992E-01	4.96323E-02	1.10873E-03	1.04012	1.07992E-01	1.250E-01	1.6616

(a) Output from case with u_e specified.

Figure 18.- Output from two-dimensional boundary-layer calculation.

U2 = 9.40277E 03
 DEL = 3.02421E 05
 NU2 = 3.27443E-02

AX	UTAU	DFI,TA	DEL ST	THETA	CF	UC/UZ	BLIST+H	JX	MIN
1.07500E 01	2.75853E 02	1.78872E-01	7.00000E-02	2.49773E-02	7.71981E-04	1.35316	9.52500E-01	0.0	1.0001
1.38750E 01	2.40572E 02	1.88064E-01	7.64997E-02	2.64890E-02	6.43730E-04	1.33210	9.42750E-01	3.125E-02	2.0024
1.61333E 01	2.21472E 02	1.90021E-01	8.29599E-02	2.79512E-02	5.37044E-04	1.31357	9.33000E-01	3.175E-02	2.1801
1.81500E 01	1.46280E 02	2.45650E-01	1.12030E-01	3.39078E-02	2.60483E-04	1.25296	8.87000E-01	1.250E-01	2.5041
1.20000E 01	9.16353E 01	3.04655E-01	1.48000E-01	4.03973E-02	1.12045E-04	1.20558	8.48000E-01	1.250E-01	2.9501
1.25000E 01	8.20830E 00	4.23961E-01	2.31000E-01	4.79095E-02	-9.75678E-07	1.17132	8.31000E-01	1.250E-01	4.0877
1.30000E 01	5.42523E 01	5.44706E 01	3.14000E-01	5.36157E-02	-4.33315E-05	1.15567	8.14000E-01	1.250E-01	5.1343
1.35000E 01	6.56214E 01	6.38768E-01	3.75000E-01	5.95115E-02	-6.51881E-05	1.14165	7.49500E-01	1.250E-01	5.6144
1.40000E 01	7.71282E 01	7.29138E-01	4.35000E-01	6.35875E-02	-9.13034E-05	1.13480	6.85000E-01	1.250E-01	6.2043
1.45000E 01	7.18564E 01	7.70348E-01	4.60000E-01	6.92785E-02	-4.11766E-05	1.12291	5.85000E-01	1.250E-01	6.3171
1.50000E 01	4.45044E 01	7.73524E-01	4.40000E-01	7.83358E-02	-3.26269E-05	1.10182	4.40000E-01	1.250E-01	4.9422
1.55000E 01	2.00228E 01	7.15603E-01	3.73000E-01	8.64426E-02	6.84464E-06	1.08002	3.73000E-01	1.250E-01	3.7074
1.60000E 01	8.27965E 01	6.58124E-01	3.06000E-01	9.05431E-02	1.20372E-04	1.06939	3.06000E-01	1.250E-01	2.8750
1.65000E 01	1.25059E 02	6.34677E-01	2.68000E-01	9.15319E-02	2.80038E-04	1.06617	2.68000E-01	1.250E-01	2.3087
1.70000E 01	1.72094E 02	6.12617E-01	2.30000E-01	8.94214E-02	5.21237E-04	1.07271	2.30000E-01	1.250E-01	2.3342
1.75000E 01	2.02841E 02	6.08530E-01	2.10000E-01	8.76884E-02	7.08257E-04	1.07886	2.10000E-01	1.250E-01	1.8524
1.80000E 01	2.14176E 02	6.03411E-01	1.90000E-01	8.43694E-02	9.19959E-04	1.09125	1.90000E-01	1.250E-01	1.6961

(b) Output from case with c^* specified.

Figure 18.- Concluded.

NASA DATA COMPARISON - CONFIGURATION 1
 JET SIMULATED WITH A SOLID STING
 ROATTAIL L/D = 0.8

0	0	700			
-1	0	0	1	1	0
1.4		0.9			
98					
0.0		0.0			
0.1		0.025013			
0.2		0.059026			
0.3		0.075038			
0.4		0.100051			
0.5		0.125064			
0.6		0.150077			
0.7		0.175090			
0.8		0.200102			
0.9		0.225115			
1.0		0.250128			
1.1		0.275141			
1.2		0.300154			
1.3		0.325166			
1.4		0.350179			
1.5		0.375192			
1.6		0.400205			
1.7		0.425218			
1.8		0.450230			
1.9		0.473630			
2.0		0.489760			
2.1		0.498366			
2.2		0.500000			
2.3		0.500000			
2.5		0.500000			
3.0		0.500000			
3.5		0.500000			
4.0		0.500000			
5.0		0.500000			
6.0		0.500000			
7.0		0.500000			
7.5		0.500000			
8.0		0.500000			
8.025		0.499781			
8.05		0.499125			
8.075		0.498030			
8.1		0.496496			
8.125		0.494521			
8.15		0.492104			
8.175		0.489241			
8.2		0.485931			
8.225		0.482171			
8.25		0.477956			

(a) First 50 cards.

Figure 19.- Input data for inviscid calculation.

8.275	0.473282
8.3	0.468146
8.325	0.462542
8.35	0.456463
8.375	0.449905
8.4	0.442859
8.425	0.435319
8.45	0.427277
8.475	0.418722
8.5	0.409646
8.525	0.400037
8.55	0.389885
8.575	0.379176
8.6	0.367897
8.625	0.356032
8.65	0.343565
8.675	0.330479
8.7	0.316753
8.725	0.302368
8.75	0.287298
8.775	0.271518
8.8	0.255000
8.81	0.255000
8.82	0.255000
8.83	0.255000
8.84	0.255000
8.85	0.255000
8.86	0.255000
8.87	0.255000
8.88	0.255000
8.89	0.255000
8.9	0.255000
8.92	0.255000
8.94	0.255000
8.96	0.255000
8.98	0.255000
9.0	0.255000
9.025	0.255000
9.05	0.255000
9.075	0.255000
9.1	0.255000
9.15	0.255000
9.2	0.255000
9.3	0.255000
9.4	0.255000
9.5	0.255000
9.7	0.255000
9.9	0.255000
10.1	0.255000
10.3	0.255000

(b) Next 50 cards.

Figure 19.- Continued.

10.5		0.255000						
10.8		0.255000						
11.2		0.255000						
11.6		0.255000						
12.0		0.255000						
81	31	0	0	0				
0.0		0.0		0.0	0.0	8.8	1.0	8.0
F								

(c) Remaining 7 cards.

Figure 19.- Concluded.

----- NORMAL COORD. STRETCH FOR ALF= 1.300 -----

J	AN	G	GH
1	-0.6900E-76	0.0	0.7725E-04
2	0.1617E+03	0.1545E-03	0.4607E-03
3	0.6339E+02	0.7668E-03	0.1365E-02
4	0.3608E+02	0.1964E-02	0.2900E-02
5	0.2391E+02	0.3836E-02	0.5149E-02
6	0.1720E+02	0.6450E-02	0.8183E-02
7	0.1303E+02	0.9905E-02	0.1207E-01
8	0.1022E+02	0.1424E-01	0.1687E-01
9	0.8215E+01	0.1951E-01	0.2265E-01
10	0.6729E+01	0.2579E-01	0.2947E-01
11	0.5585E+01	0.3314E-01	0.3739E-01
12	0.4690E+01	0.4161E-01	0.4643E-01
13	0.3968E+01	0.5126E-01	0.5670E-01
14	0.3377E+01	0.6215E-01	0.6824E-01
15	0.2886E+01	0.7433E-01	0.8110E-01
16	0.2474E+01	0.8787E-01	0.9535E-01
17	0.2123E+01	0.1028E+00	0.1110E+00
18	0.1822E+01	0.1193E+00	0.1280E+00
19	0.1551E+01	0.1372E+00	0.1470E+00
20	0.1334E+01	0.1569E+00	0.1674E+00
21	0.1135E+01	0.1780E+00	0.1895E+00
22	0.9585E+00	0.2010E+00	0.2134E+00
23	0.8070E+00	0.2258E+00	0.2371E+00
24	0.6670E+00	0.2524E+00	0.2667E+00
25	0.5371E+00	0.2810E+00	0.2963E+00
26	0.4245E+00	0.3116E+00	0.3289E+00
27	0.3227E+00	0.3443E+00	0.3517E+00
28	0.2304E+00	0.3792E+00	0.3977E+00
29	0.1465E+00	0.4163E+00	0.4360E+00
30	0.7000E-01	0.4552E+00	0.4767E+00
31	0.1150E-06	0.4976E+00	0.5198E+00

(a) Normal coordinates.

Figure 20.- Output for inviscid calculation.

I	S	X	Y	THET	THETB	AK	F
1	0.0	0.0	0.0	0.9000E+02	0.9000E+02	0.3392E-04	0.1786E+00
2	0.7013E-01	0.6804E-01	0.1702E-01	0.1404E+02	0.1404E+02	0.3263E-04	0.1776E+00
3	0.1411E+00	0.1369E+00	0.3423E-01	0.1404E+02	0.1404E+02	0.3508E-04	0.1746E+00
4	0.2136E+00	0.2072E+00	0.5183E-01	0.1404E+02	0.1404E+02	0.1710E-03	0.1698E+00
5	0.2885E+00	0.2799E+00	0.7001E-01	0.1404E+02	0.1404E+02	0.1137E-03	0.1637E+00
6	0.3666E+00	0.3556E+00	0.8896E-01	0.1404E+02	0.1404E+02	0.6476E-04	0.1565E+00
7	0.4486E+00	0.4352E+00	0.1098E+00	0.1404E+02	0.1404E+02	0.3181E-04	0.1484E+00
8	0.5351E+00	0.5191E+00	0.1292E+00	0.1404E+02	0.1404E+02	0.3862E-05	0.1403E+00
9	0.6269E+00	0.6082E+00	0.1521E+00	0.1404E+02	0.1404E+02	0.4738E-04	0.1321E+00
10	0.7246E+00	0.7030E+00	0.1758E+00	0.1404E+02	0.1404E+02	0.2102E-03	0.1240E+00
11	0.8288E+00	0.8040E+00	0.2011E+00	0.1404E+02	0.1404E+02	0.2119E-03	0.1162E+00
12	0.9399E+00	0.9118E+00	0.2281E+00	0.1404E+02	0.1404E+02	0.5590E-04	0.1089E+00
13	0.1058E+01	0.1027E+01	0.2568E+00	0.1404E+02	0.1404E+02	0.2978E-04	0.1021E+00
14	0.1185E+01	0.1149E+01	0.2875E+00	0.1404E+02	0.1404E+02	0.3230E-04	0.9586E-01
15	0.1319E+01	0.1280E+01	0.3201E+00	0.1404E+02	0.1404E+02	0.1697E-03	0.9013E-01
16	0.1452E+01	0.1419E+01	0.3548E+00	0.1404E+02	0.1404E+02	0.9192E-04	0.8493E-01
17	0.1614E+01	0.1556E+01	0.3916E+00	0.1404E+02	0.1404E+02	0.3839E-03	0.8022E-01
18	0.1774E+01	0.1721E+01	0.4304E+00	0.1406E+02	0.1406E+02	0.1258E-03	0.7599E-01
19	0.1943E+01	0.1885E+01	0.4705E+00	0.1221E+02	0.1221E+02	0.7319E+00	0.7220E-01
20	0.2120E+01	0.2060E+01	0.4959E+00	0.4519E+01	0.4519E+01	0.7878E+00	0.6891E-01
21	0.2306E+01	0.2246E+01	0.5000E+00	-0.1302E+00	-0.1302E+00	0.1413E-01	0.6579E-01
22	0.2500E+01	0.2440E+01	0.5000E+00	0.0	0.9817E-02	-0.1476E-02	0.6312E-01
23	0.2702E+01	0.2642E+01	0.5000E+00	0.0	0.1970E-02	0.7913E-03	0.6078E-01
24	0.2917E+01	0.2851E+01	0.5000E+00	0.0	-0.3575E-02	0.1335E-03	0.5873E-01
25	0.3127E+01	0.3058E+01	0.5000E+00	0.0	-0.1543E-02	-0.2754E-03	0.5695E-01
26	0.3350E+01	0.3290E+01	0.5000E+00	0.0	0.7465E-03	-0.8351E-04	0.5544E-01
27	0.3570E+01	0.3518E+01	0.5000E+00	0.0	0.5621E-03	0.9205E-04	0.5417E-01
28	0.3811E+01	0.3751E+01	0.5000E+00	0.0	-0.1860E-03	0.2000E-04	0.5314E-01
29	0.4048E+01	0.3988E+01	0.5000E+00	0.0	0.4014E-04	-0.5329E-04	0.5234E-01
30	0.4289E+01	0.4229E+01	0.5000E+00	0.0	0.5544E-03	-0.1603E-04	0.5176E-01
31	0.4531E+01	0.4471E+01	0.5000E+00	0.0	0.4761E-03	0.2730E-04	0.5140E-01
32	0.4775E+01	0.4715E+01	0.5000E+00	0.0	-0.2088E-03	0.7093E-04	0.5126E-01
33	0.5018E+01	0.4958E+01	0.5000E+00	0.0	-0.1502E-02	0.1144E-03	0.5135E-01
34	0.5261E+01	0.5201E+01	0.5000E+00	0.0	-0.2547E-02	0.1074E-04	0.5169E-01
35	0.5502E+01	0.5442E+01	0.5000E+00	0.0	-0.1779E-02	-0.1221E-03	0.5227E-01
36	0.5739E+01	0.5679E+01	0.5000E+00	0.0	0.7712E-03	-0.2531E-03	0.5314E-01
37	0.5972E+01	0.5912E+01	0.5000E+00	0.0	0.5005E-02	-0.3817E-03	0.5430E-01
38	0.6199E+01	0.6139E+01	0.5000E+00	0.0	0.9360E-02	-0.1491E-03	0.5580E-01
39	0.6419E+01	0.6359E+01	0.5001E+00	0.0	0.8405E-02	0.2994E-03	0.5769E-01
40	0.6632E+01	0.6572E+01	0.5001E+00	0.0	0.2130E-02	0.7309E-03	0.6001E-01
41	0.6836E+01	0.6776E+01	0.5001E+00	0.0	-0.8812E-02	0.1144E-02	0.6285E-01
42	0.7029E+01	0.6970E+01	0.5000E+00	0.0	-0.2370E-01	0.1538E-02	0.6630E-01
43	0.7212E+01	0.7153E+01	0.4999E+00	0.0	-0.2564E-01	-0.1553E-02	0.7049E-01
44	0.7384E+01	0.7324E+01	0.4999E+00	0.0	0.6027E-02	-0.5098E-02	0.7556E-01

(b) Tangential coordinates.

Figure 20.- Continued.

45	0.7543E+01	0.7483E+01	0.5000E+00	0.0	0.6755E-01	-0.8370E-02	0.8172E-01
46	0.7690E+01	0.7630E+01	0.5002E+00	0.0	0.1002E+00	0.2183E-02	0.8924E-01
47	0.7823E+01	0.7763E+01	0.5004E+00	0.0	0.4047E-01	0.1342E-01	0.5845E-01
48	0.7944E+01	0.7884E+01	0.5004E+00	0.0	-0.8710E-01	0.2756E-01	0.1058E+00
49	0.8051E+01	0.7991E+01	0.5000E+00	0.0	-0.2597E+00	0.3260E-01	0.1237E+00
50	0.8146E+01	0.8086E+01	0.4974E+00	0.0	-0.3447E+01	0.7092E+00	0.1409E+00
51	0.8227E+01	0.8167E+01	0.4900E+00	0.0	-0.6787E+01	0.7148E+00	0.1618E+00
52	0.8301E+01	0.8241E+01	0.4796E+00	0.0	-0.9704E+01	0.7329E+00	0.1866E+00
53	0.8353E+01	0.8293E+01	0.4674E+00	0.0	-0.1225E+02	0.7509E+00	0.2145E+00
54	0.8410E+01	0.8350E+01	0.4544E+00	0.0	-0.1451E+02	0.7702E+00	0.2426E+00
55	0.8467E+01	0.8407E+01	0.4402E+00	0.0	-0.1656E+02	0.7926E+00	0.2647E+00
56	0.8513E+01	0.8453E+01	0.4261E+00	0.0	-0.1850E+02	0.8233E+00	0.2727E+00
57	0.8560E+01	0.8500E+01	0.4097E+00	0.0	-0.2049E+02	0.8550E+00	0.2609E+00
58	0.8610E+01	0.8550E+01	0.3899E+00	0.0	-0.2264E+02	0.8942E+00	0.2376E+00
59	0.8664E+01	0.8605E+01	0.3658E+00	0.0	-0.2507E+02	0.9434E+00	0.2192E+00
60	0.8724E+01	0.8664E+01	0.3362E+00	0.0	-0.2771E+02	0.1053E+01	0.1997E+00
61	0.8790E+01	0.8730E+01	0.2954E+00	0.0	-0.3126E+02	0.1177E+01	0.1812E+00
62	0.8863E+01	0.8803E+01	0.2547E+00	0.0	-0.2635E+01	-0.4422E+02	0.1635E+00
63	0.8943E+01	0.8883E+01	0.2550E+00	0.0	-0.2683E-04	-0.1016E-02	0.1467E+00
64	0.9033E+01	0.8973E+01	0.2550E+00	0.0	-0.1808E-05	0.2323E-06	0.1309E+00
65	0.9135E+01	0.9075E+01	0.2550E+00	0.0	-0.0403E-09	-0.1933E-08	0.1159E+00
66	0.9250E+01	0.9190E+01	0.2550E+00	0.0	0.3146E-10	-0.4979E-11	0.1019E+00
67	0.9381E+01	0.9321E+01	0.2550E+00	0.0	-0.2712E-11	-0.3307E-11	0.8877E-01
68	0.9533E+01	0.9473E+01	0.2550E+00	0.0	-0.7623E-12	0.1610E-12	0.7654E-01
69	0.9710E+01	0.9650E+01	0.2550E+00	0.0	0.2602E-12	-0.1067E-13	0.6522E-01
70	0.9919E+01	0.9859E+01	0.2550E+00	0.0	-0.7049E-13	-0.4717E-15	0.5490E-01
71	0.1017E+02	0.1011E+02	0.2550E+00	0.0	0.1153E-13	0.3913E-14	0.4529E-01
72	0.1048E+02	0.1042E+02	0.2550E+00	0.0	0.9092E-15	-0.3215E-15	0.3669E-01
73	0.1086E+02	0.1080E+02	0.2550E+00	0.0	-0.3641E-15	-0.5504E-16	0.2899E-01
74	0.1135E+02	0.1129E+02	0.2550E+00	0.0	0.2997E-16	0.1040E-16	0.2219E-01
75	0.1201E+02	0.1195E+02	0.2550E+00	0.0	0.4933E-17	0.1323E-17	0.1630E-01
76	0.1293E+02	0.1287E+02	0.2550E+00	0.0	0.0	0.0	0.1135E-01
77	0.1431E+02	0.1425E+02	0.2550E+00	0.0	0.0	0.0	0.7247E-02
78	0.1661E+02	0.1655E+02	0.2550E+00	0.0	0.0	0.0	0.4076E-02
79	0.2121E+02	0.2115E+02	0.2550E+00	0.0	0.0	0.0	0.1812E-02
80	0.3501E+02	0.3495E+02	0.2550E+00	0.0	0.0	0.0	0.4530E-03
81	0.1000E+31	0.1000E+31	0.2550E+00	0.0	0.0	0.0	0.1000E-29

(b) Concluded.

Figure 20.- Continued.

ITERATION NO. 1

IT	DMAX	ID	JD	RMAX	IR	JR	ISUB	ISUP	RAVG	PF1	QF3	NS	SEC/CYC
1	0.408E-01	61	31	0.312E+02	1	31	1	0	0.149E+00	1.400	0.100	0	0.180
2	0.237E-01	2	31	0.119E+02	1	31	1	0	0.104E+00	1.400	0.100	0	0.180
3	0.186E-01	1	31	0.168E+02	1	31	1	0	0.963E-01	1.400	0.100	0	0.180
4	0.164E-01	2	31	0.666E+01	59	31	1	0	0.825E-01	1.400	0.100	0	0.180
5	0.138E-01	1	31	0.125E+02	1	31	1	0	0.788E-01	1.400	0.100	0	0.180
6	0.967E-02	58	31	0.444E+01	58	31	1	0	0.705E-01	1.400	0.100	0	0.180
7	0.845E-02	59	31	0.411E+01	62	31	1	0	0.637E-01	1.400	0.100	0	0.180
8	0.757E-02	57	31	0.384E+01	62	31	1	0	0.603E-01	1.400	0.100	0	0.180
9	0.681E-02	57	31	0.362E+01	62	31	1	0	0.580E-01	1.400	0.100	0	0.180
10	0.617E-02	56	31	0.366E+01	1	31	1	0	0.567E-01	1.400	0.100	0	0.180
11	0.562E-02	56	31	0.326E+01	62	31	1	0	0.534E-01	1.400	0.100	0	0.180
12	0.507E-02	55	31	0.311E+01	62	31	1	0	0.507E-01	1.400	0.100	0	0.180
13	0.474E-02	61	31	0.292E+01	62	31	1	0	0.491E-01	1.400	0.100	0	0.180
14	0.454E-02	61	31	0.286E+01	62	31	1	0	0.486E-01	1.400	0.100	0	0.180
15	0.435E-02	61	31	0.275E+01	62	31	1	0	0.474E-01	1.400	0.100	0	0.180
16	0.417E-02	61	31	0.265E+01	62	31	1	0	0.461E-01	1.400	0.100	3	0.180
17	0.401E-02	61	31	0.255E+01	62	31	1	0	0.447E-01	1.400	0.100	4	0.170
18	0.387E-02	61	31	0.246E+01	62	31	1	0	0.439E-01	1.400	0.100	4	0.170
19	0.373E-02	61	31	0.238E+01	62	31	1	0	0.431E-01	1.400	0.100	5	0.180
20	0.361E-02	61	31	0.230E+01	62	31	1	0	0.423E-01	1.400	0.100	5	0.180

RMAX= 0.23E+01, COVR= 0.15E-01

(c) Iteration history.

Figure 20.- Continued.

ITERATION NO. 1

PLOT OF CP AT EQUAL XI-INCREMENTS

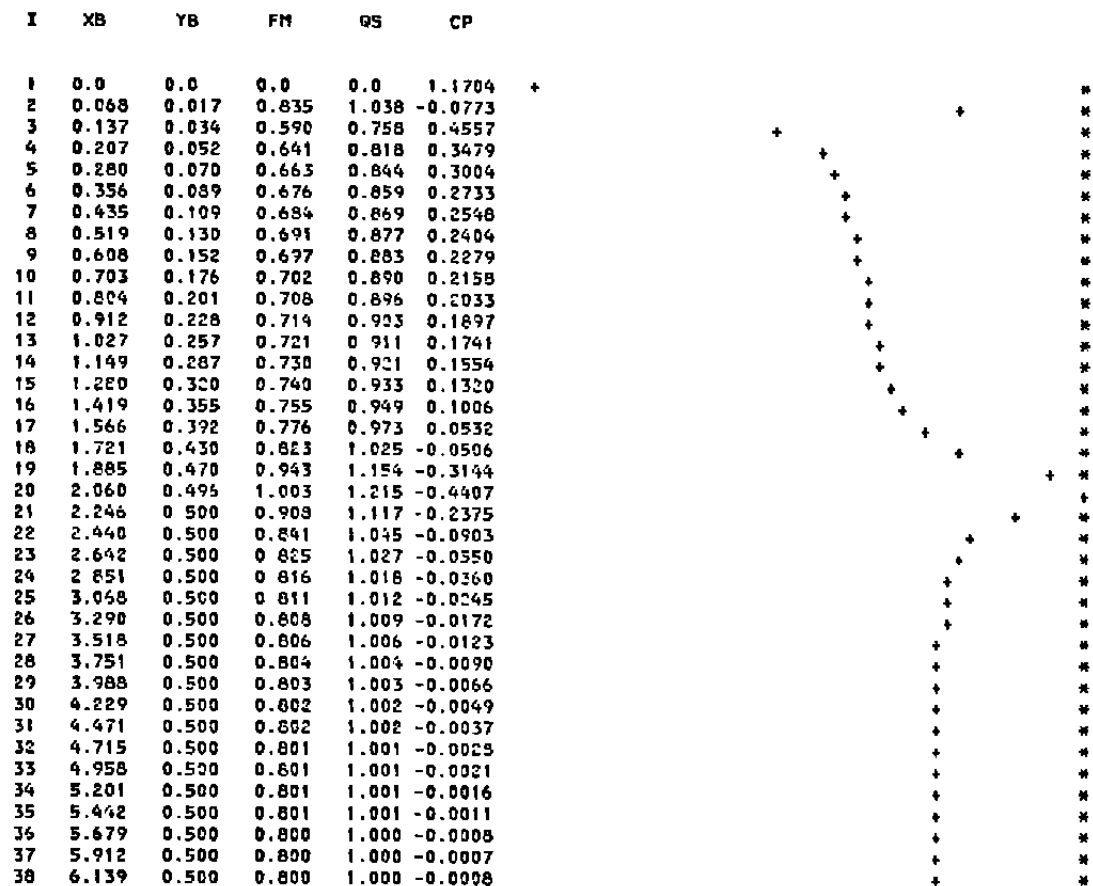
(d) Tabulated solution and plot of C_p .

Figure 20.- Continued.

39	6.359	0.500	0.801	1.001	-0.0012
40	6.572	0.500	0.801	1.001	-0.0018
41	6.776	0.500	0.801	1.001	-0.0026
42	6.970	0.500	0.802	1.002	-0.0036
43	7.153	0.500	0.802	1.002	-0.0049
44	7.324	0.500	0.804	1.004	-0.0083
45	7.483	0.500	0.808	1.008	-0.0168
46	7.630	0.500	0.815	1.017	-0.0340
47	7.763	0.500	0.828	1.031	-0.0628
48	7.884	0.500	0.851	1.055	-0.1118
49	7.991	0.500	0.912	1.122	-0.2473
50	8.086	0.497	0.973	1.202	-0.4190
51	8.169	0.490	1.031	1.234	-0.4985
52	8.241	0.480	1.040	1.234	-0.5170
53	8.303	0.467	1.033	1.217	-0.5037
54	8.358	0.454	1.013	1.186	-0.4623
55	8.407	0.441	0.989	1.151	-0.4111
56	8.453	0.426	0.963	1.114	-0.3565
57	8.500	0.410	0.923	1.061	-0.2712
58	8.550	0.390	0.868	0.992	-0.1509
59	8.605	0.366	0.794	0.900	0.0134
60	8.664	0.336	0.685	0.770	0.2531
61	8.730	0.299	0.490	0.544	0.6544
62	8.803	0.255	0.487	0.532	0.6401
63	8.833	0.255	0.561	0.702	0.5158
64	8.974	0.255	0.627	0.801	0.3783
65	9.075	0.255	0.673	0.856	0.2791
66	9.190	0.255	0.708	0.896	0.2029
67	9.321	0.255	0.735	0.927	0.1444
68	9.473	0.255	0.755	0.949	0.1002
69	9.650	0.255	0.770	0.966	0.0676
70	9.859	0.255	0.780	0.978	0.0441
71	10.110	0.255	0.787	0.986	0.0277
72	10.417	0.255	0.792	0.992	0.0167
73	10.800	0.255	0.796	0.995	0.0096
74	11.293	0.255	0.798	0.997	0.0051
75	11.950	0.255	0.799	0.999	0.0025
76	12.870	0.255	0.799	0.999	0.0011
77	14.250	0.255	0.800	1.000	0.0004
78	16.550	0.255	0.800	1.000	0.0001
79	21.150	0.255	0.800	1.000	0.0000
80	34.948	0.255	0.800	1.000	0.0
81*****	0.255	0.800	1.000	0.0	

TOTAL BODY DRAG COEFFICIENT= 0.07332

AFTERBODY DRAG COEFFICIENT= 0.04269

(d) Concluded.
Figure 20.- Continued.

ITERATION NO. 1

NO. OF SONIC PTS. ON EACH CONSAANT-J LINE, STARTING WITH J-JMAX (BODY SURFACE) AT LEFT

4 0

N= 4

XS(K), K=1,...,N

0.205E+01 0.207E+01 0.810E+01 0.838E+01

YS(K), K=1,...,N

0.495E+00 0.496E+00 0.495E+00 0.497E+00

(e) Sonic point distribution.

Figure 20.- Concluded.

TABLE I. RELATION BETWEEN EXTERNAL DATA SETS
AND INPUT/OUTPUT LOGICAL UNIT NUMBERS

<u>Data File</u> <u>(fig. 12)</u>	<u>Logical Unit</u>	
	<u>Input</u>	<u>Output</u>
1	14	9
2	13	8
3	12	2
4	15	10
5	11	3

TABLE II. BASIC INPUT DATA

<u>Item No.</u>	<u>Variables</u>	<u>Format</u>
1	TITLE (three cards)	20A4
2	NRSTRT,N3,ILIM If NRSTRT \neq 0 and N3 \neq 0, skip to item 12 If NRSTRT \neq 0 and N3 \neq 0 stop. No further input is necessary	3I5
3	LPROG,N1,N2,IBL,IUNIT,MIT	6I5
4	GAM,AMINF If LPROG = 1 skip to item 13	
5	IXY If IXY = 0, skip next card	I5
6	XO,YO (IXY cards)	2F10.0
7	IMAX,JMAX,MHALF,KLOSE,LREADP	5I5
8	DNDZO,XIXM,XM,DSDXIM,XBT,DMAX,XZNEW	7F10.0
9	PLUMIN If PLUMIN = FALSE, skip next card	L5
10	GAMAP,PTPPFS,AMP,THETAP,TTP,GMP,XJ,GC If LPROG = -1, skip remaining cards	7F10.0
11	LSEP,LITER,LNSHK If LSEP = FALSE, skip next card	L5
12	XSEP,DTHET If NRSTRT \neq 0 stop. No further input is necessary	2F10.0

TABLE II. CONCLUDED

<u>Item No.</u>	<u>Variables</u>	<u>Format</u>
13	IOPT,K,LVAR1,LSHAPE,LIC,LDSTAR,LSHPBL If LPROG \neq 1 or if LPROG = 1 and both IOPT = 1 and LVAR1 = 2, skip items 14 and 15	7I5
14	NVAR	I5
15	XVAR,VAR	2F10.0
16	EL,PT,TT,TWONTT,VISC,RGAS,SCON,DFACT	8F10.0
17	XZ,RLEN,XT,DXP,HLIM If LSHAPE \neq 0, skip next card If LIC = 1, input CFC1 and DELTA1 If LIC = 2, input CFC1 and DELST1	5F10.0
18	CFC1,DELTA1 (or DELST1) If IOPT = 1, skip next card	2F10.0
19	UE1,DUEDX If LSHPBL = 0 and LPROG = 0, skip items 20 and 21	2F10.0
20	NR	I5
21	XRP,RL	2F10.0

TABLE III. SUMMARY OF INPUT DATA FOR RESTARTING

<u>Item No.</u>	<u>Variables</u>	<u>Format</u>
1	TITLE (Three cards)	20A4
2	NRSTRT,N3,ILIM If N3 = 0 stop. No further cards are necessary	5I5
3	XSEP,THETS	2F10.0

LIST OF SYMBOLS

A_{nj}	coefficients in eq. (24)
a	speed of sound
B_n	term in eq. (24)
b	width of mixing layer (fig. 2)
C_f	skin friction coefficient
D	maximum body diameter
G	quantity defined in eq. (14)
H_i	transformed shape factor, δ_i^*/θ_i
M	Mach number
m	$\frac{\gamma-1}{2} M^2$
p	pressure
r	radius
S	$T_t/T_{te} - 1$
s	root-mean-square error, eq. (25)
T	temperature
u, v	x, r velocity components
x, r	physical coordinates defined in figure 2
x_s	location of separation point (fig. 1)
β	eddy viscosity factor, $\tau/\mu(\partial u/\partial y)$
γ	ratio of specific heats
δ_i	transformed boundary-layer thickness
δ^*	displacement thickness
δ_i^*	transformed displacement thickness, $\int_0^{\delta_i} (1 - u/u_e) dy$
θ_s	half-angle of conical displacement surface

LIST OF SYMBOLS (Concluded)

θ_i	transformed momentum thickness, $\int_0^{\delta_i} \frac{u}{u_e} \left(1 - \frac{u}{u_e}\right) dy$
μ	molecular viscosity
ν	μ/ρ
ρ	density
τ	shear stress
ϕ	angle in eqs. (4)-(7)
ω	underrelaxation factor [eq. (2)]

Subscripts

e	refers to boundary-layer-edge
f	refers to conditions after a shock wave
i	refers to conditions preceding a shock wave, or conditions at the inner edge of an exhaust jet mixing layer
I	refers to inviscid flow
j	refers to conditions in exhaust nozzle
o	refers to the undisturbed free stream
s	refers to separation point
t	denotes stagnation point
V	refers to viscous flow
w	refers to conditions on a solid surface

Special notation

$()_x$	refers to differentiation with respect to x
---------	---